July 2020

DEPOLYMERIZABLE AND DISSIPATIVE CHEMICAL SYSTEMS: ROLE IN MATERIAL SYNTHESIS AND APPLICATIONS

Vikash Kumar
University of Massachusetts Amherst

DEPOLYMERIZABLE AND DISSIPATIVE CHEMICAL SYSTEMS: ROLE IN MATERIAL SYNTHESIS AND APPLICATIONS

A Dissertation Presented

by

VIKASH KUMAR

Submitted to the Graduate School of the

University of Massachusetts Amherst in partial fulfillment

of the requirements for the degree of

DOCTOR OF PHILOSOPHY

MAY 2020

Department of Chemistry

DEPOLYMERIZABLE AND DISSIPATIVE CHEMICAL SYSTEMS: ROLE IN MATERIAL SYNTHESIS AND APPLICATIONS

A Dissertation Presented

by

VIKASH KUMAR

Approved as to style and content by:

_____
Sankaran Thayumanavan, Chair

_____
Dhandapani Venkataraman, Member

_____
Min Chen, Member

_____
Barbara Osborne, Outside Member
Veterinary and Animal Science Department

_____

Ricardo Metz, Head,
Department of Chemistry

DEDICATION

To my lovely parents who gave me all the freedom in life

ACKNOWLEDGEMENTS

Pursuing a PhD is probably the hardest and most technical mountain I have ever climbed, and it would not have been possible without a proper support group.

First of all, I need to thank my supervisor, Professor Sankaran Thayumanavan. He is someone who has a deep desire of learning things which is something I have personally learnt from him. Getting into the details of things and learn about it. Throughout the process, he had been critical of necessary things such as writing scientific papers succinctly, presenting scientific data to any audience, and how to be efficient. I am grateful to him for those critiques because it is required to make us better. I would also take this opportunity to thank my dissertation committee members: Professor DV, Professor Min Chen and Professor Barbara Osborne. Your suggestions and valuable inputs during my qualifying exams had been a great help in outlining this dissertation work.

This work would not have been possible without my collaborators. I am grateful to Justin Harris and Professor Anne McNeil from University of Michigan Ann Arbor who helped me with the rheology measurements of hydrogels; Michael Tsuei and Professor Nick Abbott from Cornell University who tested the applicability of degradable polyelectrolyte-surfactant complex at the interface of liquid crystals, and Rui Cao and Professor Anthony Dinsmore from the physics department at Umass Amherst with whom we had a collaboration on light triggerable polymers.

Apart from research, I had some really great opportunities to work with several units at Umass Amherst such as EH&S staffs, Chemistry department staffs and Office of Professional Development (OPD). They have contributed significantly to my personal and professional

development. I am so grateful to: JMS, Chandra Hardy, Betsy Blunt, Kristi Ohr, Glenda Pons, Ryan Feyrer, Robert Sabola and Shana Passonno.

Throughout my research, several times I had to rely on Vachet lab for mass spectrometry studies. Meizhe Wang and Kong were my go to friends for that. Thank you for all the time you spent for me.

Thayumanavan lab group is huge and there was so much to learn from every past and present group member. I would like to thank Dr. Kishore Raghupathi, Dr. Youngju Bae, Dr. Oyuntuya Munkhabat, Dr. Priyaa Prasad, Dr. Subramani Swaminathan, Dr. Krishna Raghupathi, Dr. Mine Canakci, Dr. Hui Wang, Dr. Uma Sridhar and my undergraduate student Marina Franc for all the scientific inputs. I am grateful to the current group members and colleagues Dr. JingJing Gao, Hongxu Liu, Manisha Shivrayan, Pintu Kanjilal, Kingshuk Dutta, Dr. Jiaming Zhuang and Stephanie Le for sharing good as well as bad times together.

I had been pretty much a loner but I made sure I have few good friends who helped me survive grad school and I am so grateful to them. Thameez KY, Myrat Kurbanov, Ann Fernandez and Sparsh Makhaik: thank you so much!

It was great to be in touch with the undergraduate friends throughout the graduate school and they had been great stress reliever in bad times. I would like to thank Aashay Patil, Punya Plaban Sathpathy, Akash Guru and Kush Kumar for always being in touch.

I don’t think I could have made it till here without my family. I am so grateful to them for everything they have done and sacrificed for me. I was definitely lucky to be the youngest among six siblings and each of them have sacrificed their share of food and education so that I could eat well and study well. My nephews and nieces: I am so thankful to you all for all the fun we have.

Lastly, my parents, I don’t know if thanking them is enough, but I am so grateful to them for all their love and support throughout my life. They were always there for me whenever I needed someone during my hardest times. This degree is as much theirs as it is mine. Thank you!

ABSTRACT

DEPOLYMERIZABLE AND DISSIPATIVE CHEMICAL SYSTEMS: ROLE IN MATERIAL SYNTHESIS AND APPLICATIONS

MAY 2020

VIKASH KUMAR

B.S., INDIAN INSTITUTE OF SCIENCE EDUCATION AND RESEARCH PUNE

M.S., INDIAN INSTITUTE OF SCIENCE EDUCATION AND RESEARCH PUNE

PH.D., UNIVERSITY OF MASSACHUSETTS AMHERST

Directed by: Professor Sankaran Thayumanavan

Biomimetic systems which can show a functional response when treated with external stimuli are advantageous in applications such as self-healing, drug delivery, diagnostics and sensing. Depolymerizable and dissipative chemical systems are ideal tools to synthesize biomimetic systems that mimic nature. While there is abundance of synthetic chemistry tools to design depolymerizable systems, there is a lack of synthetic and formulation methodologies for developing useful materials from them. Majority of this thesis is directed towards narrowing that gap in knowledge, by utilizing depolymerizable systems to synthesize useful materials such as hydrogel and polyelectrolyte complexes for applications including self-healing, drug delivery and sensing. Minor part of this thesis involves dissipative chemical systems and it is directed towards achieving artificial systems that mimic several dynamic pathways predominant in nature which are regulated in presence of energy input.

TABLE OF CONTENTS

Page

LIST OF FIGURES

Figure **Page**

LIST OF ABBREVIATIONS

SIP	Self-immolative polymer
PBC	Poly (benzyl carbamate)
PBE	Poly (benzyl ether)
ATP	Adenosine triphosphate
ADP	Adenosine diphosphate
GTP	Guanosine triphosphate
GDP	Guanosine diphosphate
PDADMAC	Poly (diallyl) dimethylammonium chloride
HRP	Horseradish peroxidase
UV	Ultraviolet
DBTL	Dibutyltin dilaurate
ALP	Alkaline phosphatase
TFA	Trifluoroacetic acid
DCM	Dichloromethane
LC	Liquid crystal
CTAB	Cetyl trimethyl ammonium bromide
SDS	Sodium dodecyl sulfate
5CB	4-cyano-4’-pentylbiphenyl
DLS	Dynamic light scattering
TEM	Transmission electron microscopy

CHAPTER 1

INTRODUCTION

1.1 Motivation

Our daily lives involve remarkable use of polymeric materials. They are used for a variety of applications ranging from the use of plastics for storing food to their use in electronic devices. In a traditional sense, discovery of polymers is aimed towards making materials with higher mechanical strength. However, it has led to a significant increase in plastic pollution,[1–3] sparking interest in the development of degradable polymers. Inspired by this interest, along the lines of degradable materials, degradable linkers for prodrug design started to come into picture.[4] This concept further evolved at a macromolecule scale leading to the development of depolymerizable systems with significant improvements in chemical design that facilitated their degradation in response to a variety of stimulus.[5–9] Although most of the depolymerizable systems do not really serve the purpose of curbing pollution, they have turned out to be useful in a variety of other applications such as drug delivery,[10–12] sensing[13,14] and responsive plastics.[15,16]

The design strategy of depolymerizable system involves kinetically trapping an unstable state of polymer using a stable chemical functionality at the chain terminus.[17] The functionality is chosen in such a way that it can react with desired external stimulus, to unmask the reactive polymer chain. As a consequence, the polymer chain undergoes sequential depolymerization into individual building blocks. In literature, these polymeric systems are also referred as self-immolative polymers (SIP) due to their destruction in response to stimuli. This feature can be compared to the domino effect where a single disturbance event at one end of the group of dominoes supporting each other, leads to the collapse of individual dominos (Figure 1.1). Because a single chemical

event leads to depolymerization into multiple building blocks, this feature is desirable for signal amplification purposes in which a trace amount of input can be used to provide a macroscopic response.[18–21] While current state of art focuses primarily on the development of new chemical systems that undergo depolymerization, translating these chemical design guidelines to develop useful materials is relatively less explored. A part of this thesis aims towards improvement of our understanding of depolymerizable polymers in terms of formulation and their interfacial behavior. This understanding would help us in developing materials for applications such as self-healing, sensing and drug delivery.

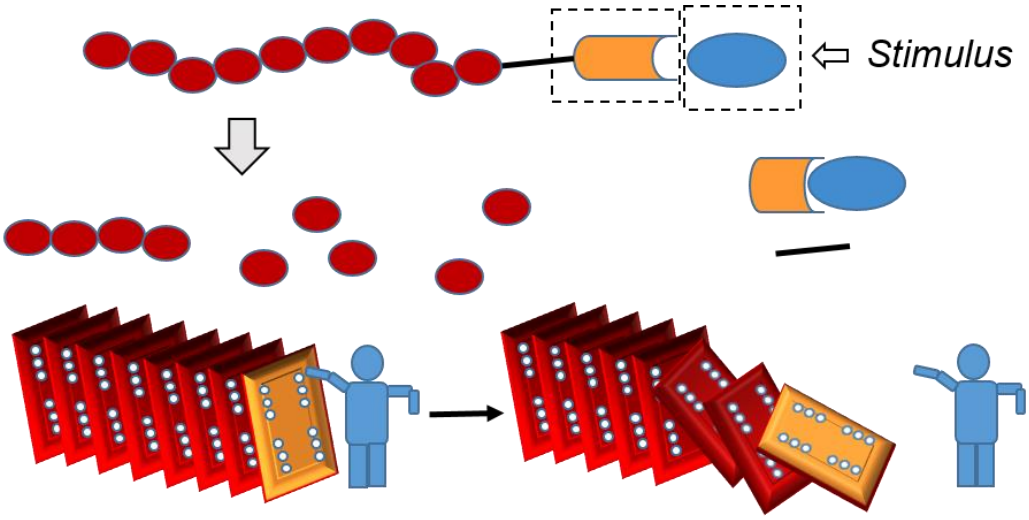

Figure 1.1: Illustration of depolymerizable polymers and its similarity to domino effect

1.2 Types of depolymerizable polymeric systems

1.2.1 Poly (benzyl carbamate) (PBC)

In these polymeric systems, a carbamate containing phenyl group is polymerized using Sn (IV) based catalyst called dibutyltin dilaurate (DBTL) at a high temperature of 115 ^{0}C.[22] After polymerization, a suitable trigger is used to cap the polymer in situ.[23] The trigger is chosen depending on the stimuli of interest for a particular application. Introduction of side chains in the

polymer backbone during monomer synthesis offers structural diversity to these polymers (Figure 1.2). Depolymerization usually proceeds through the formation of a reactive polymeric intermediate that is revealed after the cap is removed upon stimuli treatment. The reactive intermediate undergoes sequential 1, 6-elimination and decarboxylation reactions to generate highly reactive azaquinone methides that reacts with nucleophiles such as water to form 4-aminobenzyl alcohol or its derivatives as the byproduct of depolymerization (Figure 1.2).[24,25]

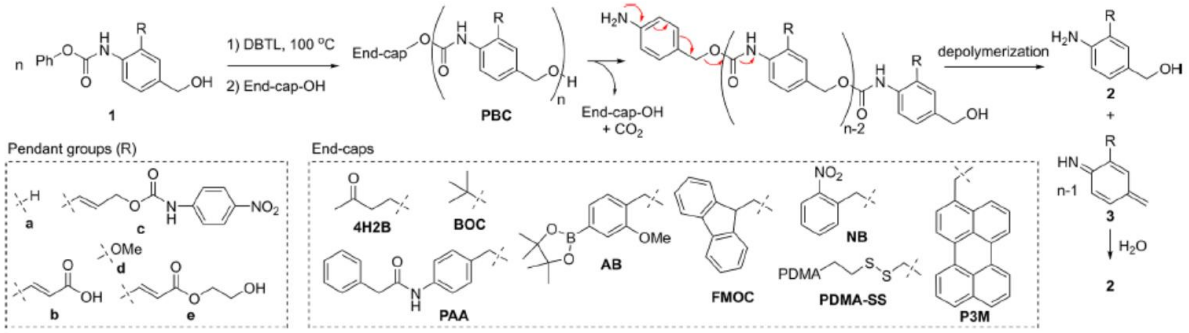

Figure 1.2: Scheme for depolymerizable poly (benzyl carbamate) synthesis and its subsequent depolymerization. Reproduced with permission from reference 25.

1.2.2 Poly (benzyl carbamate) with spacers

While poly (benzyl carbamates) were the first class of depolymerizable polymers developed, their rigid backbone provided poor solubility in a number of solvents. Although the solubility could be altered by modifying the side chains in the polymer, monomer synthesis becomes challenging. To solve these issues, poly (benzyl carbamates) with spacers were designed which solved the solubility issues[26] and provided opportunity to tune the deplymerization kinetics.[27] For example, the research group of Gillies et al. introduced N, N'-dimethylethylenediamine (DMED) as the spacer in poly (benzyl carbamates) to improve their solubility (Figure 1.3). The depolymerization

in these class of polymers goes through sequential cyclization of spacers and subsequent elimination reactions (Figure 1.3).[26]

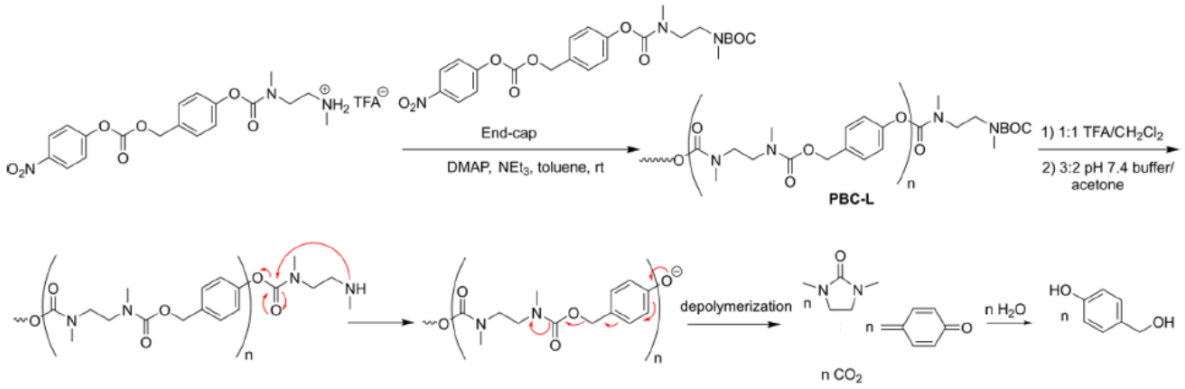

Figure 1.3: Synthesis of depolymerizable poly (benzyl carbamate) with N, N'-dimethylethylenediamine (DMED) spacer. Reproduced with permission from reference 25.

1.2.3 Poly (benzyl ether) s (PBE)

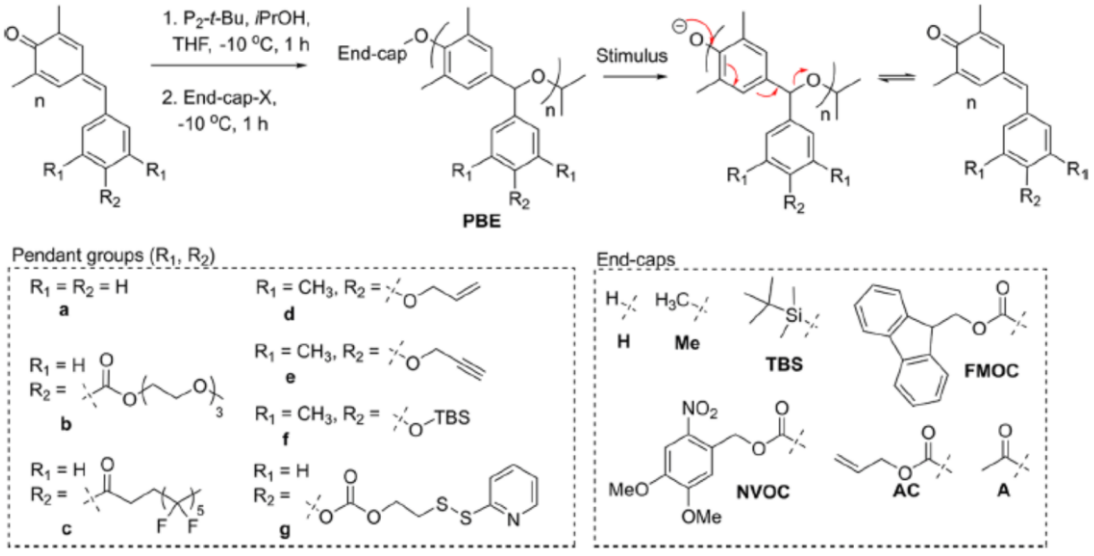

Figure 1.4: Synthesis of poly (benzyl ether) with variations in structure and end caps. Reproduced with permission from reference 25.

dimethyl-7-phenyl-1,4-benzoquinone monomer; 1-tertbutyl-2,2,4,4,4-pentakis(dimethylamino)-

2λ5,4λ5-catenadi-(phosphazene) (P2-t-Bu) as a base and alcohol as an initiator.[28] The polymer could be capped using silyl ethers, carbonates or alkyl groups to achieve the degradable PBEs under respective conditions (Figure 1.4). The depolymerization of PBE followed significantly faster kinetics compared to the PBCs. Several variations of PBE with different depolymerization kinetics have been studied by varying the functional groups on the pendant phenyl groups (Figure 1.4).[29–31]

1.2.4 Polypthalaldehydes

This class of polymers can be synthesized using cationic or anionic polymerization of pthalaldehyde in presence of catalysts such as phosphazene, $BF_3.OEt_2$, $SnCl_4$ or $TiCl_4$ at low temperature of -78 ^{0}C (Figure 1.5).[32] Similar to the other class of depolymerizable polymers, polypthalaldehydes can also be capped using a suitable trigger. Removal of the trigger using a stimulus leads to depolymerization.

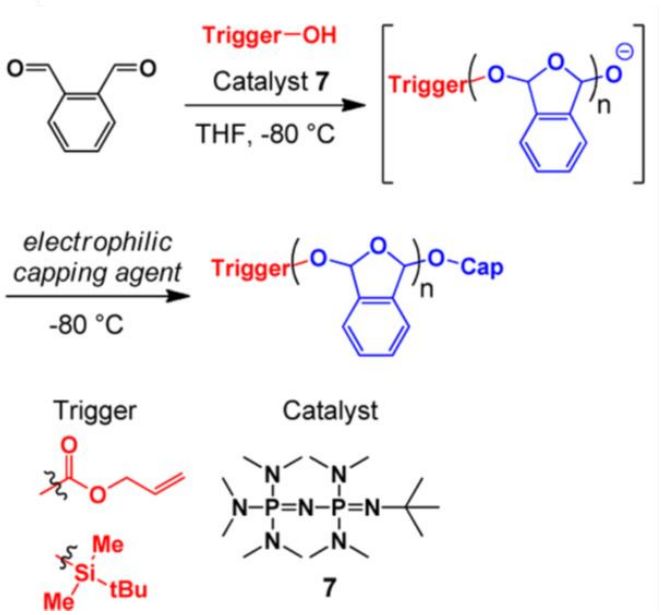

Figure 1.5: Synthesis of polypthalaldehydes using catalyst 7 and suitable triggers. Reproduced with permission from reference 24.

1.3 Use of suitable trigger and stimuli in depolymerizable systems.

While depolymerizable backbones are important in terms of the electronic cascade leading to polymer degradation, the key step leading to the electronic cascade is the reaction of stimuli with trigger or polymer cap. Several stimuli such as acid, base, redox, light, enzyme etc. can be used depending on the applications.[24,33]

In this thesis we have focused on developing materials sensitive to light and enzyme, therefore this chapter will focus on examples of systems which can be triggered using light and enzyme. For more details related to examples of other kind of triggers used, it can be found in detailed review written by Gillies et al.[24]

1.3.1 Enzyme triggered depolymerization

Enzyme specific systems are particularly attractive for biomedical applications, because of their involvement in numerous cellular metabolic pathways.[34,35] The high turnover number, preference towards specific substrates and mechanism of action under mild aqueous conditions offer the impetus for researchers to design and test enzyme responsive nanomaterials. In case of depolymerizable systems responsive to enzymes, an enzyme sensitive trigger is used to cap the polymer chain. The enzymatic cleavage event leads to the sequential elimination reactions leading to polymer degradation. For example, bovine serum albumin has been used to trigger the cleavage of 4-hydroxy-2-butanone which unravels the sequential elimination reactions leading to polymer degradation.[22] During degradation, multiple fluorescent reporter units were generated which provided a visual readout to study enzyme triggered degradation process (Figure 1.6).

Since depolymerizable systems are very sensitive to stimuli including enzymes, they have potential to be useful in a number of biological applications which involves dysfunctional enzymes for sensing and drug delivery applications. However, an important consideration that needs to be taken into account is the toxicity of the reactive intermediates formed during the sequential elimination reactions.

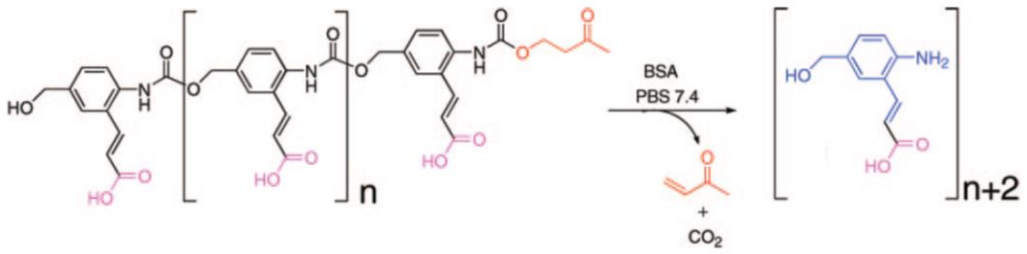

Figure 1.6: Bovine serum albumin triggered depolymerization. Reproduced with permission from reference 22.

1.3.2 Light triggered depolymerization

Light is particularly attractive stimuli because of its remote use which doesn't involve introducing additional reagent in the chemical mixture. As a result, it can be used as a stimulus for the spatiotemporal control of a material's property via depolymerization. Various light cleavable groups have been developed in recent years which can be cleaved using the suitable wavelength and intensity of light source. Examples of light sensitive group includes o-nitrobenzyl group and bromocoumarin (Figure 1.7).[36]

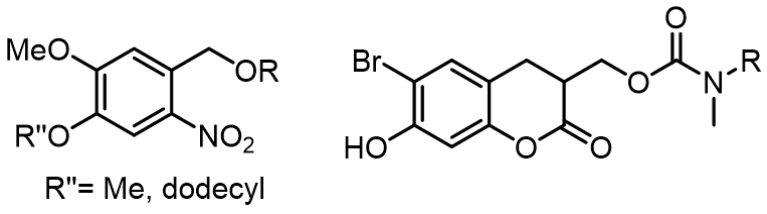

Figure 1.7: Examples of light sensitive groups used to cap depolymerizable polymers.

1.4 Applications of depolymerizable chemical systems

Due to the triggered degradation of these chemical systems, most of the applications associated with depolymerizable systems are centered towards nanomaterial degradation for molecular release. For example, by modifying the functional groups in depolymerizable systems, they can be made amphiphilic which can self-assemble under aqueous conditions into various nanostructures such as micelles and vesicles.[12,27] Interior of these nanomaterials can be used to encapsulate molecules such as drugs or enzymes, which can be released on demand using a suitable stimuli of interest. Since the depolymerization involves a single cleavage event, these materials are very sensitive and provide an amplified response to the triggering event.

Depolymerizable systems have also been used as solid state materials which can undergo patterned degradation upon treatment with external stimuli. These examples provide a direction of their use in lithography applications.[15,16]

1.5 Dissipative chemical systems

Another class of chemical systems that have gained significant attention in past decade are dissipative or non-equilibrium chemical systems that requires chemical input to function. While most of the self-assembled structures are thermodynamic in nature due to the reversibility of non-covalent forces of interaction experienced by amphiphilic molecules, dissipative system can form self-assembled structures only in the presence of chemical input.[37]

Most natural systems have evolved to undergo self-assembly process under non-equilibrium conditions i.e. the self-assembly process is sustained in the presence of an energy input. Once the energy input is ceased, transiently formed nanoassemblies can dissipate the energy to revert back to their equilibrium state. The self-assembly and energy dissipation process can be repeated over

multiple cycles by continuously supplying energy input to the system. As a result, the entire process is highly dynamic and adaptive which allows the natural systems to achieve energetically uphill functions. For example, the dynamic growth of microtubules using guanosine triphosphate (GTP) bound tubulin dimers as building block and their shrinkage due to the hydrolysis of GTP into guanosine diphosphate (GDP) is a classic non-equilibrium system deployed in cellular processes such as cell division.[38,39] Similarly, the use of adenosine triphosphate (ATP) as an energy input by enzyme kinase to sustain various cellular functions is another example of non-equilibrium process predominant in nature.[40,41]

Designing artificial systems which mimic such natural processes using the principles of supramolecular chemistry has been gaining significant attention. It involves designing building blocks which can transiently self-assemble in the presence of a chemical input.[42] Once the supply of chemical input is ceased, the transiently formed self-assembled nanostructures can dissipate the energy to revert back to its resting or thermodynamic state. Dissipation of energy is usually triggered by stimuli such as pH,[43] light[44] or enzyme[45] which is an inherent part of the system. Enzymes, in particular are useful trigger for energy dissipation because of their resemblance to natural systems which constantly use enzymes in tandem to achieve non-equilibrium processes. Using this strategy, the non-equilibrium assembly is maintained by constantly supplying an energy input to the system.

As a demonstration of artificial non-equilibrium system, ATP was used as an energy input to template the self-assembly of positively charged surfactants into transient vesicles in the presence of potato apyrase.[45] Gradual hydrolysis of ATP by potato apyrase led to the disassembly of vesicles, which could be reassembled by adding more ATP to the system. The lifetime of vesicles was dependent on the concentration of potato apyrase which dictated the consumption of ATP or

energy dissipation. The transiently formed vesicles were also used as nanoreactor to carry out a transient chemical reaction between two hydrophobic reactants which was otherwise not possible.

The non-equilibrium supramolecular chemistry concept can also be applied to transiently control the nature of supramolecular conformation. In a recent report, hexokinase and creatine phopsphokinase were used in tandem to temporally tune the conformation of Zinc (II) dipicolylethylenediamine derived naphthalene diamide (NDPA).[46] NDPA gives rise to P-helix like conformation upon binding to ATP while an M helix upon binding to ADP (Figure 9a). By temporally controlling the relative concentration of ATP and ADP using hexokinase and creatine phopsphokinase in presence of their respective substrates (Figure 9b), it was found that a specific supramolecular conformation can be transiently achieved. Apart from the dynamic nature of conformations due to the enzymatic formation of ATP and ADP, tunability in the lifetime of each conformation was also achieved by varying the concentration of enzyme or the substrate. This demonstration is reminiscent of kinase and phosphatase mediated cellular processes used in dynamic way to constantly carry out the non-equilibrium processes using ATP as an energy input.

1.6 Summary and overview of the thesis

While there is tremendous scope in applications of depolymerizable systems, several inherent limitations of depolymerizable polymers such as low molecular weight and poor solubility of PBCs limits their applicability in constructing useful materials. Additionally, the use of depolymerizable materials which show varying properties before and after degradation at the interface of two phases is not well explored. Chapter 2, 3 and 4 of this thesis are aimed towards improving the scope of applications of depolymerizable systems.

The development of dissipative chemical systems is in a state of infancy and creating artificial chemical systems which mimics the dynamic behavior of natural systems is highly desirable for

materials which can show dynamic and adaptive behavior in response to stimuli. Chapter 5 of this thesis is aimed towards the development of dissipative systems using ATP as an energy input.

1) In chapter 2, the depolymerization strategy has been used to "construct" cross-linked network like structures. A UV triggerable poly (benzyl carbamate) based vesicle has been formulated using electrostatic interactions which can encapsulate water soluble enzymes in their interior. When triggered with UV light, the enzymes can get released and react with the substrate molecules present in the aqueous bulk leading to hydrogel formation
2) In chapter 3, alkaline phosphatase triggerable materials have been synthesized by modifying poly (benzyl carbamate) into a water soluble as well as water insoluble polymer. Both polymers can be used for synthesizing different nanomaterials which showed contrasting degradation kinetics depending on the exposure of substrate to alkaline phosphatase.
3) In chapter 4, alkaline phosphatase triggerable poly (benzyl carbamate) and surfactant based complex has been studied at the interface of liquid crystals. When the complex at interface is triggered with alkaline phosphatase, their interaction with liquid crystal changes drastically which was reflected in the optical signature of liquid crystal.
4) In chapter 5, with an aim to mimic ATP fueled kinase-phosphatase mediated enzymatic pathway in biological systems, artificial peptide based amphiphilic systems were studied. These artificial systems were designed and studied in such a way that they could undergo self-assembly process in the presence of ATP as an energy input.

1.7 References

(1) Vince, J.; Hardesty, B. D. Plastic Pollution Challenges in Marine and Coastal Environments: From Local to Global Governance. *Restor. Ecol.* **2017**, *25* (1), 123–128.

(2) Borrelle, S. B.; Rochman, C. M.; Liboiron, M.; Bond, A. L.; Lusher, A.; Bradshaw, H.; Provencher, J. F. Why We Need an International Agreement on Marine Plastic Pollution. *Proc. Nat. Acad. Sci. U. S. A.* **2017,** *114* (38), 9994–9997.

(3) Haward, M. Plastic Pollution of the World's Seas and Oceans as a Contemporary Challenge in Ocean Governance. *Nat. Commun*. **2018**, 9 (1), 1-3.

(4) Carl, P. L.; Chakravarty, P. K.; Katzenellenbogen, J. A. A Novel Connector Linkage Applicable in Prodrug Design. *J. Med. Chem*. **1981**, *24* (5), 479–480.

(5) Shabat, D. Self-Immolative Dendrimers as Novel Drug Delivery Platforms. *J. Polym. Sci. Part A Polym. Chem.* **2006**, *44* (5), 1569–1578.

(6) Wang, W.; Alexander, C. Self-Immolative Polymers. *Angew. Chem. Int. Ed*. **2008**, *47* (41) 7804–7806.

(7) Amir, R. J.; Pessah, N.; Shamis, M.; Shabat, D. Self-Immolative Dendrimers. *Angew. Chem. Int. Ed.* **2003**, *42* (37), 4494–4499.

(8) Li, S.; Szalai, M. L.; Kevwitch, R. M.; McGrath, D. V. Dendrimer Disassembly by Benzyl Ether Depolymerization. *J. Am. Chem. Soc.* **2003**, *125* (35), 10516–10517.

(9) Haba, K.; Popkov, M.; Shamis, M.; Lerner, R. A.; Barbas, C. F.; Shabat, D. Single-Triggered Trimeric Prodrugs. *Angew. Chem. Int. Ed.* **2005**, *44* (5), 716–720.

(10) Fomina, N.; McFearin, C.; Sermsakdi, M.; Edigin, O.; Almutairi, A. UV and Near-IR

Triggered Release from Polymeric Nanoparticles. *J. Am. Chem. Soc.* **2010**, *132* (28), 9540–9542.

(11) De Gracia Lux, C.; Joshi-Barr, S.; Nguyen, T.; Mahmoud, E.; Schopf, E.; Fomina, N.; Almutairi, A. Biocompatible Polymeric Nanoparticles Degrade and Release Cargo in Response to Biologically Relevant Levels of Hydrogen Peroxide. *J. Am. Chem. Soc.* **2012**, *134* (38), 15758–15764.

(12) Liu, G.; Wang, X.; Hu, J.; Zhang, G.; Liu, S. Self-Immolative Polymersomes for High-Efficiency Triggered Release and Programmed Enzymatic Reactions. *J. Am. Chem. Soc.* **2014**, *136* (20), 7492–7497.

(13) Gnaim, S.; Shabat, D. Self-Immolative Chemiluminescence Polymers: Innate Assimilation of Chemiexcitation in a Domino-like Depolymerization. *J. Am. Chem. Soc.* **2017**, *139* (29), 10002–10008.

(14) Liu, G.; Zhang, G.; Hu, J.; Wang, X.; Zhu, M.; Liu, S. Hyperbranched Self-Immolative Polymers (HSIPs) for Programmed Payload Delivery and Ultrasensitive Detection. *J. Am. Chem. Soc.* **2015**, *137* (36), 11645–11655.

(15) Seo, W.; Phillips, S. T. Patterned Plastics That Change Physical Structure in Response to Applied Chemical Signals. *J. Am. Chem. Soc.* **2010**, *132* (27), 9234–9235.

(16) DiLauro, A. M.; Lewis, G. G.; Phillips, S. T. Self-Immolative Poly(4,5-Dichlorophthalaldehyde) and Its Applications in Multi-Stimuli-Responsive Macroscopic Plastics. *Angew. Chem. Int. Ed.* **2015**, *127* (21), 6298–6303.

(17) Alouane, A.; Labruère, R.; Le Saux, T.; Schmidt, F.; Jullien, L. Self-Immolative Spacers:

Kinetic Aspects, Structure-Property Relationships, and Applications. *Angew. Chem. Int. Ed*. **2015**, *54* (26), 7492–7509.

(18) Roth, M. E.; Green, O.; Gnaim, S.; Shabat, D. Dendritic, Oligomeric, and Polymeric Self-Immolative Molecular Amplification. *Chem. Rev*. **2016**, *116* (3), 1309–1352.

(19) Weinstain, R.; Sagi, A.; Karton, N.; Shabat, D. Self-Immolative Comb-Polymers: Multiple-Release of Side-Reporters by a Single Stimulus Event. *Chem. - A Eur. J.* **2008**, *14* (23), 6857–6861.

(20) Lewis, G. G.; Robbins, J. S.; Phillips, S. T. Phase-Switching Depolymerizable Poly(Carbamate) Oligomers for Signal Amplification in Quantitative Time-Based Assays. *Macromolecules* **2013**, *46* (13), 5177–5183.

(21) Lewis, G. G.; Robbins, J. S.; Phillips, S. T. Point-of-Care Assay Platform for Quantifying Active Enzymes to Femtomolar Levels Using Measurements of Time as the Readout. *Anal. Chem.* **2013**, *85* (21), 10432–10439.

(22) Sagi, A.; Weinstain, R.; Karton, N.; Shabat, D. Self-Immolative Polymers. *J. Am. Chem. Soc.* **2008**, *130* (16), 5434–5435.

(23) Esser-Kahn, A. P.; Sottos, N. R.; White, S. R.; Moore, J. S. Programmable Microcapsules from Self-Immolative Polymers. *J. Am. Chem. Soc.* **2010**, *132* (30), 10266–10268.

(24) Peterson, G. I.; Larsen, M. B.; Boydston, A. J. Controlled Depolymerization: Stimuli-Responsive Self-Immolative Polymers. *Macromolecules* **2012**, *45* (18), 7317–7328.

(25) Yardley, R. E.; Kenaree, A. R.; Gillies, E. R. Triggering Depolymerization: Progress and Opportunities for Self-Immolative Polymers. *Macromolecules* **2019**, *52* (17), 6342-6360.

(26) DeWit, M. A.; Gillies, E. R. A Cascade Biodegradable Polymer Based on Alternating Cyclization and Elimination Reactions. *J. Am. Chem. Soc.* **2009**, *131* (51), 18327–18334.

(27) Chen, E. K. Y.; McBride, R. A.; Gillies, E. R. Self-Immolative Polymers Containing Rapidly Cyclizing Spacers: Toward Rapid Depolymerization Rates. *Macromolecules* **2012**, *45* (18), 7364–7374.

(28) Olah, M. G.; Robbins, J. S.; Baker, M. S.; Phillips, S. T. End-Capped Poly(Benzyl Ethers): Acid and Base Stable Polymers That Depolymerize Rapidly from Head-to-Tail in Response to Specific Applied Signals. *Macromolecules* **2013**, *46* (15), 5924–5928.

(29) Ergene, C.; Palermo, E. F. Cationic Poly(Benzyl Ether)s as Self-Immolative Antimicrobial Polymers. *Biomacromolecules* **2017**, *18* (10), 3400–3409.

(30) Xiao, Y.; Li, H.; Zhang, B.; Cheng, Z.; Li, Y.; Tan, X.; Zhang, K. Modulating the Depolymerization of Self-Immolative Brush Polymers with Poly(Benzyl Ether) Backbones. *Macromolecules* **2018**, *51* (8), 2899–2905.

(31) Baker, M. S.; Kim, H.; Olah, M. G.; Lewis, G. G.; Phillips, S. T. Depolymerizable Poly(Benzyl Ether)-Based Materials for Selective Room Temperature Recycling. *Green Chem.* **2015**, *17* (9), 4541–4545.

(32) Aso, C.; Tagami, S.; Kunitake, T. Polymerization of Aromatic Aldehydes. II. Cationic Cyclopolymerization of Phthalaldehyde. *J. Polym. Sci. Part A-1 Polym. Chem.* **1969**, *7* (2), 497–511.

(33) Weinstain, R.; Baran, P. S.; Shabat, D. Activity-Linked Labeling of Enzymes by Self-Immolative Polymers. *Bioconjug. Chem.* **2009**, *20* (9), 1783–1791.

(34) Dhanasekaran, S. M.; Barrette, T. R.; Ghosh, D.; Shah, R.; Varambally, S.; Kurachi, K.; Pienta, K. J.; Rubin, M. A.; Chinnaiyan, A. M. Delineation of Prognostic Biomarkers in Prostate Cancer. *Nature* **2001**, *412* (6849), 822–826.

(35) Robinson, P. K. Enzymes: Principles and Biotechnological Applications. *Essays Biochem.* **2015**, *59*, 1–41.

(36) De Gracia Lux, C.; McFearin, C. L.; Joshi-Barr, S.; Sankaranarayanan, J.; Fomina, N.; Almutairi, A. Single UV or near IR Triggering Event Leads to Polymer Degradation into Small Molecules. *ACS Macro Lett.* **2012**, *1* (7), 922–926.

(37) Mattia, E.; Otto, S. Supramolecular Systems Chemistry. *Nat. Nanotechnol*. **2015**, *10* (2), 111-119.

(38) Heald, R.; Nogales, E. Microtubule Dynamics. *J. Cell Sci.* **2002**, *115* (1).

(39) Cassimeris, L.; Pryer, N. K.; Salmon, E. D. Real-Time Observations of Microtubule Dynamic Instability in Living Cells. *J. Cell Biol.* **1988**, *107* (6 I), 2223–2231.

(40) Dhiman, S.; Jain, A.; Kumar, M.; George, S. J. Adenosine-Phosphate-Fueled, Temporally Programmed Supramolecular Polymers with Multiple Transient States. *J. Am. Chem. Soc.* **2017**, *139* (46), 16568–16575.

(41) Tatsumi, T.; Shiraishi, J.; Keira, N.; Akashi, K.; Mano, A.; Yamanaka, S.; Matoba, S.; Fushiki, S.; Fliss, H.; Nakagawa, M. Intracellular ATP Is Required for Mitochondrial Apoptotic Pathways in Isolated Hypoxic Rat Cardiac Myocytes. *Cardiovasc. Res.* **2003**, *59* (2), 428–440.

(42) Rieß, B.; Grötsch, R. K.; Boekhoven, J. The Design of Dissipative Molecular Assemblies

Driven by Chemical Reaction Cycles. *Chem* **2019**, *6* (3), 552–578.

(43) Boekhoven, J.; Hendriksen, W. E.; Koper, G. J. M.; Eelkema, R.; Van Esch, J. H. Transient Assembly of Active Materials Fueled by a Chemical Reaction. *Science* **2015**, *349* (6252), 1075–1079.

(44) Klajn, R.; Bishop, K. J. M.; Grzybowski, B. A. Light-Controlled Self-Assembly of Reversible and Irreversible Nanoparticle Suprastructures. *Proc. Natl. Acad. Sci. U. S. A.* **2007**, *104* (25), 10305–10309.

(45) Maiti, S.; Fortunati, I.; Ferrante, C.; Scrimin, P.; Prins, L. J. Dissipative Self-Assembly of Vesicular Nanoreactors. *Nat. Chem.* **2016**, *8* (7), 725–731.

(46) Dhiman, S.; Jain, A.; George, S. J. Transient Helicity: Fuel-Driven Temporal Control over Conformational Switching in a Supramolecular Polymer. *Angew. Chem. Int. Ed.* **2017**, *56* (5), 1329–1333.

CHAPTER 2

UV TRIGGERED DEPOLYMERIZATION STRATEGY TO CONSTRUCT HYDROGELS

Used with permission from Kumar, V.; Harris, J. T.; Ribbe, A.; Franc, M.; Bae, Y.; McNeil, A. J.; Thayumanavan, S. Construction from Destruction: Hydrogel Formation from Triggered Depolymerization-Based Release of an Enzymatic Catalyst. *ACS Macro Lett.* **2020**, 377–381.

2.1 Introduction

One of the key features of natural system is their rapid and amplified response to trace external stimulus or signal.[1,2] Upon sensing an input signal, the signal is transduced across multiple length scales to bring the desired response which is a macroscopically observed phenomenon. This sense and respond signal is predominant in number of living organisms such as hagfish. As a defense mechanism, they secrete a slime or gel like matrix around them in response to predator attack such as a shark bite which gags the predator. The gel formation is a result of protein containing vesicle secretion by hagfish after the attack.[3–5] In presence of seawater, vesicles disassemble leading to the cross-linked network of proteins resulting in gel formation. Biomimetic systems that undergo similar macroscopic phase transformations by amplifying external input signal could be useful in number of applications such as self-healing. For example, creating on demand cross-linked network in response to an external signal could be used to heal the cracks developed in a material.

"Self-immolative" or depolymerizable chemical systems have been gaining significant attention in recent years due to their ability to undergo degradation into multiple building block components in response to a single cleavage event at the chain terminus.[6] This feature is used for signal

amplification purposes where a trace input signal brings macroscopic change in the property of material. For example, solid-state materials which can be triggered to show a macroscopic change in their property after experiencing an input signal has been well studied.[7,8] Similarly, self-immolative dendrimers and polymers have also been used in sensing applications where a trace amount of analyte can be detected due to the generation of multiple reporter units.[9–11] These processes take advantage of the triggered destruction of self-immolative dendrimers or polymers to small molecule components.

In this chapter, we were interested in developing a strategy to construct cross-linked hydrogel network by taking advantage of the depolymerization process primarily because it offers advantage in applications where on-demand material formation is desired. Herein, the depolymerization process forms the basis for triggered disassembly of vesicles, where the ensuing molecular release is utilized to obtain a change in property of material from solution to hydrogel which can be macroscopically visualized.

In order to achieve self-assembled vesicles and their triggered disassembly, we took advantage of polyvalent interaction between two polyelectrolytes which has been shown to form a variety of nanoscale and mesoscale assemblies.[12–15] Because the basis for forming these assemblies is polyvalency, we hypothesized that the depolymerization process can be leveraged to alter the strength of interaction between the polyelectrolytes and, thus, the stability of the assembly. One of the polyelectrolytes is designed to undergo chain unzipping in response to UV light as trigger. As the degree of polymerization reduces towards the monomeric state after triggering with UV light, the polyvalent interaction weakens, leading to the disassembly of vesicles. To accomplish hydrogel formation from this disassembly process, we envisioned encapsulation of gelating agents into the vesicles, which upon release into the bulk aqueous phase would result in the formation of hydrogel.

The components of vesicular interior and the bulk aqueous phase has to be such that the gel formation is encouraged only when the components present in both phases come in contact with each other which is possible after the triggered depolymerization of one polyelectrolyte. The self-assembly of two polyelectrolytes, disassembly and gel formation is illustrated in Figure 2.1.

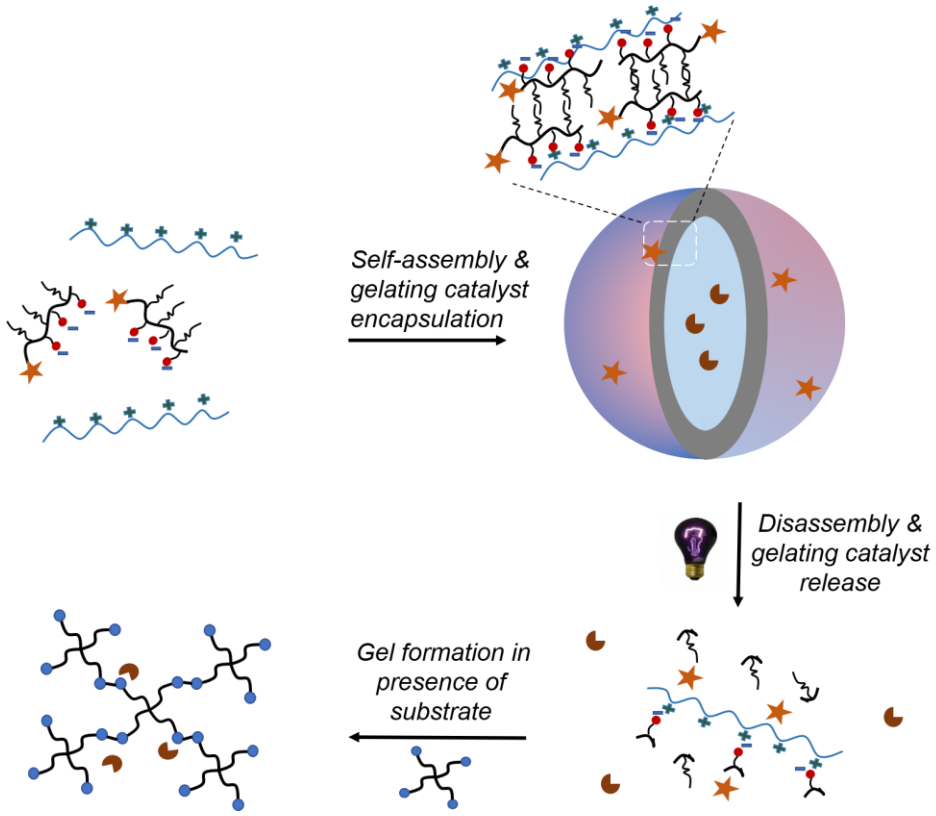

Figure 2.1: Schematic representation of self-assembly of polyelectrolytes into vesicles, gelating agent encapsulation, disassembly using UV trigger and gel formation.

2.2 Results and Discussion

2.2.1 Molecular Design and Synthetic Scheme

Synthetic scheme of monomer used in the synthesis of UV triggerable depolymerizable poly(benzylcarbamate) is shown in Figure 2.2. Step growth polymerization technique reported earlier was used for polymer synthesis.[16] The polymer chain was capped using o-nitrobenzyl

moiety to achieve UV degradable polymer P1.[17,18] The *t*-butyl ester containing side chains from P1 were deprotected in a controlled way using TFA: DCM mixture to achieve P2 which contained

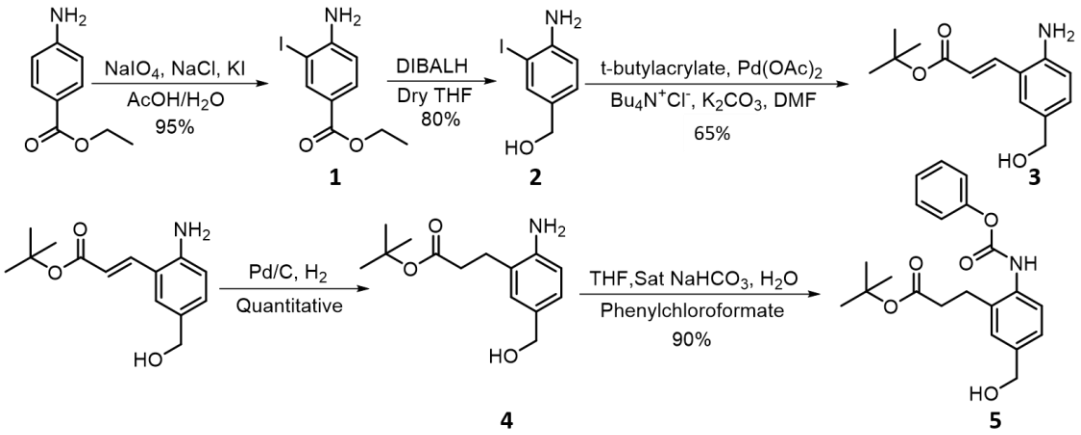

Figure 2.2: Monomer synthesis scheme.

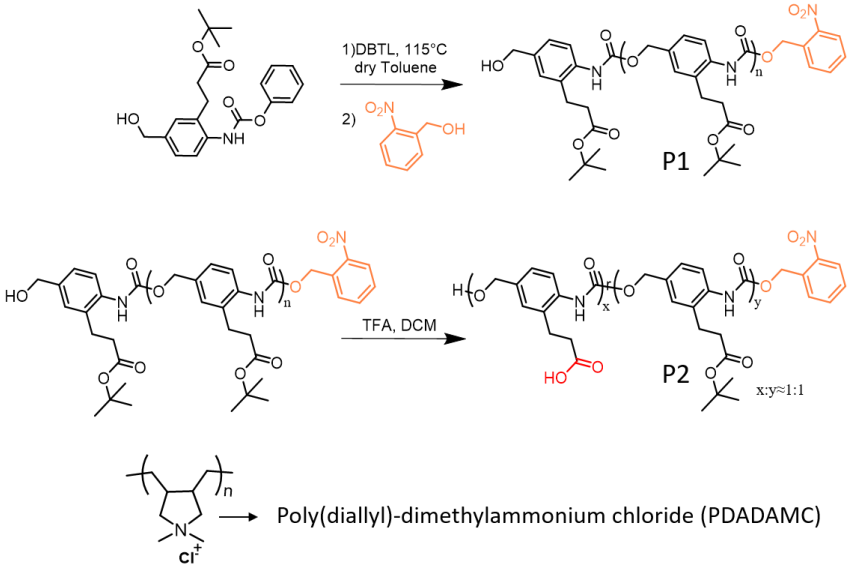

Figure 2.3: Synthesis and structure of polymers used in this chapter.

random and equal distribution of carboxylic acid and *t*-butyl ester groups (Figure 2.3). Poly (diallyl)dimethylammonium chloride (PDADMAC) was used as positively charged polyelectrolyte in the self-assembly process.

2.2.2 Depolymerization studies of P2

Depolymerization of P1 or P2 is a multistep process as shown in Figure 2.4. Upon UV irradiation, o-nitrobenzyl unit is cleaved first, resulting into an unstable intermediate polymer which can undergo an electronic cascade to depolymerize the entire chain.

P2 offered good solubility in polar solvents such as methanol. In order to study the

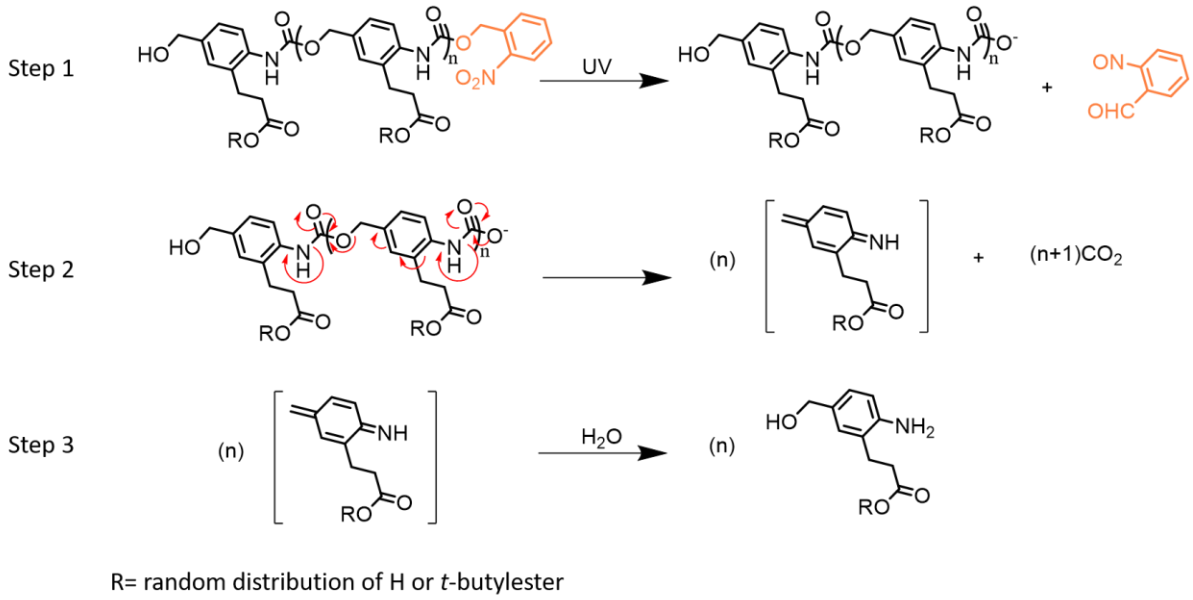

Figure 2.4: Mechanism of degradation of **P2** in presence of UV light.

depolymerization of P2, it was dissolved in a MeOD/D_2O mixture (2:1) and irradiated with 350 nm UV light of intensity of 2.2 mW/cm^2. The resultant solution was monitored using ^{1}H NMR spectroscopy and it was found that the complete cleavage of o-nitrobenzyl group takes 2 h. It was determined using the disappearance of peak at 5.6 ppm corresponding to the methylene protons of o-nitrobenzyl group. A temporal increase in the intensity of proton signals corresponding to the small molecule products after depolymerization was observed in ^{1}H NMR (Figure 2.5A). Using relative integration values of polymer and small molecule, it was found that 70% of the polymer depolymerized in ~24 h (Figure 2.5B).

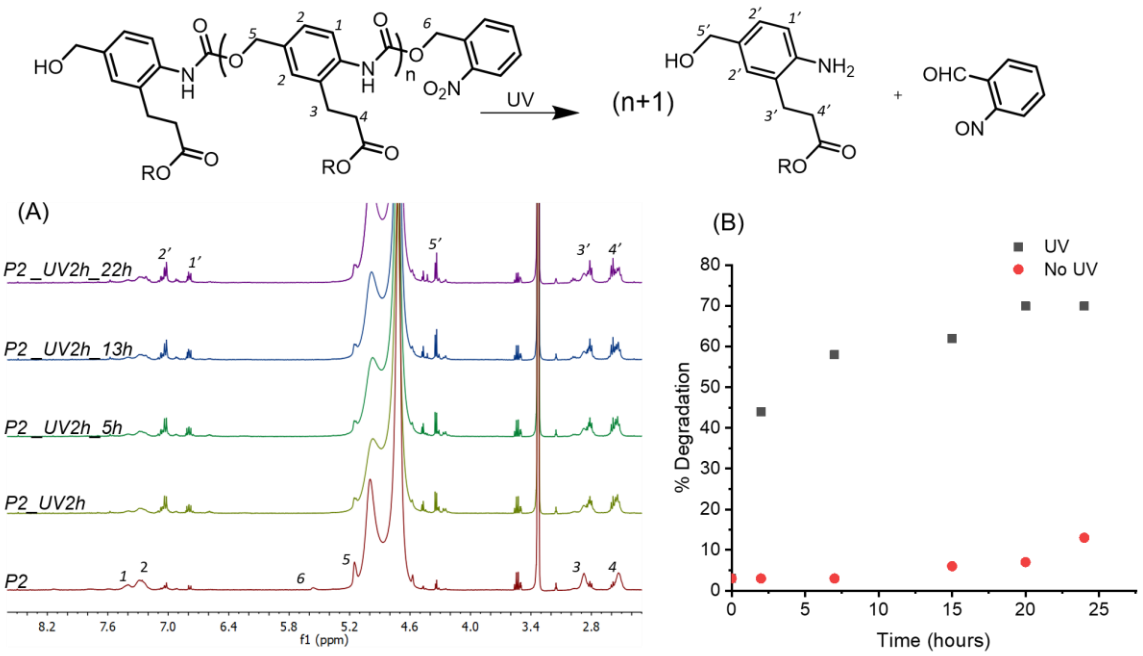

Figure 2.5: (A) ^{1}H NMR of **P2** solution at different time intervals after UV irradiation for 2 h; (B) Black: Percentage of polymer degraded at different time intervals, Red: Percentage of polymer degraded due to hydrolysis.

2.2.3 Self-assembly studies of P2

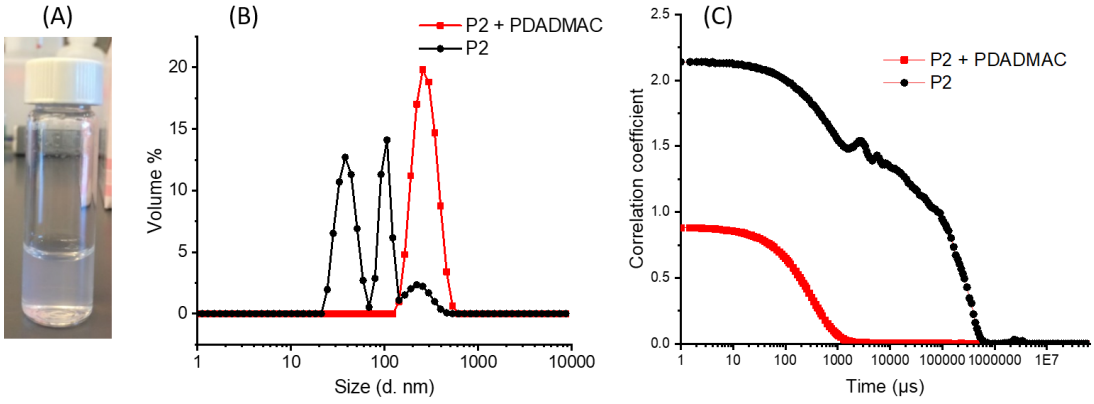

Figure 2.6: (A) Image of colloidal dispersion of **P2** + PDADMAC; (B) DLS size profile of **P2** and **P2** + PDADMAC; (C) Correlation coefficient of **P2** and **P2** + PDADMAC.

Since P2 was inherently amphiphilic, we expected it to self-assemble in water, but it exhibited poor self-assembly characteristics under aqueous conditions as observed in the dynamic light

scattering (DLS) studies. It showed multimodal size distribution and poor correlation coefficient

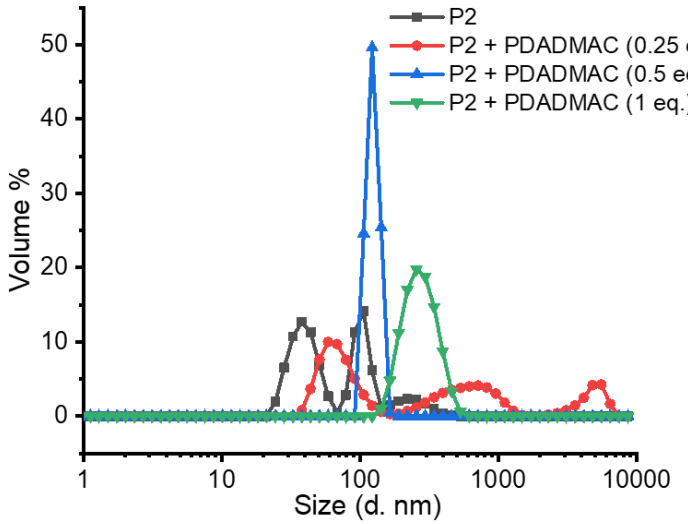

Figure 2.7: DLS size profile of **P2** when mixed with different charge equivalents of PDADMAC. The dispersity value was 0.587 for **P2**, 0.752 for **P2** + PDADMAC (0.25 eq.), 1 for **P2** + PDADMAC (0.5 eq.) and 0.206 for **P2** + PDADMAC (1 eq.).

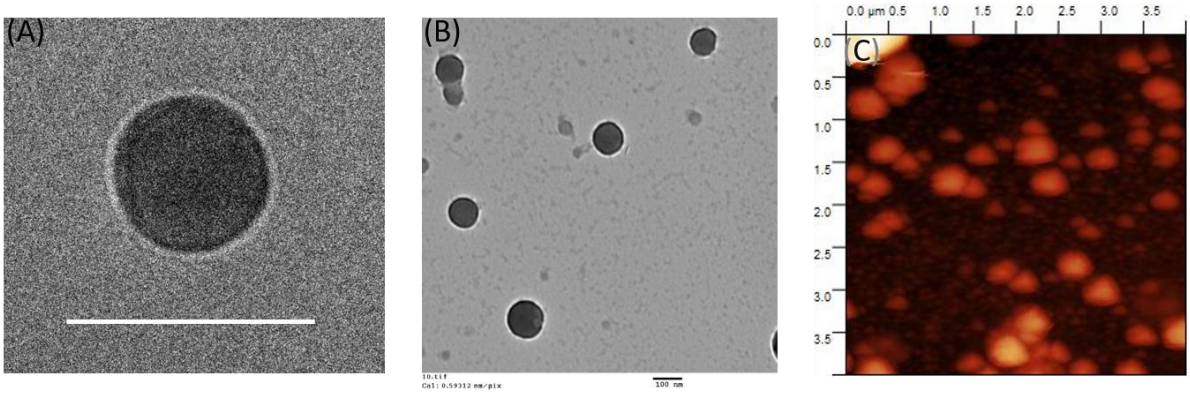

Figure 2.8: Images of **P2** + PDADMAC nanoparticles. (A) cryogenic TEM image (scale bar 90 nm); (B) Dry state TEM image; (C) AFM image.

with a dispersity value of 0.587 (Figure 2.6B, C). Interestingly, however P2 assembled into stable colloidal nanoparticles in the presence of stoichiometrically equivalent amount (based on charge) of poly(dially)dimethylammonium chloride (PDADMAC) (Figure 2.6A, B, C). By titrating the P2 solution with different equivalents of PDADMAC (based on charge), it was found that an

equivalent amount of PDADMAC was required for stable nanoparticle formation (Figure 2.7). In the presence of equivalent amount of PDADMAC, P2 self-assembled into nanoparticles of size ~250 nm with excellent correlation function and dispersity value of 0.206.

Particle morphology of (P2 + PDADMAC) nanoparticles was studied using cryogenic and dry state electron microscopy (TEM) as well as atomic force microscopy (AFM) which revealed a vesicle like morphology and spherical nature of the particles.

To further confirm if the self-assembled nanoparticles were vesicles, we tested their ability to encapsulate hydrophilic or water-soluble dyes. Vesicles have aqueous lumen which could be used to accommodate water-soluble dyes such as rhodamine 6G. Rhodamine 6G was encapsulated during the particle formulation followed by the removal of unencapsulated dye through dialysis. If rhodamine 6G dye molecules are encapsulated in the aqueous lumen, they show significantly less fluorescence because of self-quenching features at high local concentration (Figure 2.9A). However, same amount of free dye in water shows higher fluorescence. Indeed, the fluorescence of dye molecules was significantly less when they were encapsulated in the vesicles compared to the same concentration of dye in water (Figure 2.9B, C).

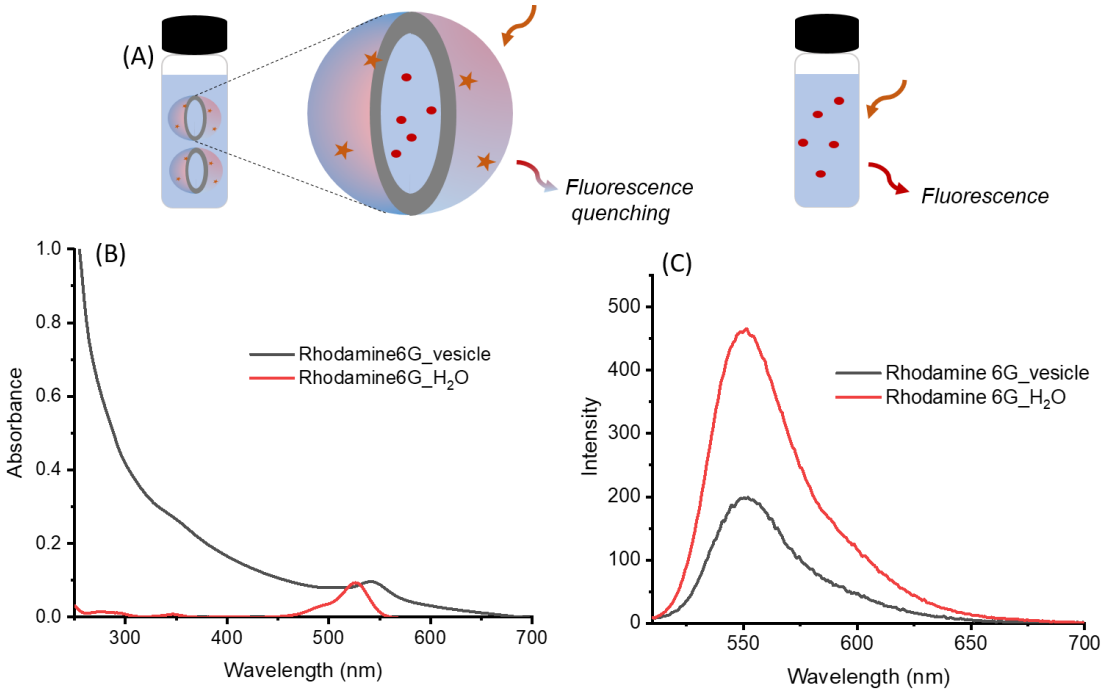

Figure 2.9: (A) Schematic showing self-quenching feature of rhodamine 6G molecules when encapsulated in vesicle compared with free molecules in water; (B) Absorption spectra of similar concentration of rhodamine 6G in vesicle vs in water; (C) Fluorescence spectra of rhodamine 6G in vesicle vs in water using an excitation wavelength of 510 nm.

2.2.4 Vesicle disassembly studies upon UV exposure

After confirming the vesicular morphology of nanoparticles using microscopy and dye encapsulation experiments, we subsequently investigated their disassembly upon UV exposure. We hypothesized that upon UV irradiating the solution containing vesicles with rhodamine 6G encapsulated inside, there should be an increase in their fluorescence. This is because after UV triggered disassembly, the dye molecules are released from aqueous lumen of vesicles to the aqueous bulk where they have significantly less local concentration. This should result in higher fluorescence of dye molecules after UV irradiation. We observed an increase in the fluorescence

of rhodamine 6G, where the increase is commensurate with that expected for free dye molecules in the aqueous phase (Figure 2.10).

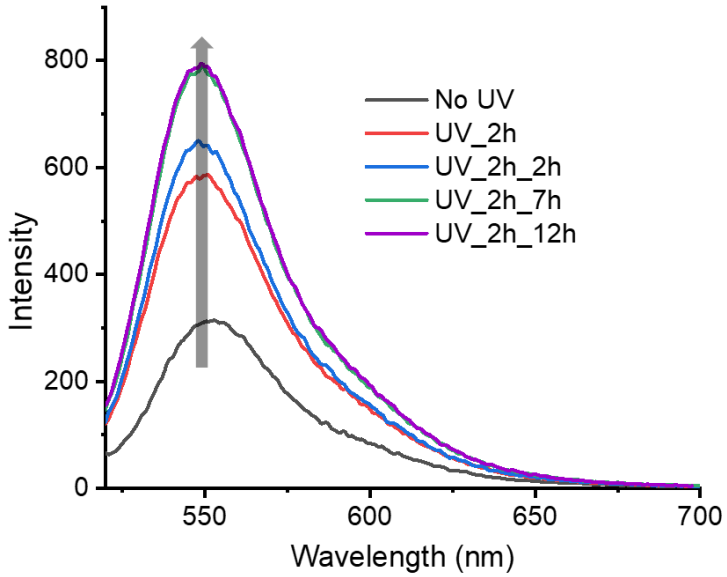

Figure 2.10: Emission profile of rhodamine 6G molecules encapsulated in vesicles after UV exposure for 2 h and subsequent time intervals.

Disassembly of vesicles was further studied using TEM and DLS. After triggering the vesicles with UV light, they lost their spherical nature and the resultant product morphology was ill defined (Figure 2.11).

In DLS, we observed a multimodal size distribution of the particles with poor correlation coefficient after UV treatment (Figure 2.12A, B). The control solution without UV treatment showed similar size distribution of the vesicles implying that the samples were stable in the absence of UV exposure. These experiments confirm that robust nanoassemblies do not exist in solution after UV exposure.

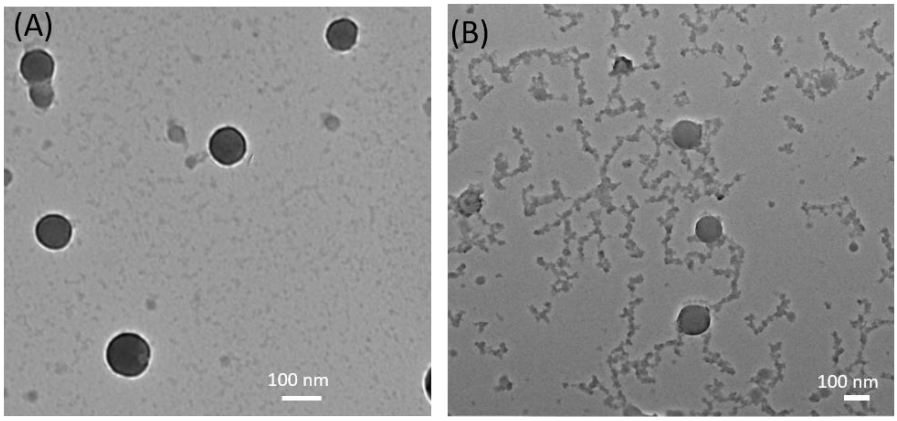

Figure 2.11: TEM images of vesicles (A) before UV exposure; (B) after UV exposure.

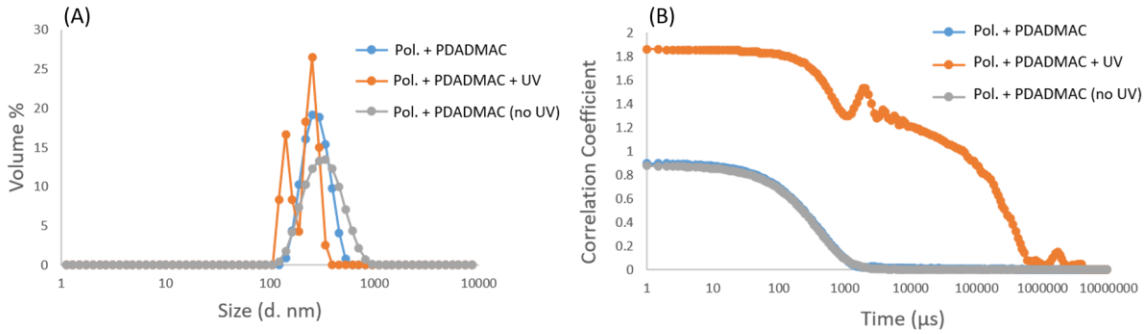

Figure 2.12: (A) DLS profile of assemblies before and after UV exposure; (B) Correlation coefficient of assemblies before and after UV exposure.

2.2.5 Approach for triggered gelation

Successful encapsulation and triggered release of rhodamine 6G from the assemblies laid the foundation for encapsulating a water-soluble catalyst in the aqueous lumen of vesicles. Enzymes are suitable candidates towards this objective because of their high solubility and turnover number under aqueous conditions. If encapsulated or compartmentalized inside, the barrier provided by vesicle boundary restricts their accessibility to substrate present in aqueous bulk. However, when triggered with UV light, the depolymerization induced disassembly can lead to the release of

enzymes to react with substrate. The idea of encapsulating an enzyme and releasing it in response to UV signal, offers an inherent signal amplification capacity, because a single enzyme molecule can react with multiple substrate species to bring about a desired response.

Towards this objective, in our initial attempts we tried to encapsulate enzymes such as alkaline phosphatase and chymotrypsin. These enzymes have been well known to cleave water soluble peptides for hydrogel formation.[19] However, we encountered the following issues during the studies:

1) When the particle formulation was done in the presence of enzyme, we observed aggregation. This was primarily because under the experimental conditions, both enzymes carry a net negative charge which led to charge mediated cross-linking of particles.
2) Substrate for these enzymes were relatively hydrophobic and they offered poor solubility under aqueous conditions which was well below their critical gelation concentration.

To circumvent these issues, we decided to use a charge neutral enzyme under experimental conditions of pH 9. Accordingly, we chose horseradish peroxidase (HRP) (pI ~ 9; MW 44 kDa) to encapsulate in the aqueous lumen of vesicles. In the presence of H_2O_2, HRP catalyzes the oxidation of tyrosine methyl ester into its radical form which can cross-link to form dimer or higher order polymeric products.[20–22]

We envisioned the possibility of HRP-catalyzed hydrogel formation through cross-linking 4-arm-polyethyleneglycol polymers, which has previously been shown to form hydrogels.[23] Thus, we modified commercially available 4-arm-PEG-succinimidyl carbonate with tyrosine methyl ester to obtain tyrosine containing branched substrate (P3) (Figure 2.13). It should be noted that by using

polyethyleneglycol polymers as substrate for HRP, the substrate aqueous solubility issue can also be addressed.

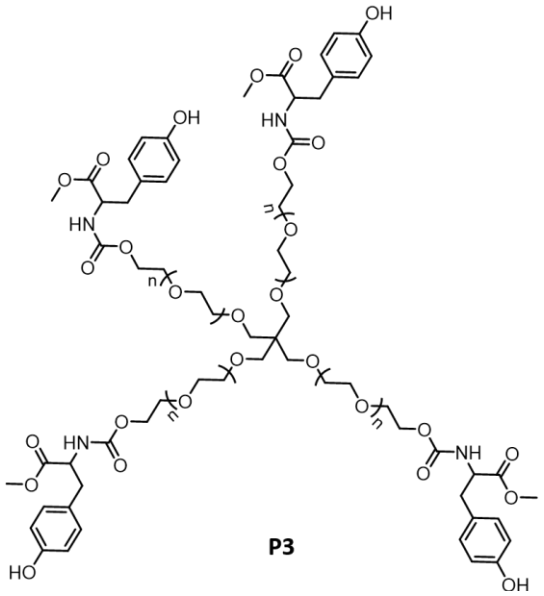

Figure 2.13: Structure of horseradish peroxidase substrate.

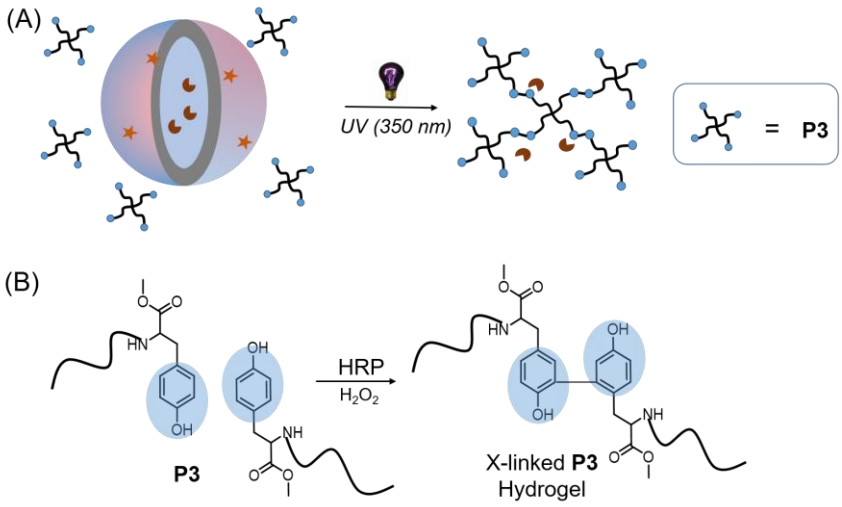

Figure 2.14: (A) Schematic of UV triggered vesicle disassembly to release HRP leading to hydrogel formation; (B) Schematic of HRP induced cross-linking in **P3**.

Using this approach, we envisioned the strategy to construct hydrogels from UV triggered release of enzymatic catalyst by destruction of nanoscopic vesicles (Figure 2.14).

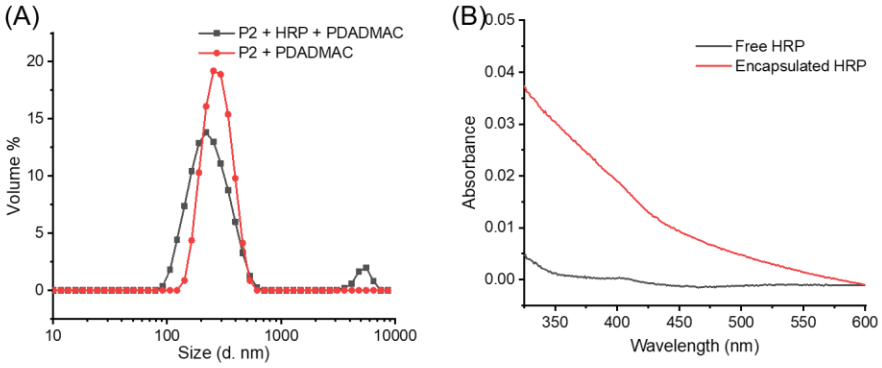

Figure 2.15: (A) DLS profile of **P2** + HRP + PDADMAC (black) and **P2** + PDADMAC (red); (B) UV-vis spectra of vesicles with HRP encapsulated (red) and filtrate after repeated washing (black).

Prior to testing this triggered gelation process, we characterized the encapsulation of enzyme inside the vesicles. HRP was incorporated during the polyelectrolyte complexation-based vesicle formation. As the presence of unencapsulated enzyme could prematurely cause gelation, the vesicular solution was washed multiple times using a centrifuge filter of 100 kDa MW cut off. DLS studies revealed that the enzyme-containing particles have approximately the same size distribution as empty particles (Figure 2.15A). The encapsulated HRP was characterized using UV-vis spectroscopy in which we observed the characteristics absorbance peak corresponding to the Soret band of porphyrin ring in HRP at 403 nm[24] (Figure 2.15B).

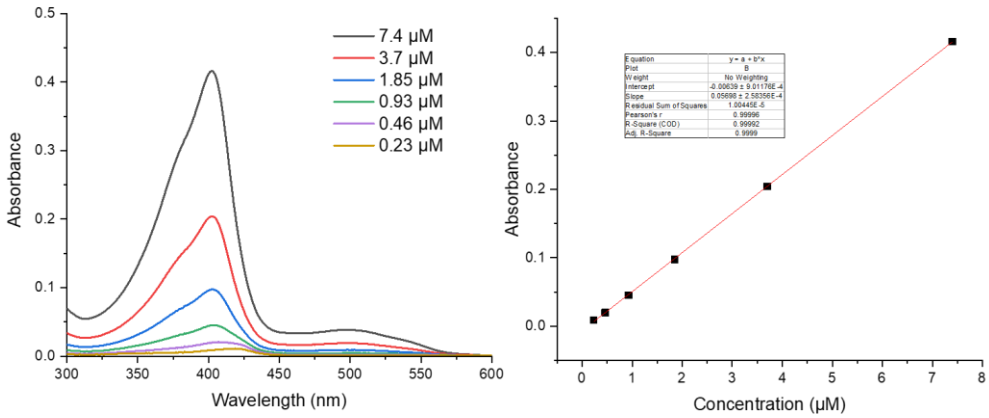

Figure 2.16: Calibration curve for HRP quantification using the Soret band of HRP at 403 nm.

The concentration of enzyme inside the vesicles was 4.2 μM which was determined using the calibration curve of the absorbance spectra of HRP (Figure 2.16).

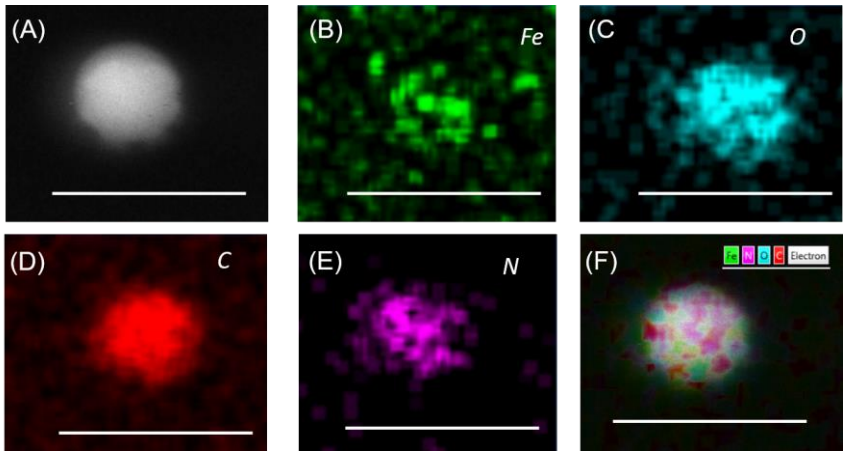

Figure 2.17: (A) Bright field electron microscopy image of **P2** + HRP + PDADMAC; Energy-dispersive X-ray spectroscopy (EDS) electron mapping profile of particle in (A) for different elements mentioned as (B) iron; (C) oxygen; (D) carbon; (E) nitrogen; (F) combined electron mapping of all elements. (Scale bar is 500 nm).

Since the shoulder from the Soret band was rather weak, we further confirmed its presence using

elemental mapping in energy-dispersive X-ray spectroscopy (EDS). HRP is a metalloenzyme containing an iron-based porphyrin cofactor. Indeed, EDS elemental mapping analysis of the nanoparticles clearly showed the presence of iron and thus the enzyme within the vesicles (Figure 2.17, Figure 2.18).

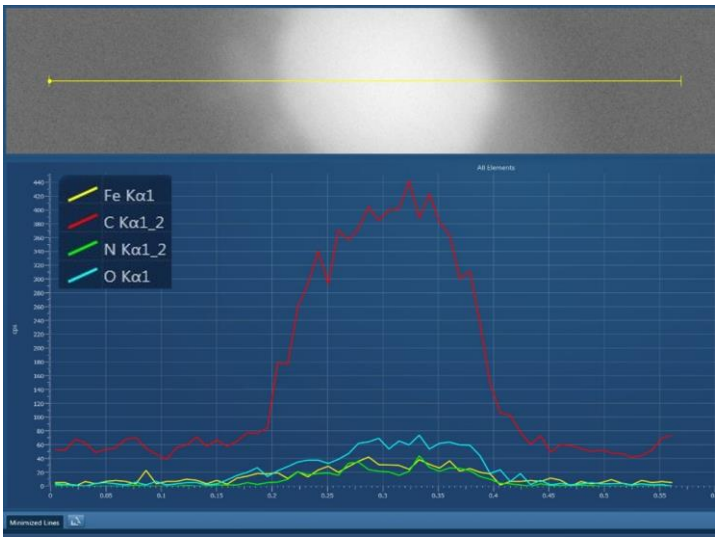

Figure 2.18: Relative elemental distribution of different elements in vesicle along the yellow line.

The possibility of light-triggered release of the enzyme and catalyzed amplification to form hydrogels was then investigated. The vesicles containing HRP were dispersed in a solution containing substrate P3 (5 wt. %). In the presence of H_2O_2, no gelation was observed, presumably due to the fact that that HRP is compartmentalized inside the vesicle. However, when irradiated with UV light for 45 minutes, gelation was observed in an hour as evidenced by the inverted vial test (Figure 2.19). This result suggests that HRP was released in the aqueous bulk after vesicle disassembly, then reacting with P3 to form cross-links.

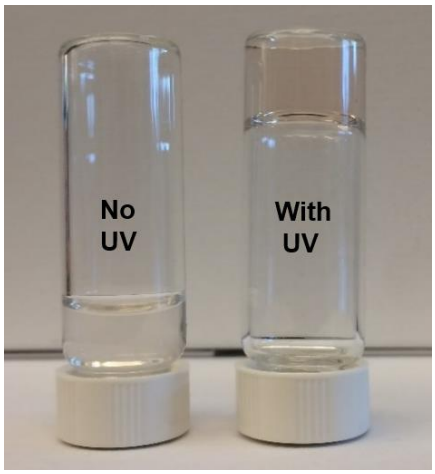

Figure 2.19: Inverted vial-test before and after applying UV trigger.

Next, we investigated the dependence of irradiation time on the extent of gel formation. The complete cleavage of light sensitive o-nitrobenzyl group took 2 h to cleave which makes depolymerization reaction the rate determining step in the process. However, by illuminating the enzyme containing assemblies for less than 2 h, UV irradiation time can dictate the extent of depolymerization. The UV irradiation time, therefore, can dictate the extent of enzyme release which should be reflected in the strength of hydrogels. To test this hypothesis, irradiation time was varied for 15, 30, 45, and 60 min. Oscillatory shear rheology was utilized to characterize the storage (G') and loss (G'') moduli of the hydrogels. Frequency sweeps show that G' is greater than G'' from 0.1 to 100 rad/s and is nearly independent of frequency, suggesting that the gels are elastic, cross-linked materials. The G' of hydrogels increased with irradiation time, demonstrating that the gels were stronger with more UV exposure (Figure 2.20). Interestingly, the G' value upon 60 min of UV exposure was lower than that for 45 min. ^{1}H NMR study of HRP mediated oxidation of tyrosine methyl ester revealed that when enzyme was pretreated with UV for 60 min, the amount of cross-linked product was significantly less compared to when enzyme was used without UV

pretreatment (Figure 2.21). This was reflected in the storage modulus of hydrogels. It should be noted that the loss modulus or G'' values represent the liquid like property of the material and should not represent the trend for hydrogel strength in a material.

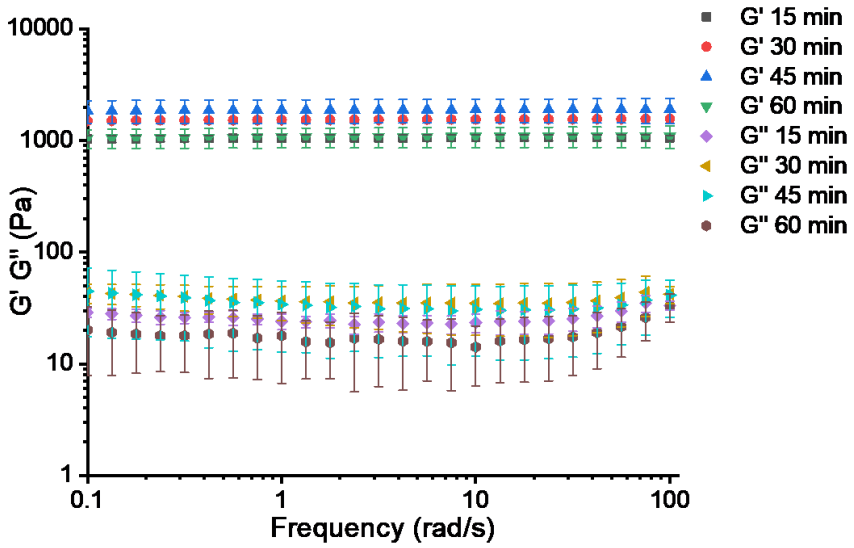

Figure 2.20: Storage (G') and loss (G'') modulus of hydrogels with 15, 30, 45 and 60 min of UV irradiation. Values represent the average of two samples with error bars.

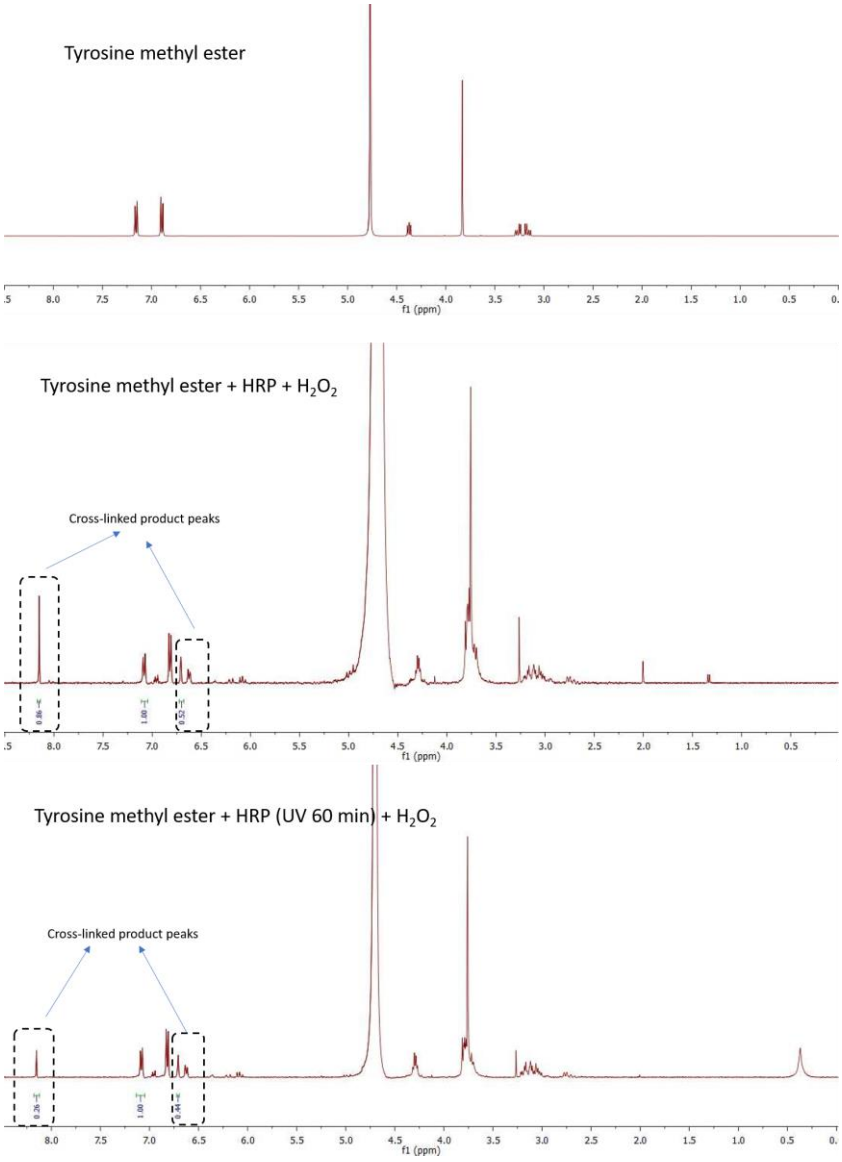

Figure 2.21: ^{1}H NMR spectrum depicting the cross-linking of tyrosine methyl ester after UV exposure for 60 min compared to without any UV treatment.

2.3 Conclusion

In this chapter, we utilize a depolymerization-based modulation of polyvalent interactions to disassemble a vesicle. The triggered disassembly of vesicles resulted in hydrogel formation due to enzymatic release. We show that anionic poly(benzylcarbamate) polymers can form vesicles on complexation with cationic PDADMAC. When the former polymer is triggered for depolymerization, the vesicle is destabilized, presumably due to the weaker interaction strength between the polyelectrolytes with decreasing polymer chain length. This process has been used to encapsulate an enzyme and then release it in the presence of the specific trigger. The catalytic nature of the enzyme amplifies the signal, as a single enzymatic molecule can cause multiple cross-linking reactions. The fact that the resultant product causes a phase change in the form of a self-supporting hydrogel, the amplification event is even macroscopically visualized. This work is a demonstration of a triggered "destruction" of a polymeric molecule to "construct" a different species. This construction from destruction principle has been previously explored in the context of mechanical disruption of microcapsules. Extending this idea to a molecularly addressable depolymerization process through polyvalency significantly expands its scope in many applications that require controlled or triggered release.

2.4 Experimental details

2.4.1 Materials

Ethyl 4-amino benzoate, sodium periodate, potassium iodide, diisobutylaluminium hydride (DIBALH), t-butyl acrylate, palladium acetate, tetrabutylammonium chloride, palladium on carbon (10 wt. %), phenylchloroformate, dibutyltin dilaurate (DBTL), 2-nitrobenzyl alcohol, polydiallyldimethylammonium chloride, 20 wt**.** % in water (PDADMAC), rhodamine 6g and

peroxidase from horseradish (Type VI-A, salt free, lyophilized powder, >= 250 units/mg solid) were purchased from Sigma Aldrich and were used as such unless mentioned otherwise. Sodium chloride, acetic acid, potassium carbonate and sodium bicarbonate were purchased from Fischer Scientific and used as such unless mentioned otherwise.

2.4.2 Instruments

- **Nuclear Magnetic Resonance (NMR)**

^{1}H NMR spectra were recorded using 400 MHz Bruker NMR spectrometer with residual proton for solvent as a standard. ^{13}C NMR spectra were recorded in 100 MHz Bruker NMR spectrometer using carbon signal of the deuterated solvent as a standard.

- **Dynamic Light Scattering (DLS)**

DLS was performed using Malvern nanozetasizer with a 637 nm laser source with noninvasive backscattering detected at 173°. Standard operating procedure was set up with the following parameters: sample equilibration for 1 min at 25 ^{o}C and then three measurements were taken while each measurement recorded 16 runs.

- **Transmission Electron Microscopy (TEM)**

The sample for DLS was drop casted on carbon coated copper grid and the sample was left for drying overnight. Subsequently, the imaging was done using JEOL-2000FX transmission electron microscope.

- **Cryogenic Transmission Electron Microscopy (cryo-TEM)**

Cryo-tem sample preparation was done using a fei vitrobot mkii plunge freezer at 4°C. The samples were cryo-transferred to a fei tecnai-t12 (120kV) and observed at-175°C under low-dose conditions.

- **Energy Dispersive X-ray Spectroscopy**

Eds was performed using a JEOL jem-2200fs eftem equipped with an oxford x-max 80mm^2 eds detector. Samples were prepared as for TEM above but only allowed to dry for 5 minutes prior to observation. The samples appeared sufficiently stable at room temperature to obtain eds spectra for the confirmation of iron content without obvious beam damage.

- **Atomic Force Microscopy (AFM)**

Samples were analyzed using a Veeco Bioscope AFM. AppNano ANSCM-PA probes were used for all measurements, which consist of an ~125 mm long Si cantilever that has been coated with PtIr resulting in tips with ~ 30nm radius and a resonant frequency of ca. 300 kHz. Measurements were performed with scans sizes of between 1.35 and 20 µm, at speeds between 1.0 and 1.5 Hz, and with either 256 x 256 or 512 x 512 pixel x lines of resolution. Analysis of topography images was performed in Gwyddion. Sample was cast on glass slide and dried overnight before analyzing.

- **UV-Vis Spectroscopy**

UV-Vis measurement of the samples was done using PerkinElmer Lambda 35 spectrometer.

- **Fluorescence Spectroscopy**

Fluorescence measurement of the samples was done using PerkinElmer LS 55 spectrometer. All the samples were excited at a wavelength of 510 nm.

- **Rheology**

An AR2000ex rheometer (TA Instruments) equipped with a stainless steel 20 mm crosshatch parallel plate was used to perform rheological measurements.

2.4.3 Synthetic details

- **Synthesis of 1**

This compound was synthesized according to a previously reported procedure.

Briefly, ethyl-4-aminobenzoate (10 g, 60.54 mmol), sodium periodate (12.94 g, 60.54 mmol), sodium chloride (7.08 g, 121.08 mmol) and potassium iodide (10.05 g, 60.54 mmol) were added in 500 mL round bottom flask and purged with argon for 10 minutes. Mixture of acetic acid (120 mL, 60.54 mmol) and water (13 mL) was added to the reaction mixture to dissolve all the starting materials and the solution was left for stirring overnight and monitored using TLC for completion. The reaction mixture was filtered and the filtrate was diluted with ethyl acetate. The solution was washed twice each time with brine solution, saturated solution of sodium thiosulfate and saturated solution of sodium bicarbonate respectively. Organic layer was collected and evaporated to obtain the crude product which was purified using column chromatography with pure product eluting at 30 % ethyl acetate in hexane mixture. (Yield 95 %).

^{1}H NMR (400 MHz, $CDCl_3$) δ= 8.38 (1H, s), 7.82-7.81 (1H, d), 6.71-6.79 (1H, d), 4.50 (2H, s), 4.34-4.29 (2H, q), 1.38-1.34 (3H, t).

- **Synthesis of 2**

This compound was synthesized according to a previously reported procedure.

Compound 1 (2.15 g, 7.41 mmol) was dissolved in 10 mL dry THF, cooled to 0 ^{0}C and purged with argon gas. DIBAL-H (3.96 mL, 22.23 mmol) was mixed with 5 mL THF and was added to the solution of compound 1 dropwise. The reaction was continued for an hour and was monitored for completion using TLC. To quench excess DIBAL-H, the reaction mixture was diluted with 20 mL methanol slowly followed by the addition of 20 mL THF and celite which led to the formation of suspension which was stirred for an hour. The solid was filtered and washed multiple times with THF to wash out the crude product as filtrate. The crude product was concentrated and purified using column chromatography with pure product eluting out at 30 % ethyl acetate in hexane mixture. (Yield 80 %).

^{1}H NMR (400 MHz, $CDCl_3$) δ= 7.66-7.65 (1H, d), 7.15-7.13 (1H, d), 6.74-6.72 (1H, d), 4.52(2H, d), 4.10 (2H, s).

- **Synthesis of 3**

This compound was synthesized according to a previously reported procedure.

Compound 2 (1.3 g, 5.22 mmol) was dissolved in 15 mL dry DMF and purged with argon. Subsequently Bu_4NBr (2.1 g, 6.53 mmol), $Pd(OAc)_2$ (59 mg, 0.26 mmol), *t*-butyl acrylate (1.13 mL, 7.83 mmol) and K_2CO_3 (3.6 g, 26.1 mmol) were added to the reaction mixture. The reaction was continued for 3 h at 65 ^{0}C and was monitored to completion using TLC. The reaction mixture was cooled, diluted with ethyl acetate and washed twice with brine and water each. The organic layer was concentrated to obtain crude product which was purified using column chromatography and the pure product eluted out at 35 % ethyl acetate in hexane mixture. (Yield 65 %).

^{1}H NMR (400 MHz, $CDCl_3$) δ= 7.70-7.67 (1H, d), 7.36 (1H, s), 7.17-7.15 (1H, d), 6.68-6.67 (1H, d), 6.31-6.28 (1H, d), 4.56-4.54 (2H, d), 3.95 (2H, s), 1.52 (9H, s).

- **Synthesis of 4**

Compound 3 (1.6 g, 6.42 mmol) was dissolved in 200 mL methanol in a hydrogenation flask. Palladium on carbon (0.16 g, 0.65 mmoles) was added to the solution of compound 3. The reaction mixture was introduced to the Parr hydrogenation set up where the flask was filled with hydrogen at a pressure of 40 psi. The reaction was continued for an hour after which the flask containing reaction mixture was removed and reaction was monitored using TLC for completion. The reaction mixture was filtered and the solvent from the resulting filtered solution was evaporated to yield yellowish oil like crude product. The crude product was purified using column chromatography with pure product eluting at 30 % ethyl acetate in hexane mixture. The pure product was characterized using ^{1}H NMR, ^{13}C NMR and ESI-MS. (Yield=1.5 g, quantitative).

^{1}H NMR (400 MHz, $CDCl_3$) δ= 7.05-7.03 (2H, m), 6.67-6.65 (1H, d), 4.54 (2H, s), 3.80 (3H, s), 2.81-2.77 (2H, t), 2.58-2.53 (2H, t), 1.44 (9H, s).

^{13}C NMR (100 MHz, $CDCl_3$) δ= 172.92, 144.02, 131.24, 128.90, 126.72, 125.24, 115.84, 80.68, 65.28, 34.86, 28.10, 26.24.

ESI-MS: $[M + Na]^{+}$= 274.13

- **Synthesis of 5**

Compound 4 (1.5 g, 5.95 mmol) was suspended in a 20 mL solution of THF: sat. $NaHCO_3$: H_2O (ratio of 2:2:1) in a round bottomed flask. Phenylchloroformate (0.85 mL, 6.55 mmol) was added dropwise to the suspension of 4 and the reaction mixture was stirred for 30 minutes while monitoring it using TLC for completion. The reaction mixture was diluted with ethyl acetate and was washed twice using saturated NH_4Cl. Solvent was evaporated to obtain crude product which

was purified using column chromatography. Pure product was eluted at 30 % ethyl acetate in hexane mixture and was characterized using ^{1}H NMR, ^{13}C NMR and ESI-MS. (Yield 90 %).

^{1}H NMR (400 MHz, $CDCl_3$) δ= 8.34 (1H, s), 7.80 (1H, s), 7.41-7.37 (2H, m), 7.24-7.20 (5H, m), 4.66-4.65 (2H, d), 2.94-2.91 (2H, t), 2.68-2.65 (2H, t), 1.42 (9H, s).

^{13}C NMR (100 MHz, $CDCl_3$) δ= 173.65, 152.75, 150.95, 134.90, 129.31, 128.55, 125.97, 125.44, 121.76, 81.53, 64.99, 36.32, 28.06, 25.47.

ESI-MS: $[M + Na]^{+}$= 394.15

- **Synthesis of polymer P1**

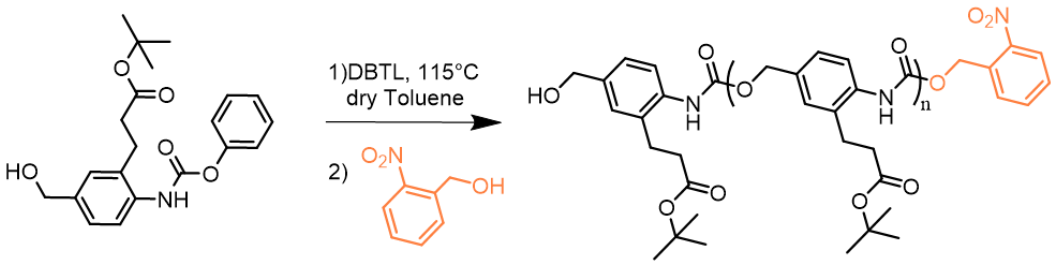

Monomer/Compound 5 (50 mg, 0.13 mmol) was dissolved in anhydrous toluene (0.15 mL) and to the mixture was added DBTL (8 µL, 0.013 mmol). The mixture was purged with argon for 5 minutes and subsequently transferred to an oil bath at 115 ^{o}C under argon atmosphere. The reaction mixture was stirred for 20 minutes after which 2- nitrobenzylalcohol (20 mg, 0.13 mmol) in a solution of anhydrous toluene (0.1 mL) was added dropwise. The reaction was stirred for 2 hours after which it was cooled to room temperature and purified by precipitation using cold diethyl ether. Brownish polymer powder was dried using high vacuum and characterized using ^{1}H NMR

and ^{13}C NMR. (Yield=30 mg). Note: *The average repeat units in the polymer varied between 8-10 in different trials.*

^{1}H NMR (400 MHz, $CDCl_3$) δ= 8.14-8.12, 7.84, 7.77, 7.30-7.28, 7.21, 5.65, 5.15, 4.63, 2.85-2.82, 2.61-2.58, 1.38.

^{13}C NMR (100 MHz, $CDCl_3$) δ= 173.32, 154.31, 135.74, 129.79, 127.27, 81.33, 70.58, 66.50, 36.09, 28.04, 25.47.

- **Synthesis of polymer P2**

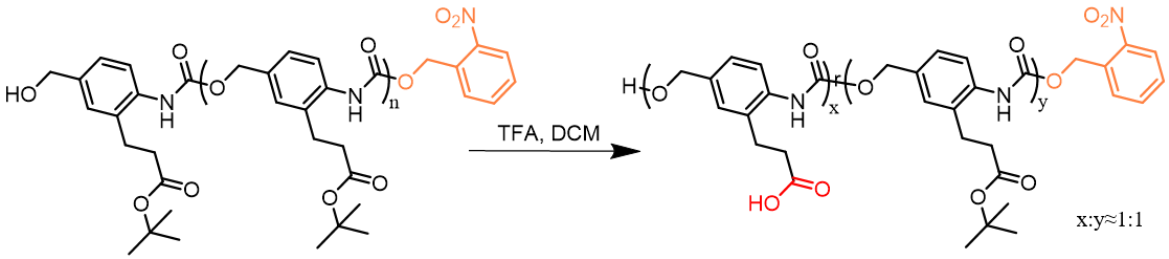

P2

Polymer P1 (30 mg) was dissolved in a mixture of trifluoroacetic acid (0.1 mL) and dichloromethane (0.4 mL) and was stirred for three minutes at room temperature. It was diluted using cold diethyl ether to obtain cloudy solution after which solvent and trifluoroacetic acid was evaporated using rotary evaporator. The solid was washed further with excess diethyl ether several times to obtain light brown polymer powder. The polymer was dried using high vacuum and characterized using ^{1}H NMR and ^{13}C NMR. (Yield=5 mg). *Note: This precursor polymer is very sensitive to trifluoroacetic acid and continuing the reaction even for a few extra minutes lead to polymer degradation.*

^{1}H NMR (400 MHz, MeOD) δ= 8.16-8.13, 7.77, 7.46, 7.28, 5.59, 5.16, 4.57, 2.91, 1.40.

^{13}C NMR (100 MHz, MeOD) δ= 173.04, 155.60, 135.35, 129.05, 126.18, 125.17, 115.11, 80.51, 66.02, 35.29, 30.12, 26.94, 25.97

- **Synthesis of P3**

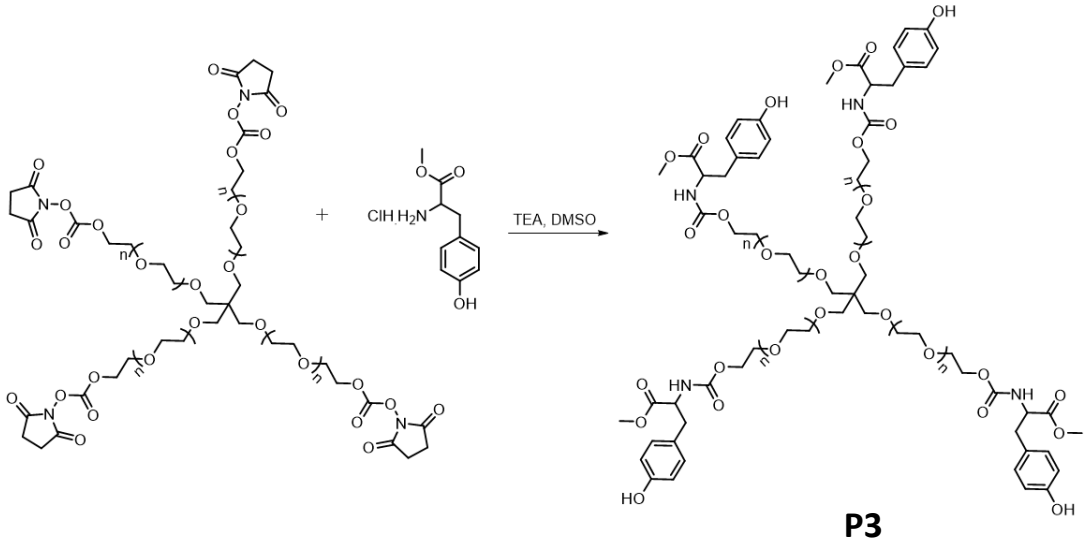

P3

4arm-poly(ethylene glycol)-succinimidyl carbonate (average MW 10000) (1 g, 0.09 mmol) was dissolved in 10 mL DMSO in a round bottomed flask. In a vial, L-tyrosine methyl ester hydrochloride (208 mg, 0.9 mmol) was dissolved in 3 mL DMSO and triethyl amine (124 µL, 0.9 mmol) was added which led to a dark brown solution. The mixture was added dropwise to the solution of 4arm-poly(ethylene glycol)-succinimidyl carbonate and the reaction was continued for 3 hours. Upon completion of reaction, the reaction mixture was dialyzed using dialysis membrane of 6000-8000 MW cut off against methanol: chloroform (70: 30) mixture for 24 hours (solvent was changed for 5 times during dialysis). The product was concentrated and characterized using ^{1}H NMR and ^{13}C NMR.

^{1}H NMR (400 MHz, $CDCl_3$) δ= 7.10 (1H, s), 6.95-6.93 (8H, d), 6.79-6.77 (8H, d), 5.23-5.21 (4H, d), 4.59-4.54 (4H, m), 4.28-4.09 (8H, m), 3.83-3.80 (8H, t), 3.74 (12H, t), 3.64-3.41 (1132H, m), 3.11-3.06 (4H, dd), 2.98-2.93 (4H, dd).

^{13}C NMR (100 MHz, $CDCl_3$) δ= 172.10, 155.87, 130.24, 115.70, 70.96, 70.56, 70.35, 70.03, 69.50, 64.39, 54.82, 52.29, 45.53, 37.18

2.4.4 Formulation of empty polymeric vesicles

P2 (1 mg) was suspended in 2 mL deionized water and to the suspension, a catalytic amount of triethyl amine was added to obtain a clear solution. In a different vial, a stock solution of Polydiallyldimethylammonium chloride, 20 wt**.** % in water (PDADMAC) was prepared by dissolving 20 µL of 20 wt. % PDADMAC in 5 mL water. 100 µL PDADMAC from the stock solution was added dropwise to the P2 solution under stirring conditions. The mixture was left for stirring for 2 hours after which the vesicles were characterized using DLS and TEM. All the steps were performed at 25 ^{o}C.

2.4.5 Formulation of polymeric vesicles with horseradish peroxidase encapsulation

P2 (1 mg) was suspended in 2 mL deionized water and to the suspension, a catalytic amount of triethyl amine was added to obtain a clear solution. 1 mg (HRP) was added to the polymer solution to obtain a clear solution. pH of the solution was adjusted to 9 by carefully adding small amount of HCl. 100 µL PDADMAC from the stock solution was added dropwise to the (P2 + HRP) solution under stirring conditions. The mixture was left for stirring for 6 hours after which the free enzyme was washed out using centrifuge filter (100 kD MW cut off) and volume of nanoparticle solution was maintained by adding deionized water. The samples were centrifuged for 2 minutes at 5000 rpm multiple times until no absorbance peak corresponding to HRP's characteristic Soret band was observed in the UV-Vis spectrum of the filtrate.

Vesicle solution with encapsulated HRP was diluted 10 times and its absorbance was measured using UV-Vis spectrum (by using empty nanoparticles as a blank) which indicated the characteristics Soret band of HRP. All the steps were performed at 25 ^{o}C.

2.4.6 Gelation experiments

5 wt. % concentration of substrate was prepared in 1 mL water. To the substrate solution, 1 mL of nanoparticle solution with loaded enzyme was added and mixed gently. The mixture was irradiated with UV light for required durations in a UV chamber (350 nm, 2.2 mW/cm^2). After irradiation, sample was taken out and stoichiometric amount of H_2O_2 relative to P3 was added. In the control experiment, similar procedure was followed except the UV irradiation step. All the steps were performed at 25 ^{o}C.

2.4.7 Rheology experiments

Hydrogels were loaded on the rheometer using a spatula. The upper geometry was lowered to a gap of ~1000 microns, based on the height of the gel, and a solvent trap filled with water was utilized to limit the solvent evaporation. All measurements were then performed at 25 °C using a normal force control of 1.50 ± 0.1 N (the normal force includes forces resulting from the solvent trap and the geometry compressing the sample). Each sample was pre-sheared using a stress of 0.06366 Pa for 30 s and then equilibrated for 5 min before performing a frequency sweep experiment. Frequency sweep experiments were performed from 100–0.1 rad/s using a 10% strain.

2.5 References

(1) Ahmad, H.; Sehgal, S.; Mishra, A.; Gupta, R. Mimosa Pudica L. (Laajvanti): An Overview. *Pharm. Rev.* **2012**, *6* (12), 115–124.

(2) Volkov, A. G.; Adesina, T.; Markin, V. S.; Jovanov, E. Kinetics and Mechanism of Dionaea Muscipula Trap Closing. *Plant Physiol.* **2008**, *146* (2), 694–702.

(3) Fudge, D. S.; Levy, N.; Chiu, S.; Gosline, J. M. Composition, Morphology and Mechanics of Hagfish Slime. *J. Exp. Biol.* **2005**, *208* (24), 4613–4625.

(4) Downing, S. W.; Spitzer, R. H.; Koch, E. A.; Salo, W. L. The Hagfish Slime Gland Thread Cell. I. A Unique Cellular System for the Study of Intermediate Filaments and Intermediate Filament-Microtubule Interactions. *J. Cell Biol.* **1984**, *98* (2), 653–669.

(5) Koch, E. A.; Spitzer, R. H.; Pithawalla, R. B.; Parry, D. A. An Unusual Intermediate Filament Subunit from the Cytoskeletal Biopolymer Released Extracellularly into Seawater by the Primitive Hagfish (Eptatretus Stouti). *J. Cell Sci.* **1994**, *107* (11), 3133-3144.

(6) Peterson, G. I.; Larsen, M. B.; Boydston, A. J. Controlled Depolymerization: Stimuli-Responsive Self-Immolative Polymers. *Macromolecules* **2012**, *45* (18), 7317–7328.

(7) Kim, H.; Mohapatra, H.; Phillips, S. T. Rapid, On-Command Debonding of Stimuli-Responsive Cross-Linked Adhesives by Continuous, Sequential Quinone Methide Elimination Reactions. *Angew. Chemi. Int. Ed.* **2015**, *127* (44), 13255–13259.

(8) Seo, W.; Phillips, S. T. Patterned Plastics That Change Physical Structure in Response to Applied Chemical Signals. *J. Am. Chem. Soc.* **2010**, *132* (27), 9234–9235.

(9) Roth, M. E.; Green, O.; Gnaim, S.; Shabat, D. Dendritic, Oligomeric, and Polymeric Self-Immolative Molecular Amplification. *Chem. Rev.* **2016**, *116* (3), 1309–1352.

(10) Gnaim, S.; Shabat, D. Self-Immolative Chemiluminescence Polymers: Innate Assimilation of Chemiexcitation in a Domino-like Depolymerization. *J. Am. Chem. Soc.* **2017**, *139* (29), 10002–10008.

(11) Alouane, A.; Labruère, R.; Le Saux, T.; Schmidt, F.; Jullien, L. Self-Immolative Spacers: Kinetic Aspects, Structure-Property Relationships, and Applications. *Angew. Chem. Int. Ed.* **2015**, *54* (26), 7492–7509.

(12) Sui, Z.; Jaber, J. A.; Schlenoff, J. B. Polyelectrolyte Complexes with PH-Tunable Solubility. *Macromolecules* **2006**, *39* (23), 8145–8152.

(13) Kishimura, A. Development of Polyion Complex Vesicles (PICsomes) from Block Copolymers for Biomedical Applications. *Polymer Journal* **2013**, *45* (9), 892–897.

(14) Wang, Q.; Schlenoff, J. B. The Polyelectrolyte Complex/Coacervate Continuum. *Macromolecules* **2014**, *47* (9), 3108–3116.

(15) Kogej, K.; Theunissen, E.; Reynaers, H. Effect of Polyion Charge Density on the Morphology of Nanostructures in Polyelectrolyte−Surfactant Complexes. *Langmuir* **2002**, *18* (23), 8799–8805.

(16) Sagi, A.; Weinstain, R.; Karton, N.; Shabat, D. Self-Immolative Polymers. *J. Am. Chem. Soc.* **2008**, *130* (16), 5434–5435.

(17) Zhao, H.; Sterner, E. S.; Coughlin, E. B.; Theato, P. O-Nitrobenzyl Alcohol Derivatives: Opportunities in Polymer and Materials Science. *Macromolecules* **2012**, *45* (4), 1723–

1736.

(18) Patchornik, A.; Amit, B.; Woodward, R. B. Photosensitive Protecting Groups. *J. Am. Chem. Soc.* **1970**, *92* (21), 6333–6335.

(19) Yang, Z.; Gu, H.; Fu, D.; Gao, P.; Lam, J. K.; Xu, B. Enzymatic Formation of Supramolecular Hydrogels. *Adv. Mater.* **2004**, *16* (16), 1440–1444.

(20) Michon, T.; Chenu, M.; Kellershon, N.; Desmadril, M.; Guéguen, J. Horseradish Peroxidase Oxidation of Tyrosine-Containing Peptides and Their Subsequent Polymerization: A Kinetic Study. *Biochemistry* **1997**, *36* (28), 8504–8513.

(21) Sisco Bayse, G.; Michaels, A. W.; Morrison, M. The Peroxidase-Catalyzed Oxidation of Tyrosine. *BBA - Enzymol.* **1972**, *284* (1), 34–42.

(22) Lopes, G. R.; Pinto, D. C. G. A.; Silva, A. M. S. Horseradish Peroxidase (HRP) as a Tool in Green Chemistry. *RSC Adv.* **2014**, *4* (70), 37244–37265.

(23) Zustiak, S. P.; Leach, J. B. Characterization of Protein Release from Hydrolytically Degradable Poly(Ethylene Glycol) Hydrogels. *Biotechnol. Bioeng.* **2011**, *108* (1), 197–206.

(24) Spulber, M.; Najer, A.; Winkelbach, K.; Glaied, O.; Waser, M.; Pieles, U.; Meier, W.; Bruns, N. Photoreaction of a Hydroxyalkyphenone with the Membrane of Polymersomes: A Versatile Method to Generate Semipermeable Nanoreactors. *J. Am. Chem. Soc.* **2013**, *135* (24), 9204–9212.

CHAPTER 3

ENZYME TRIGGERED DEGRADATION OF POLYMERIC NANOASSEMBLIES

3.1 Introduction

Enzymes play a fundamental role in key biological processes and their malfunction is implied in a variety of pathological conditions.[1–3] Development of nanomaterials that can respond to enzymes and bring a desired outcome are being increasingly pursued in applications such as therapeutic delivery, diagnostics and sensing.[4–8] For example, numerous nanostructures derived from polymers and dendrimers have been shown to undergo degradation and release encapsulated cargo in response to specific enzymes.[9–15] This is attributed to the substrate specific and catalytic action of enzymes under mild aqueous conditions. However, a major limitation associated to these systems is their slow response upon enzymatic treatment, compared to small molecule substrate counterpart in water. This is primarily because the substrate for enzymes are buried in hydrophobic core of self-assembled structures, rendering poor accessibility for enzymes.[16–19]

To achieve an amplified output in response to a stimulus, depolymerizable systems are increasingly being pursued in several applications.[20–23] A single cleavage or deprotection event at the polymer chain terminus driven by suitable stimulus leads to the degradation of polymer chain from head to tail. This property makes depolymerizable systems sensitive to trace amount of input signal.[24,25] Utilizing enzyme as an input signal to trigger the degradation of nanoassemblies formulated using depolymerizable polymers is a promising yet relatively less explored approach to address the slow kinetics of enzyme triggerable materials. For a rapid enzyme triggered

response, one of the key requirements is that the substrate should be exposed on the surface of nanoparticles.

In this chapter, we envisioned to synthesize alkaline phosphatase (ALP) triggerable poly(benzylcarbamate), P0 and its hydrophilic (P1) and hydrophobic (P2) analogues which can undergo triggered depolymerization upon enzymatic cleavage of phosphate groups (Figure 3.1A). Due to the hydrophilic nature of phosphate group, we hypothesized that nanoparticles formulated using P1 and P2 can display phosphate groups on their surface, providing easier accessibility to enzyme. The surface enzymatic cleavage event can be propagated in the nanoparticle interior through depolymerization, leading to particle disassembly and subsequent guest release (Figure 3.1B).

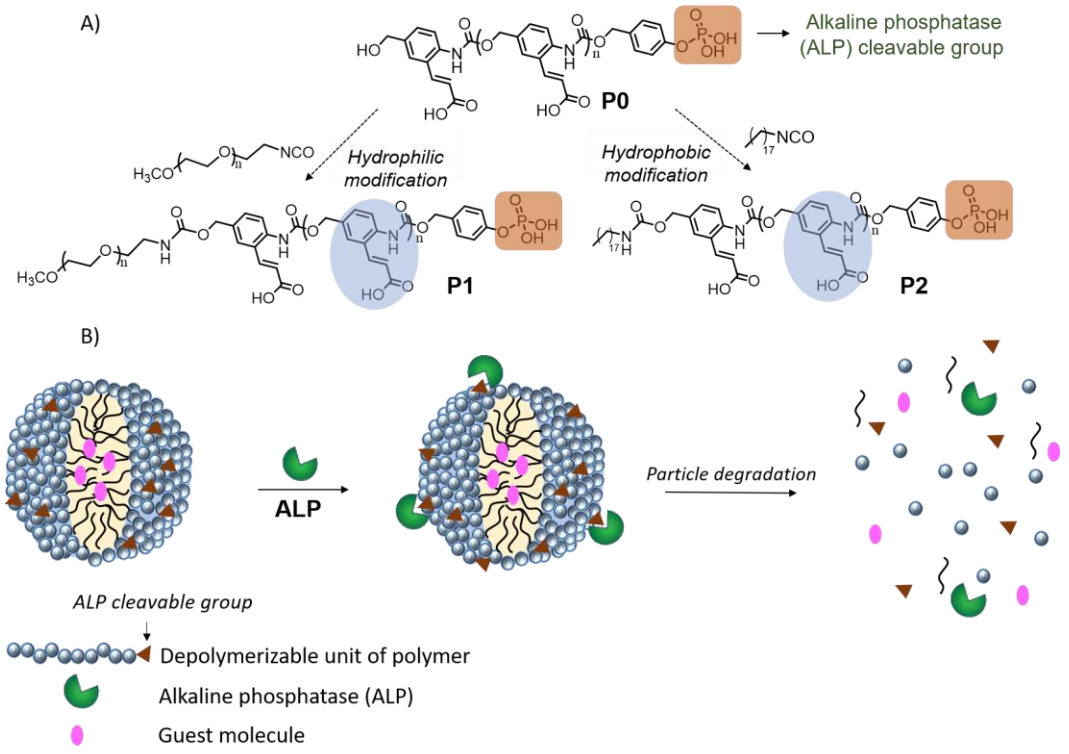

Figure 3.1: (A) Structure of ALP triggerable polymer, **P0**; its hydrophilic and hydrophobic modification into **P1** and **P2**; (B) Proposed schematic of particle formulation using **P1** and **P2** and its triggered degradation in response to ALP.

3.2 Results and Discussion

3.2.1 Molecular Design and Synthetic Scheme

Synthetic scheme of monomer used is shown in Figure 3.2. ALP triggerable polymer was synthesized using step growth polymerization discussed in chapter 2. Briefly, the polymer chain was capped using a derivative of benzyl ether protected phosphonate trigger. Deprotection of benzyl ether group from the cap and t-butyl ester groups from the side chain was carried out to synthesize P0 (Figure 3.3).

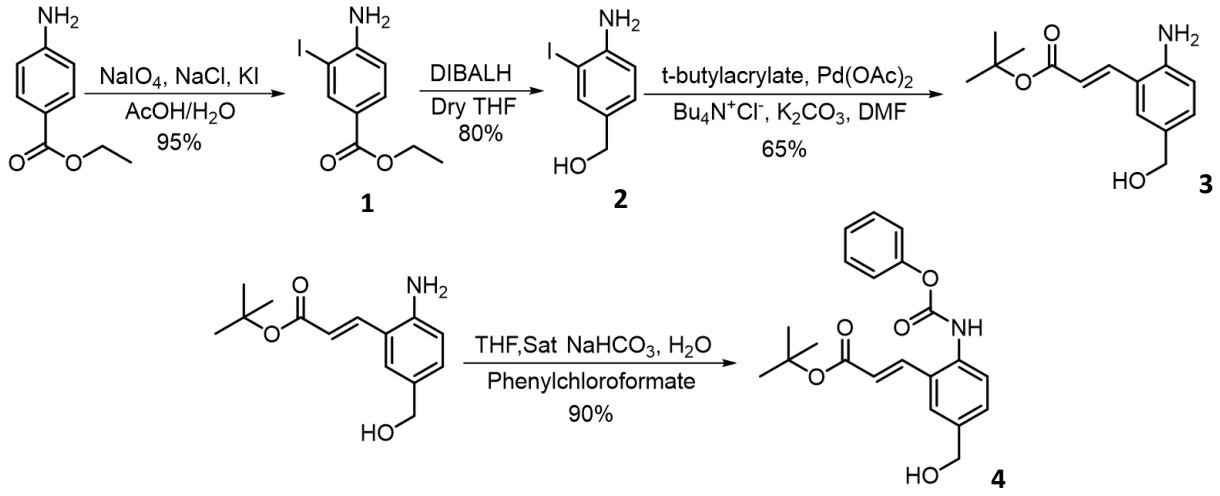

Figure 3.2: Monomer synthesis scheme.

For the synthesis of hydrophilic polymer P1, P0 was modified with polyethylene glycol isocyanate. Subsequently, the deprotection of benzyl ether groups from the cap and t-butyl ester groups from the side chain was carried out to achieve P1. The synthesis of hydrophobic polymer P2 was carried out by modifying P0 with octadecyl isocyanate and subsequent de-protection of benzyl ether and t-butyl groups (Figure 3.4).

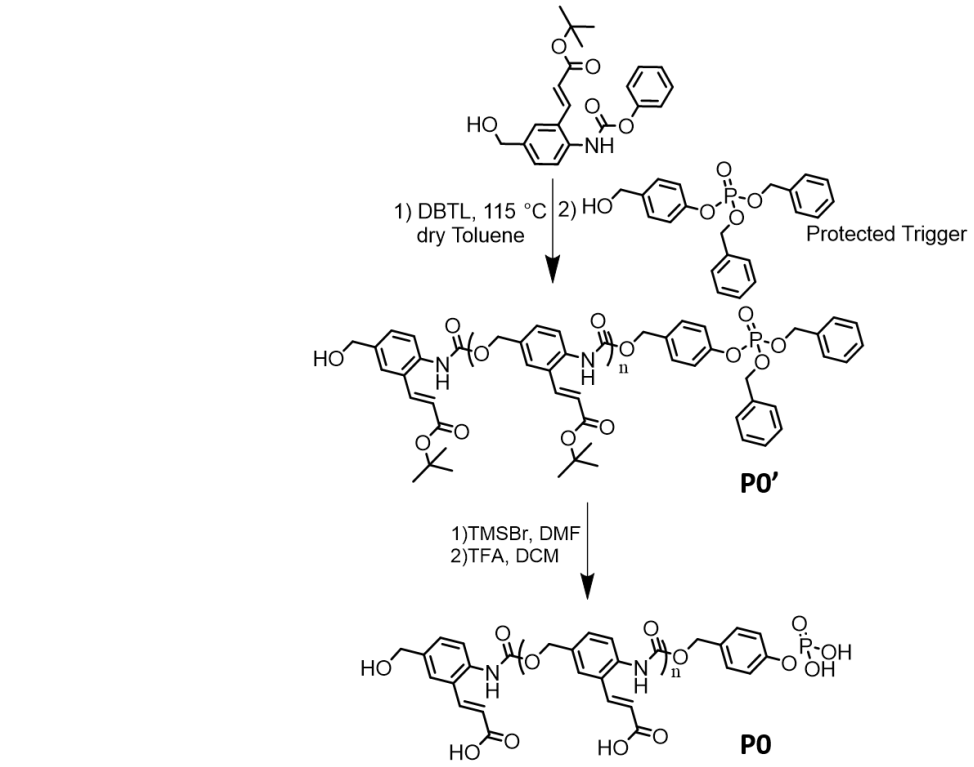

Figure 3.3: Synthetic scheme for **P0.**

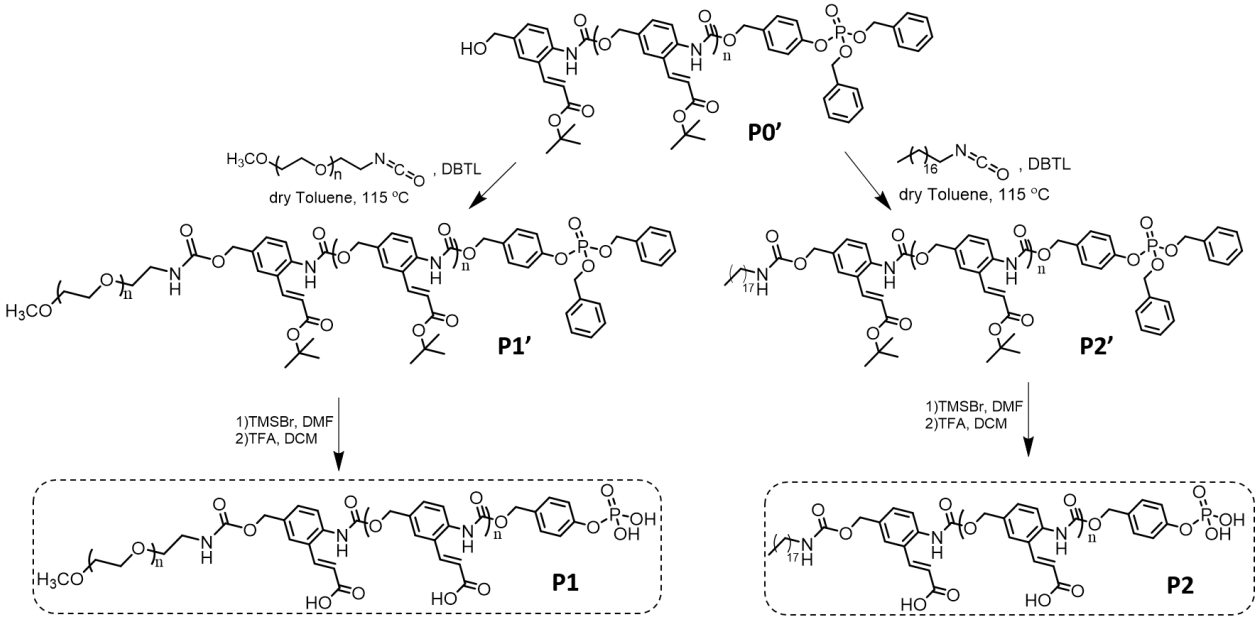

Figure 3.4: Synthetic scheme for **P1** and **P2.**

3.2.2 Depolymerization studies of P0

Depolymerization of P0 is a multi-step process, similar to the light triggered degradation of polymer discussed in chapter 2. In presence of ALP, phosphate group at the polymer chain terminus is cleaved which leads to the formation of reactive intermediate that undergoes sequential elimination to form small molecule reporter, R1 (Figure 3.5).

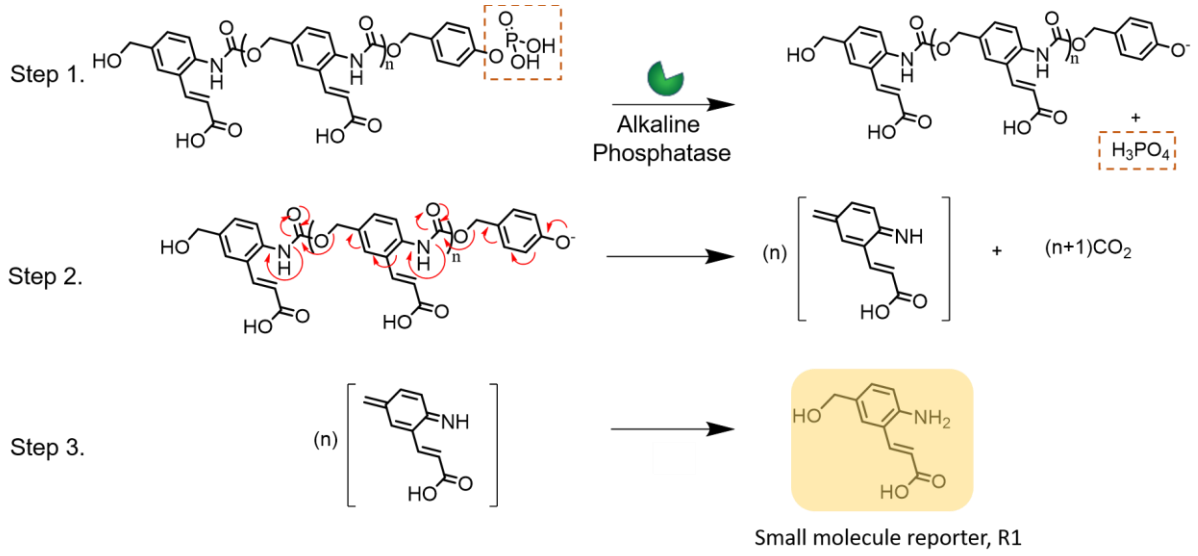

Figure 3.5: Mechanism of degradation of **P0** in presence of ALP.

Depolymerization study of P0 in the presence of ALP was studied in 250 mM bicarbonate buffer using ^{31}P NMR spectroscopy. Before cleavage, the phosphate group at the chain terminus of P0 showed characteristics NMR peak at 0 ppm. However, in the presence of ALP, we observed the disappearance of peak at 0 ppm and appearance of a new peak at 2.5 ppm, characteristics of phosphoric acid which is formed after enzymatic cleavage (Figure 3.6). The cleavage of phosphate group took less than 10 min for completion.

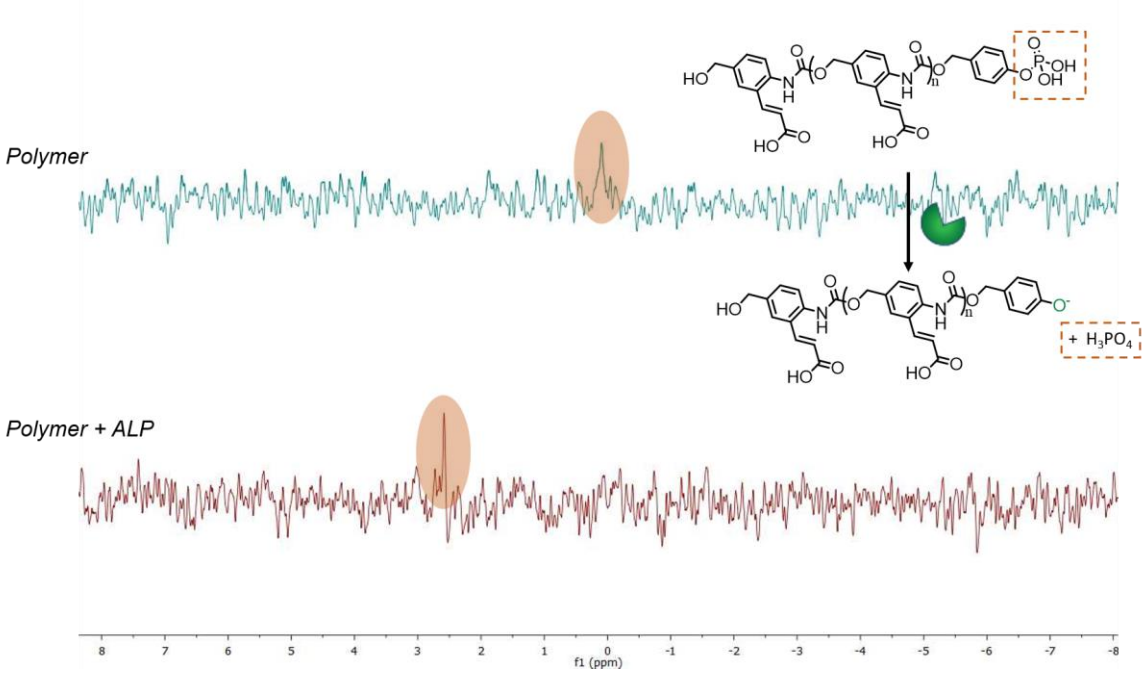

Figure 3.6: ^{31}P NMR of **P0** solution before enzyme incubation (top spectrum) and after enzyme incubation (bottom spectrum).

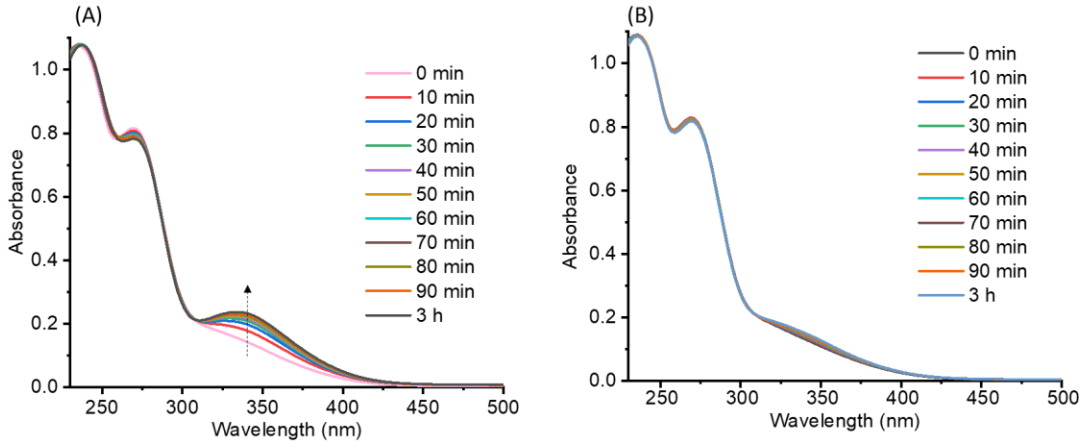

Figure 3.7: UV-Vis spectrum of **P0** solution (A) with ALP; (B) without ALP.

The resultant solution was further studied using UV-vis spectroscopy, where a temporal increase in the absorbance at 348 nm was observed after incubating the polymer solution with ALP (Figure 3.7A). However, in the control solution without enzyme, no such peak was observed (Figure 3.7B).

As another control experiment, the polymer solution was incubated with non-specific enzyme esterase and no change in the absorbance spectrum of the polymer was observed (Figure 3.8A). ALP also did not show any inherent absorbance under the working conditions (Figure 3.8B).

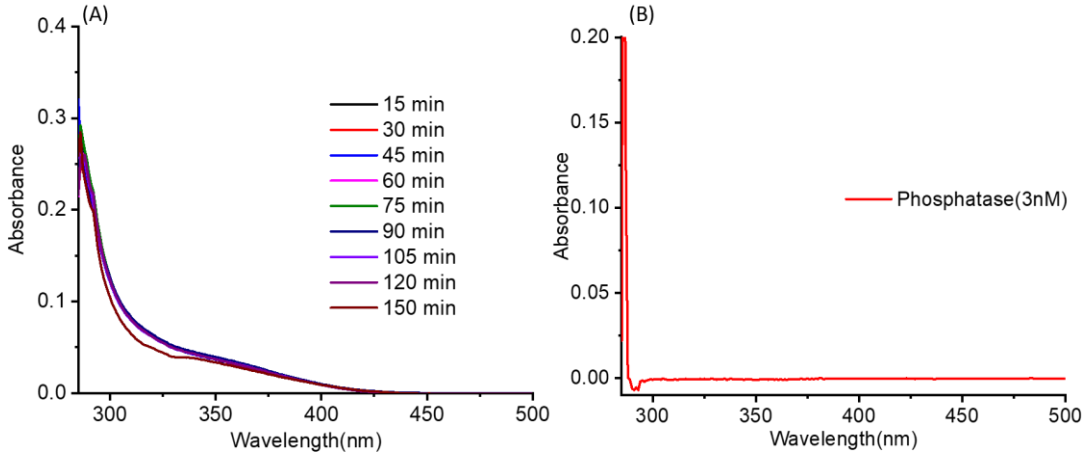

Figure 3.8: UV-Vis spectrum of (A) **P0** solution in the presence of esterase; (B) ALP solution.

We hypothesized that the increase in peak at 348 nm was due to the formation of small molecule reporter, R1 upon triggering the polymer with ALP.

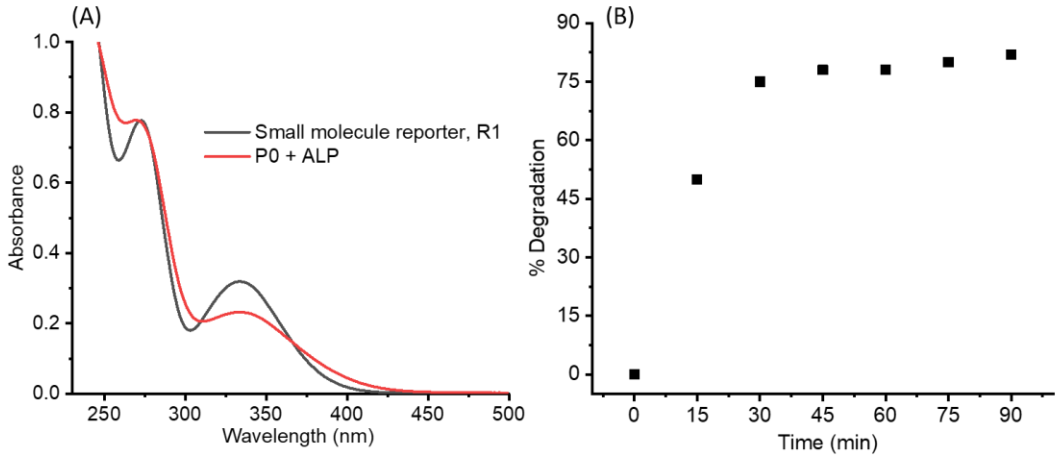

Figure 3.9: (A) Comparison between UV-Vis spectrum of **P0** incubated with ALP and small molecule reporter, R1; (B) % degradation of **P0** upon incubating with ALP.

To test this hypothesis, R1 was synthesized and its absorbance was compared with the polymer solution incubated with ALP. The signature absorbance for both solutions were similar, confirming that the absorbance peak at 348 nm was indeed due to the formation of small molecule reporter, R1 (Figure 3.9A). Using a calibration curve of R1, it was found that around 75% polymer degraded within an hour (Figure 3.9B).

3.2.3 Hydrophilic modification of P0 to P1 and poly-ion complex formation

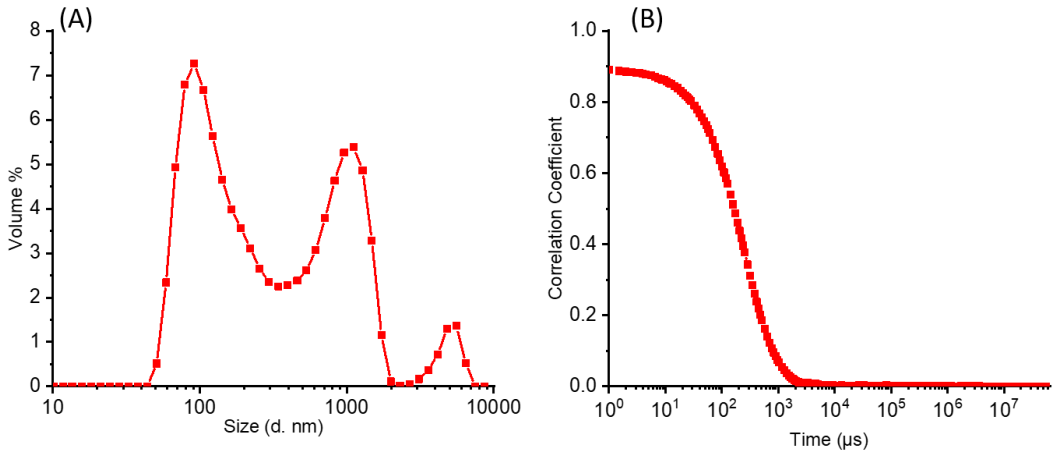

Figure 3.10: (A) DLS size distribution of **P1** + PDADMAC complex; (B) Correlation function of **P1** + PDADMAC complex.

The self-assembly behaviour of P0 was studied to test if the enzyme triggered molecular-scale depolymerization behaviour can be translated to nanomaterials with similar kinetics. P0 offered poor solubility under aqueous conditions. Therefore, hydrophilic modification of P0 was carried out by carbamate bond formation using terminal alcohol group of P0 and poly (ethylene glycol) isocyanate to synthesize water soluble polymer, P1. Carboxylic acid functionalities from the side chain of P1 were used to form polyelectrolyte complex with charge stoichiometric amount of positively charged poly (diallyldimethylammonium chloride) (PDADMAC).

Average size of the polyelectrolyte complex particles was found to be ≈183 nm with a trimodal size distribution and excellent correlation coefficient in dynamic light scattering (DLS) (Figure 3.10). Particle morphology was studied using transmission electron microscopy (TEM) which revealed spherical micelle like morphology (Figure 3.11). The particles were also used to non-covalently encapsulate hydrophobic guest or molecular probes such as DiI dye.

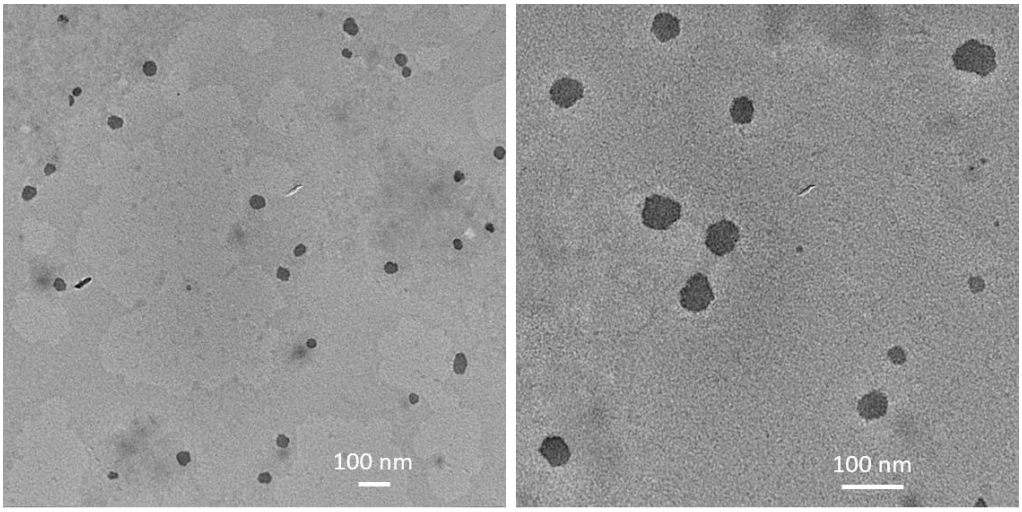

Figure 3.11: TEM images of **P1** + PDADMAC complex nanoparticles.

3.2.4 Degradation studies of P1 + PDADMAC poly-ion complex

After the formulation of poly-ion complex, effect of ALP on complex nanoparticles was studied. UV-Vis study of particles revealed the formation of small molecule reporter, R1 but the kinetics of particle degradation was significantly slower compared to the degradation of P0 in solution (Figure 3.12A, B). If compared, degradation of P0 reached saturation within 60 min but the degradation of complex took 24 hours. Significantly less release of encapsulated guest molecules was also observed (Figure 3.12A). Based on slow degradation kinetics issue observed in previous literature reports,[26] we hypothesized that

the slow degradation kinetics of complex was due to phosphate group being buried in the hydrophobic core of the polyelectrolyte complex, providing limited accessibility to ALP. This was because phosphate groups can also be involved in electrostatic complexation along with the carboxylate side chains to form the core of polyelectrolyte complex with PDADMAC.

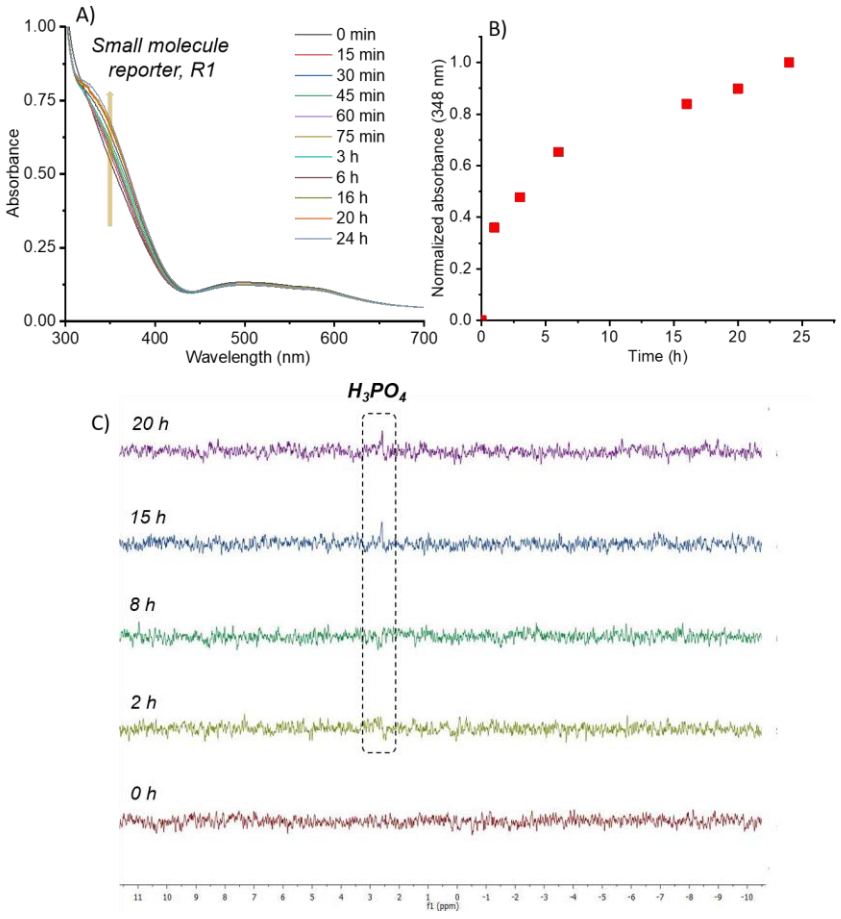

Figure 3.12: (A) UV-vis spectrum of **P1** + PDADMAC complex after treatment with ALP; (B) Kinetics of absorbance evolution at 348 nm; (C) ^{31}P NMR spectrum of complex before and after treatment with ALP.

To test this hypothesis, time dependent ^{31}P NMR study of the complex was carried out. NMR peak corresponding to the phosphate group was not observed to begin with. However, after incubating the complex particles with ALP, gradual formation of phosphoric acid was

observed (Figure 3.12C). Cleavage of phosphate groups from the complex took 20 h for completion. This led us to believe that the phosphate groups were less available for cleavage in the complex particles due to their involvement in electrostatic complexation with PDADMAC. Therefore, significantly slow degradation of the complex particles was observed.

3.2.5 Hydrophobic modification of P0 to P2 and nanoparticle formulation using P2

Our initial design principle required unhindered enzyme mediated cleavage of substrate for a rapid and amplified degradation response of particles due to depolymerization. Therefore, we targeted nanoparticle formulation approach which doesn't involve electrostatic complexation. Due to the limited aqueous solubility and lack of amphiphilicity of P0, hydrophobic modification of P0 into P2 using octadecyl isocyanate was carried out. P2 offered reasonable solubility in volatile organic solvents such as chloroform.

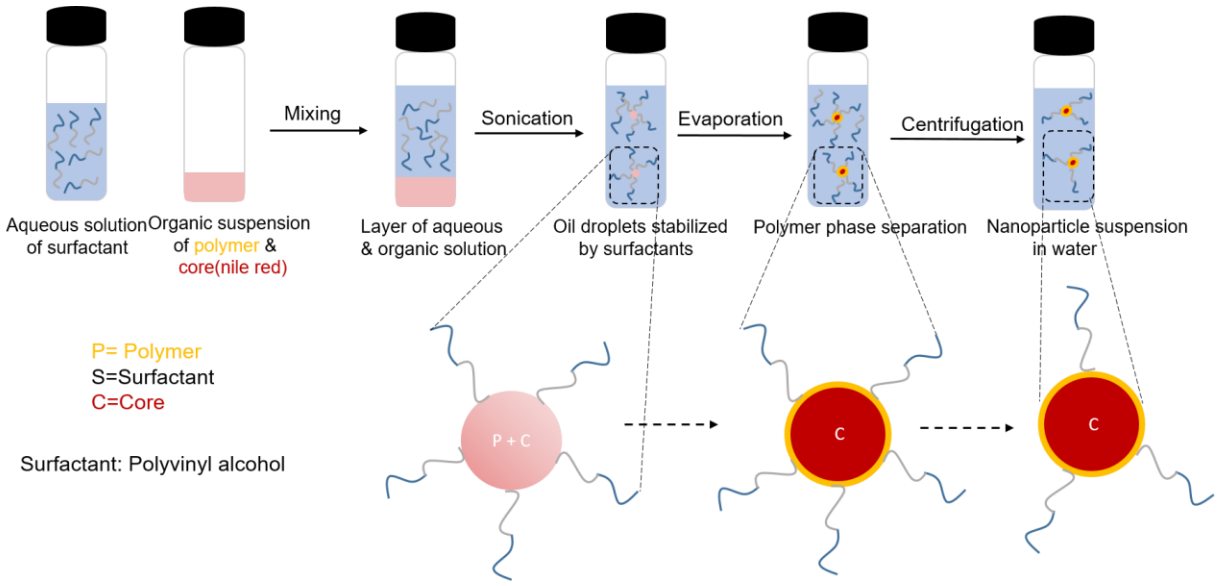

Figure 3.13: Workflow of nanoparticle formulation.

Hence, an oil in water emulsion methodology was used for nanoparticle formulation (Figure 3.13). Briefly, suspension of P2 and hydrophobic guest, nile red in chloroform (oil phase) was prepared and added to an aqueous solution of polyvinyl alcohol surfactant (water phase). Introduction of mechanical force using sonication, led to the formation of oil droplets containing polymer and guest molecules, stabilized by polyvinyl alcohol at the interface. Evaporation of organic solvent and subsequent washing of excess surfactant molecules led to the formation of P2 based nanoparticles with nile red molecules encapsulated in their interior.

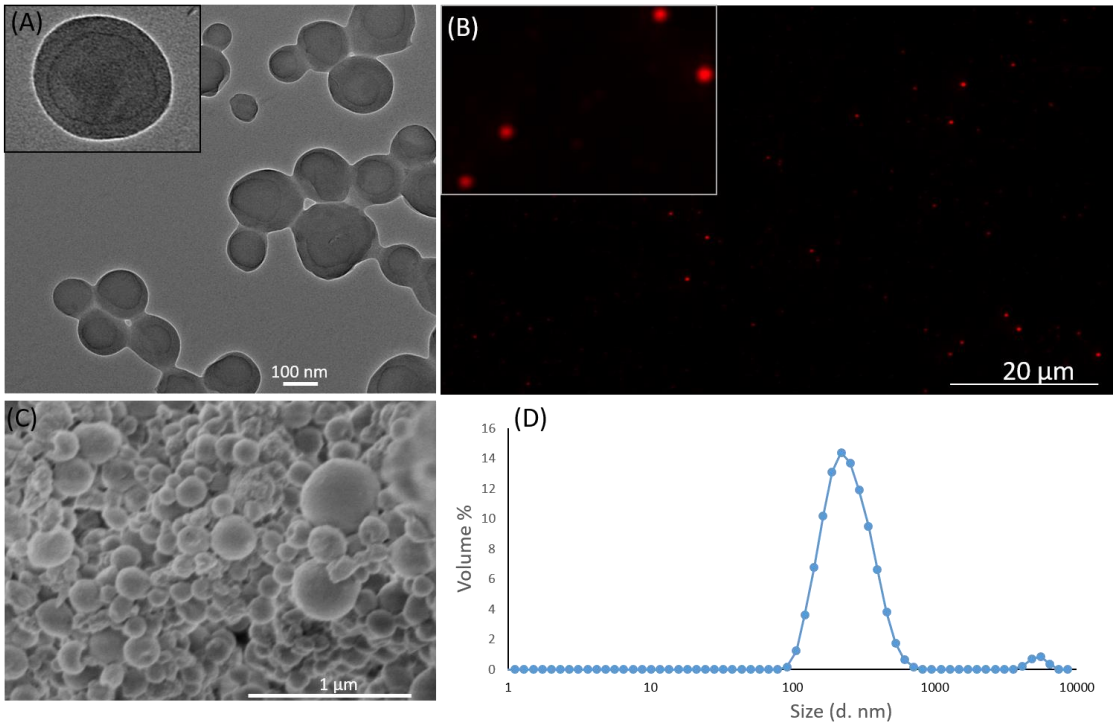

Figure 3.14: Characterization of **P2** based nanoparticles using (A) TEM; (B) Fluorescence microscope; (C) SEM and (D) DLS.

Characterization of particles was done using microscopy imaging techniques and dynamic light scattering. In TEM, spherical morphology with homogeneous distribution of the particles was observed (Figure 3.14A). Since, we used nile red as a hydrophobic guest molecule to be encapsulated during the formulation, red fluorescence was observed in fluorescence microscopy image of the particles (Figure 3.14B). This revealed the confined

location of guest molecules in the particle interior. Further, scanning electron microscopy (SEM) was also used to monitor the surface morphology of nanoparticles which revealed spherical capsule like morphology (Figure 3.14C). Size of particles was ~250 nm measured using DLS (Figure 3.14D). It should be noted that even after washing excess surfactants, small amount of polyvinyl alcohol stabilizes the nanoparticles in aqueous and buffer conditions.

3.2.6 Disassembly studies of P2 based nanoparticles

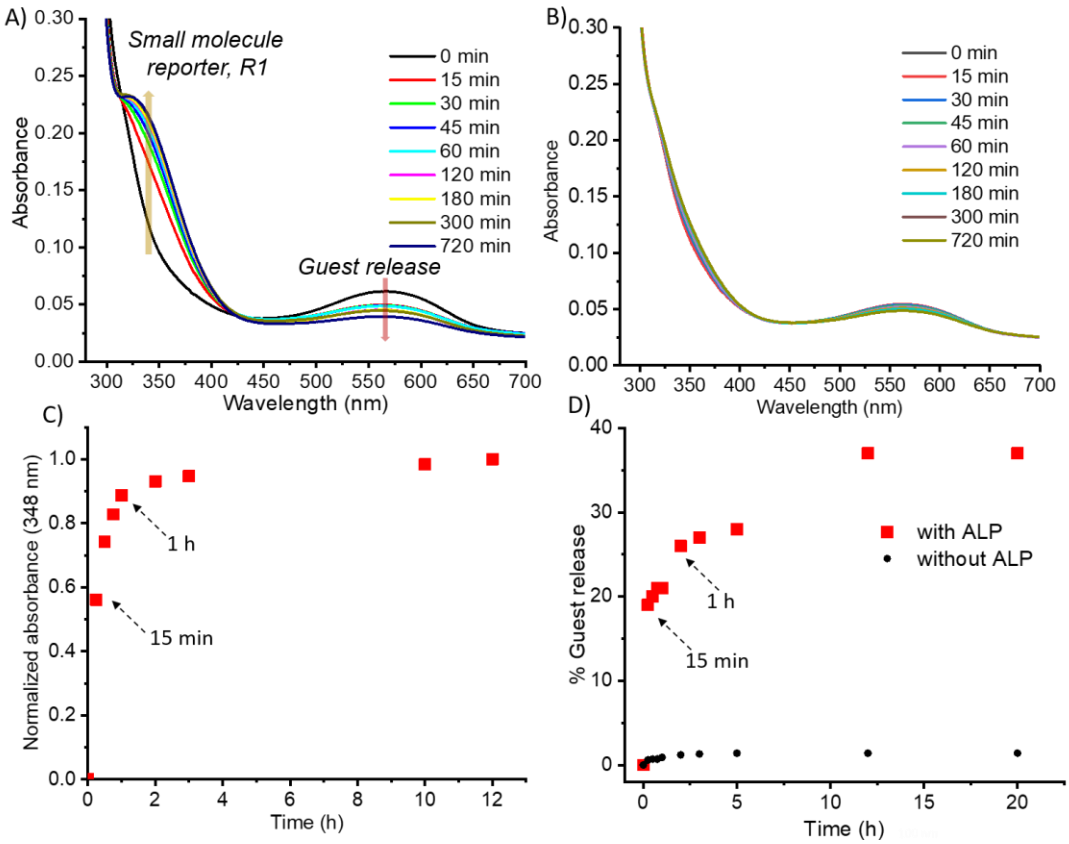

Figure 3.15: UV-Vis of **P2** based emulsion nanoparticles (A) after incubation with ALP; (B) without ALP incubation; (C) Kinetics of evolution of absorbance at 348 nm after incubating **P2** emulsion nanoparticles with ALP; (D) Guest molecule release profile from the particle (red- with ALP; black- without ALP).

After the successful formulation and characterization of nanoparticles using polymer P2, particle degradation was studied in the presence of ALP. The colloidal suspension of particles was prepared in 2.5 mM bicarbonate buffer (pH=8.5). After incubating the particles with ALP, we observed the formation of small molecule reporter, R1 because of depolymerization (Figure 3.15A, C). Simultaneous release of encapsulated guest molecules due to nanoparticle degradation after depolymerization was also observed (Figure 3.15A, D). In the control solution without ALP, small molecule reporter formation was not seen (Figure 3.15B). Additionally, there was no guest release in the absence of enzyme, implying that the particles were stable in the absence of enzyme (Figure 3.15D). After ALP addition, spherical morphology of the particles was lost, and the resultant particles were ill defined as evidenced by TEM studies (Figure 3.16).

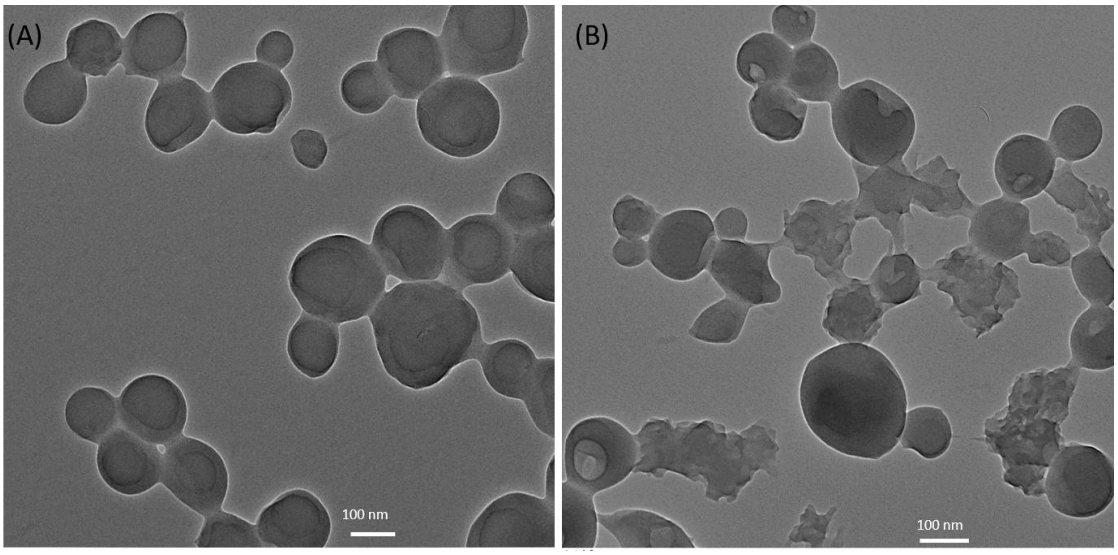

Figure 3.16: TEM images of **P2** nanoparticles (A) before ALP incubation and (B) after ALP incubation.

Kinetics of particle degradation was similar to the kinetics of P0 degradation which is significantly faster than our previous attempts with polyelectrolyte complex-based particles. This difference is attributed to the availability of phosphate groups on the surface of emulsion- based nanoparticles which provides easier accessibility by enzyme. Triggered enzymatic cleavage event on the surface of nanoparticles leads to signal propagation in the form of depolymerization. This results in a rapid and amplified response leading to nanoparticle degradation and release of guest molecular probes.

3.3 Conclusion

In summary, using ALP triggerable polymers, conditions required for nanomaterial formulation to achieve a rapid and amplified degradation response was outlined in this chapter. ALP triggerable poly (benzylcarbamate) which can depolymerize from head to tail was modified in a hydrophilic and hydrophobic fashion to achieve water and organic solvent soluble polymers. Polyelectrolyte complexation and emulsion formulation approach was utilized to synthesize nanoparticles using the respective polymers that displayed significantly varying degradation kinetics after triggering with ALP. The difference in degradation kinetics was found to be dependent on varying degree of substrate accessibility by enzyme. It was discovered that, for a rapid and amplified response in the presence of enzyme, it is crucial to formulate materials with enzyme responsive moieties present on their surface. This leads to an unhindered enzymatic reaction on the surface of nanoparticle and subsequent degradation. Results outlined in this work are applicable in designing enzyme triggerable materials for sensing and drug delivery applications where rapid and amplified response in required.

3.4 Experimental details

3.4.1 Materials

Ethyl 4-amino benzoate, sodium periodate, potassium iodide, diisobutylaluminium hydride (DIBALH), t-butyl acrylate, palladium acetate, tetrabutylammonium chloride, palladium on carbon (10 wt. %), phenylchloroformate, dibutyltin dilaurate (DBTL), 2-nitrobenzyl alcohol, polydiallyldimethylammonium chloride, 20 wt**.** % in water (PDADMAC), nile red and alkaline phosphatase were purchased from Sigma Aldrich and were used as such unless mentioned otherwise. sodium chloride, acetic acid, potassium carbonate and sodium bicarbonate were purchased from Fischer Scientific and used as such unless mentioned otherwise.

3.4.2 Instruments

- **Nuclear Magnetic Resonance (NMR)**

^{1}H NMR spectra were recorded using 400 MHz Bruker NMR spectrometer with residual proton for solvent as a standard. ^{31}P NMR spectra were recorded in 162 MHz Bruker NMR spectrometer using carbon signal of the deuterated solvent as a standard.

- **Dynamic Light Scattering (DLS)**

DLS was performed using Malvern nanozetasizer with a 637 nm laser source with noninvasive backscattering detected at 173°. Standard operating procedure was set up with the following parameters: sample equilibration for 1 min at 25 ^{o}C and then three measurements were taken while each measurement recorded 16 runs.

- **Transmission Electron Microscopy (TEM)**

The sample for DLS was drop casted on carbon coated copper grid and the sample was left for drying overnight. Subsequently, the imaging was done using JEOL-2000FX transmission electron microscope.

- **UV-Vis Spectroscopy**

UV-Vis measurement of the samples was done using PerkinElmer Lambda 35 spectrometer.

3.4.3 Synthetic details

- **Synthesis of 1**

This compound was synthesized according to a previously reported procedure.[20]

Briefly, ethyl-4-aminobenzoate (10 g, 60.54 mmol), sodium periodate (12.94 g, 60.54 mmol), sodium chloride (7.08 g, 121.08 mmol) and potassium iodide (10.05 g, 60.54 mmol) were added in 500 mL round bottom flask and purged with argon for 10 minutes. Mixture of acetic acid (120 mL, 60.54 mmol) and water (13 mL) was added to the reaction mixture to dissolve all the starting materials and the solution was left for stirring overnight and monitored using TLC for completion. The reaction mixture was filtered and the filtrate was diluted with ethyl acetate. The solution was washed twice each time with brine solution, saturated solution of sodium thiosulfate and saturated solution of sodium bicarbonate respectively. Organic layer was collected and evaporated to obtain the crude product which was purified using column chromatography with pure product eluting at 30 % ethyl acetate in hexane mixture. (Yield 95 %).

^{1}H NMR (400 MHz, $CDCl_3$) δ= 8.38 (1H, s), 7.82-7.81 (1H, d), 6.71-6.79 (1H, d), 4.50 (2H, s), 4.34-4.29 (2H, q), 1.38-1.34 (3H, t).

- **Synthesis of 2**

This compound was synthesized according to a previously reported procedure.[20]

Compound 1 (2.15 g, 7.41 mmol) was dissolved in 10 mL dry THF, cooled to 0 ^{0}C and purged with argon gas. DIBAL-H (3.96 mL, 22.23 mmol) was mixed with 5 mL THF and was added to the solution of compound 1 dropwise. The reaction was continued for an hour and was monitored for completion using TLC. To quench excess DIBAL-H, the reaction mixture was diluted with 20 mL methanol slowly followed by the addition of 20 mL THF and celite which led to the formation of suspension which was stirred for an hour. The solid was filtered and washed multiple times with THF to wash out the crude product as filtrate. The crude product was concentrated and purified using column chromatography with pure product eluting out at 30 % ethyl acetate in hexane mixture. (Yield 80 %).

^{1}H NMR (400 MHz, $CDCl_3$) δ= 7.66-7.65 (1H, d), 7.15-7.13 (1H, d), 6.74-6.72 (1H, d), 4.52(2H, d), 4.10 (2H, s).

- **Synthesis of 3**

This compound was synthesized according to a previously reported procedure.[20]

Compound 2 (1.3 g, 5.22 mmol) was dissolved in 15 mL dry DMF and purged with argon. Subsequently Bu_4NBr (2.1 g, 6.53 mmol), $Pd(OAc)_2$ (59 mg, 0.26 mmol), *t*-butyl acrylate (1.13 mL, 7.83 mmol) and K_2CO_3 (3.6 g, 26.1 mmol) were added to the reaction mixture. The reaction was continued for 3 h at 65 ^{0}C and was monitored to completion using TLC. The reaction mixture was cooled, diluted with ethyl acetate and washed twice with brine and water each. The organic layer was concentrated to obtain crude product which was purified using column chromatography and the pure product eluted out at 35 % ethyl acetate in hexane mixture. (Yield 65 %).

^{1}H NMR (400 MHz, $CDCl_3$) δ= 7.70-7.67 (1H, d), 7.36 (1H, s), 7.17-7.15 (1H, d), 6.68-6.67 (1H, d), 6.31-6.28 (1H, d), 4.56-4.54 (2H, d), 3.95 (2H, s), 1.52 (9H, s).

- **Synthesis of 4**

This compound was synthesized according to a previously reported procedure.

Compound 3 (1.5 g, 5.95 mmol) was suspended in a 20 mL solution of THF: sat. $NaHCO_3$: H_2O (ratio of 2:2:1) in a round bottomed flask. Phenylchloroformate (0.85 mL, 6.55 mmol) was added dropwise to the suspension of 4 and the reaction mixture was stirred for 30 minutes while monitoring it using TLC for completion. The reaction mixture was diluted with ethyl acetate and was washed twice using saturated NH_4Cl. Solvent was evaporated to obtain crude product which was purified using column chromatography. Pure product was eluted at 30 % ethyl acetate in hexane mixture and was characterized using (Yield 90 %).

^{1}H NMR (400 MHz, $CDCl_3$) δ= 7.85-7.79 (2H, m), 7.56 (1H, s), 7.39-7.37 (3H, m), 7.24-7.20 (3H, m), 6.98 (1H, s), 6.42-6.38 (1H, d) 4.70-4.68 (2H, d), 1.55 (9H, s).

- **Synthesis of small molecule reporter, R1**

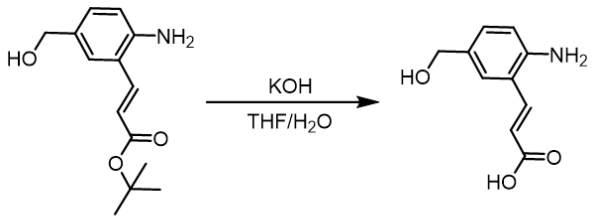

3

Compound 3 (20 mg, 0.08 mmol) was dissolved in THF (8 mL). Potassium hydroxide (45 mg, 0.8 mmol) was dissolved in 2 mL water and was added to the solution of 3. The mixture was left for stirring for 24 h under reflux conditions at 65 ^{0}C while monitoring it using TLC until completion.

After completion, the reaction mixture was washed using ethyl acetate 3 times to wash out unreacted starting material. The aqueous layer was neutralized using 2N HCl carefully to a pH of 6. It led to the formation of precipitate which was washed multiple times with methanol. Pure product was concentrated and characterized using ^{1}H NMR and ^{13}C NMR.

^{1}H NMR (400 MHz, MeOD) δ= 7.64-7.60 (d, 1H), 7.36 (s, 1H), 7.09-7.07 (d, 1H), 6.74-6.72 (d, 1H), 6.39-6.35 (d, 1H), 4.46 (s, 2H)

- **Synthesis of trigger**

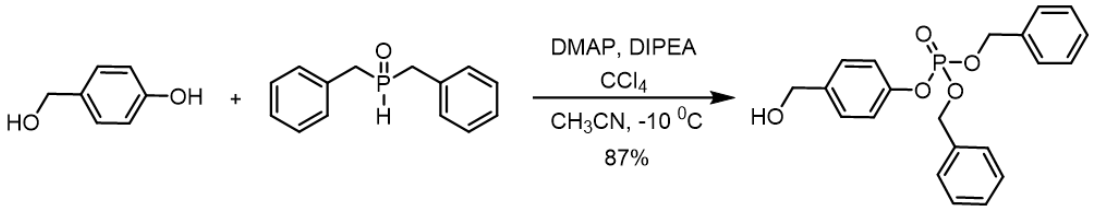

Trigger was synthesized according to a previously reported procedure.[26]

^{1}H NMR (400 MHz, MeOD) δ= 7.35-7.32 (m, 12H), 7.12-7.10 (m, 2H), 5.15-5.13 (d, 4H), 4.58 (s, 2H)

^{31}P NMR (162 MHz, d-DMSO) δ (ppm) = 6.57

- **Synthesis of P0'**

Monomer/Compound 4 (100 mg, 0.27 mmol) was dissolved in anhydrous toluene (200 µL) and purged with argon for 5 min. To the solution, was added DBTL (16 µL, 0.027 mmol) and the mixture was kept under argon atmosphere for five minutes. Subsequently, the vial containing mixture was transferred to a preheated oil bath at a temperature of 115 ^{o}C under argon atmosphere. The mixture was stirred for 10 min after which obvious signs of precipitation was observed due to polymerization. Subsequently, dibenzyl ether protected phosphate trigger (123 mg, 0.27 mmol)

dissolved in anhydrous toluene (300 µL) was added to the polymer solution dropwise using a syringe. The reaction mixture was stirred for 90 min at 115 ^{o}C under argon atmosphere after which the polymer was cooled to room temperature. The polymer was purified by precipitation using methanol multiple times to obtain light yellowish powder. The powder was dried overnight under high vacuum and analyzed using ^{1}H NMR and ^{31}P NMR (Yield 60 mg).

^{1}H NMR (400 MHz, d-DMSO) δ (ppm) = 9.60-9.49, 7.86, 7.79-7.75, 7.46, 7.37-7.36, 7.22-7.19, 6.47-6.43, 5.18-5.14, 4.50-4.48, 1.47

^{31}P NMR (162 MHz, d-DMSO) δ (ppm) = 6.32

- **Synthesis of P0**

P0' (50 mg) was dissolved in anhydrous DMF (~150 µL) and was kept under ice bath. The solution was purged with argon for 10 minutes after which TMSBr (100 µL; note: TMSBr needs to be added in excess and we found twice the volume w.r.t the weight of P0' works best) was added to the solution dropwise using a glass syringe. 15 min after the addition of TMSBr, the ice bath was removed, and the reaction was continued overnight (12 h) under argon atmosphere. After 12 h, ~10 µL methanol was added to the reaction mixture to obtain a slightly cloudy mixture. The mixture was stirred for 30 more minutes after which it was purified using precipitation by multiple washing with methanol to obtain light yellowish powder as product. The powder was dried overnight under high vacuum and characterized using ^{1}H NMR, ^{31}P NMR and ^{13}C NMR. (Yield 25 mg).

In the subsequent step for *t*-butyl ester deprotection, polymer was dissolved in 0.3 mL mixture of TFA/DCM (1:1 ratio) and was stirred for 6 min. After 6 min, TFA/DCM mixture was evaporated using rotary evaporator to obtain yellow solid. The solid was washed with diethyl ether three times

and was further dried using high vacuum. It was characterized using ^{1}H NMR, ^{31}P NMR and ^{13}C NMR. (Yield 20 mg).

^{1}H NMR (400 MHz, d-DMSO) δ (ppm) = 9.60-9.48, 7.86, 7.79-7.75, 7.46, 6.48-6.44, 5.14, 4.49

^{31}P NMR (162 MHz, d-DMSO) δ (ppm) = 6.26

^{13}C NMR (100 MHz, d-DMSO) δ (ppm) = 168.01, 163.24, 154.96, 139.88, 136.98, 130.58, 129.03, 126.95, 120.61, 66.01, 34.86

- **Synthesis of P1'**

P0' (50 mg, 0.0083 mmol) was dispersed in anhydrous toluene (200 µL) and purged with argon for five minutes. DBTL (2 µL, 0.002 mmol) was added to the P0' dispersion. Subsequently, the mixture was introduced to an oil bath at 115 ^{0}C under argon atmosphere. Polyethyleneglycol (5k) isocyanate (250 mg, 0.04 mmol), dissolved in anhydrous toluene (~200 µL) was added to the mixture and dropwise using a syringe and the mixture was stirred for 2 h. After 2 h, the reaction mixture was cooled to room temperature and was purified using precipitation by multiple washing with methanol to obtain white powder. The white solid was dried under high vacuum and was characterized using ^{1}H NMR and ^{31}P NMR. (Yield 30 mg).

^{1}H NMR (400 MHz, d-DMSO) δ (ppm) = 9.60-9.48, 7.86, 7.79-7.75, 7.46, 7.37-7.35, 7.21-7.19, 6.47-6.43, 5.17-5.14, 4.49-4.48, 3.51, 1.47

^{31}P NMR (162 MHz, d-DMSO) δ (ppm) = 6.32

- **Synthesis of P1**

P1' (25 mg) was dissolved in anhydrous DMF (~150 µL) and was kept under ice bath. The solution was purged with argon for 10 minutes after which TMSBr (50 µL) was added to the solution

dropwise using a glass syringe. 15 min after the addition of TMSBr, the ice bath was removed, and the reaction was continued overnight (12 h) under argon atmosphere. After 12 h, ~10 µL methanol was added to the reaction mixture. The mixture was stirred for 30 more minutes after which it was purified using precipitation by multiple washing with methanol to obtain white solid powder as product. The powder was dried overnight under high vacuum and characterized using ^{1}H NMR and ^{31}P NMR. (Yield 15 mg).

In the subsequent step for *t*-butyl ester deprotection, polymer was dissolved in 0.4 mL mixture of TFA/DCM (1:1 ratio) and was stirred for 6 min. After 6 min, TFA/DCM mixture was evaporated using rotary evaporator to obtain light yellow solid. The solid was washed with diethyl ether three times and was further dried using high vacuum. It was characterized using ^{1}H NMR, ^{31}P NMR and ^{13}C NMR. (Yield 10 mg).

^{1}H NMR (400 MHz, d-DMSO) δ (ppm) = 9.61-9.47, 7.86, 7.82-7.78, 7.47, 6.50-6.46, 5.42, 5.15, 4.97, 4.72, 3.51

^{31}P NMR (162 MHz, d-DMSO) δ (ppm) = 6.24

^{13}C NMR (100 MHz, d-DMSO) δ (ppm) = 167.99, 154.94, 139.78, 136.96, 134.32, 130.57, 128.96, 126.93, 120.57, 70.25, 66.01, 28.35

- **Synthesis of P2'**

P0' (80 mg, 0.02 mmol) was dispersed in anhydrous toluene (400 µL) and purged with argon for five minutes. DBTL (2 µL, 0.002 mmol) was added to the P0' dispersion. Subsequently, the mixture was introduced to an oil bath at 115 ^{0}C under argon atmosphere. Octadecyl isocyanate (60 mg, 0.2 mmol), dissolved in anhydrous toluene (~150 µL) was added to the mixture and dropwise using a syringe and the mixture was stirred for 2 h. After 2 h, the reaction mixture was cooled to

room temperature and was purified using precipitation by multiple washing with methanol to obtain white powder. It was further washed multiple times with diethyl ether. The white solid was dried under high vacuum and was characterized using ^{1}H NMR and ^{31}P NMR. (Yield 50 mg).

^{1}H NMR (400 MHz, d-DMSO) δ (ppm) = 9.55, 7.80-7.74, 7.45-7.34, 7.18-7.14, 6.43-6.39, 5.12, 4.97, 4.59, 1.46, 1.21, 0.85-0.82

^{31}P NMR (162 MHz, d-DMSO) δ (ppm) = 6.35

- **Synthesis of P2**

P2' (25 mg) was dissolved in anhydrous DMF (~150 µL) and was kept under ice bath. The solution was purged with argon for 10 minutes after which TMSBr (50 µL) was added to the solution dropwise using a glass syringe. 15 min after the addition of TMSBr, the ice bath was removed, and the reaction was continued overnight (12 h) under argon atmosphere. After 12 h, ~10 µL methanol was added to the reaction mixture. The mixture was stirred for 30 more minutes after which it was purified using precipitation by multiple washing with methanol to obtain white powder as product. The powder was dried overnight under high vacuum and characterized using ^{1}H NMR, ^{31}P NMR. (Yield 15 mg).

In the subsequent step for *t*-butyl ester deprotection, polymer was dissolved in 0.4 mL mixture of TFA/DCM (1:1 ratio) and was stirred for 6 min. After 6 min, TFA/DCM mixture was evaporated using rotary evaporator to obtain light yellow solid. The solid was washed with diethyl ether three times and was further dried using high vacuum. It was characterized using ^{1}H NMR, ^{31}P NMR and ^{13}C NMR. (Yield 10 mg).

^{1}H NMR (400 MHz, d-DMSO) δ (ppm) = 9.61-9.50, 7.86, 7.82-7.78, 7.47, 6.50-6.46, 5.15, 5.00-4.98, 4.50, 1.23, 0.88-0.83

^{31}P NMR (162 MHz, d-DMSO) δ (ppm) = 6.24

^{13}C NMR (100 MHz, d-DMSO) δ (ppm) = 168.01, 154.95, 139.80, 136.97, 130.58, 129.01, 126.92, 120.59, 66.02, 29.49

3.4.4 Formulation of P1 + PDADMAC polyelectrolyte complex nanoparticles: P1 (1 mg) was dissolved in 1 mL bicarbonate buffer (2.5 mM, pH=8.5) by sonication. In a different vial, stock solution of PDADMAC was prepared by dissolving 20 µL of 20 wt. % concentrated PDADMAC in 5 mL water. 150 µL of PDADMAC from the stock solution was added to P1 solution and the mixture was sonicated for 2 min. The resultant colloidal particles were left to stabilize for 10 min before characterizing them using DLS and TEM.

3.4.5 Formulation of P2 based nanoparticles using single emulsion approach: P2 (2.5 mg) was dispersed in chloroform (1 mL). Nile red (30 µL from 3 mM stock solution in chloroform) was added to P2 dispersion. The mixture was added to 2 mL aqueous solution of polyvinyl alcohol (0.5 wt. %). The organic and aqueous layers were emulsified using probe sonicator (100 Watt) for 2 min. After emulsification, chloroform was evaporated carefully using rotary evaporator. Subsequently, the aqueous solution of nanoparticles was centrifuged 3 times at 12000 rpm for 5 min to spin down the particles and wash out excess polyvinyl alcohol. In the end, settled nanoparticles were dispersed in 2.5 mM bicarbonate buffer and left to stabilize for 10 min before subsequent characterization and studies

3.5 References

(1) Robinson, P. K. Enzymes: Principles and Biotechnological Applications. *Essays Biochem.* **2015**, *59*, 1–41.

(2) Dhanasekaran, S. M.; Barrette, T. R.; Ghosh, D.; Shah, R.; Varambally, S.; Kurachi, K.; Pienta, K. J.; Rubin, M. A.; Chinnaiyan, A. M. Delineation of Prognostic Biomarkers in Prostate Cancer. *Nature* **2001**, *412* (6849), 822–826.

(3) Sato, H.; Takino, T.; Okada, Y.; Cao, J.; Shinagawa, A.; Yamamoto, E.; Seiki, M. A Matrix Metalloproteinase Expressed on the Surface of Invasive Tumour Cells. *Nature* **1994**, *370* (6484), 61–65.

(4) Li, Y.; Liu, G.; Wang, X.; Hu, J.; Liu, S. Enzyme-Responsive Polymeric Vesicles for Bacterial-Strain-Selective Delivery of Antimicrobial Agents. *Angew. Chem. Int. Ed.* **2016**, *128* (5), 1792–1796.

(5) Kang, J. H.; Asai, D.; Kim, J. H.; Mori, T.; Toita, R.; Tomiyama, T.; Asami, Y.; Oishi, J.; Sato, Y. T.; Niidome, T.; et al. Design of Polymeric Carriers for Cancer-Specific Gene Targeting: Utilization of Abnormal Protein Kinase Cα Activation in Cancer Cells. *J. Am. Chem. Soc.* **2008**, *130* (45), 14906–14907.

(6) Hu, J.; Zhang, G.; Liu, S. Enzyme-Responsive Polymeric Assemblies, Nanoparticles and Hydrogels. *Chem. Soc. Rev*. **2012**, *41* (18), 5933–5949.

(7) Kim, K.; Bae, B.; Kang, Y. J.; Nam, J. M.; Kang, S.; Ryu, J. H. Natural Polypeptide-Based Supramolecular Nanogels for Stable Noncovalent Encapsulation. *Biomacromolecules* **2013**, *14* (10), 3515–3522.

(8) Wong, C.; Stylianopoulos, T.; Cui, J.; Martin, J.; Chauhan, V. P.; Jiang, W.; Popovíc, Z.; Jain, R. K.; Bawendi, M. G.; Fukumura, D. Multistage Nanoparticle Delivery System for Deep Penetration into Tumor Tissue. *Proc. Natl. Acad. Sci. U. S. A.* **2011**, *108* (6), 2426–2431.

(9) Wen, J.; Anderson, S. M.; Du, J.; Yan, M.; Wang, J.; Shen, M.; Lu, Y.; Segura, T. Controlled Protein Delivery Based on Enzyme-Responsive Nanocapsules. *Adv. Mater.* **2011**, *23* (39), 4549–4553.

(10) Li, N.; Cai, H.; Jiang, L.; Hu, J.; Bains, A.; Hu, J.; Gong, Q.; Luo, K.; Gu, Z. Enzyme-Sensitive and Amphiphilic PEGylated Dendrimer-Paclitaxel Prodrug-Based Nanoparticles for Enhanced Stability and Anticancer Efficacy. *ACS Appl. Mater. Interfaces* **2017**, *9* (8), 6865–6877.

(11) Azagarsamy, M. A.; Sokkalingam, P.; Thayumanavan, S. Enzyme-Triggered Disassembly of Dendrimer-Based Amphiphilic Nanocontainers. *J. Am. Chem. Soc.* **2009**, *131* (40), 14184–14185.

(12) Wang, C.; Chen, Q.; Wang, Z.; Zhang, X. An Enzyme-Responsive Polymeric Superamphiphile. *Angew. Chem. Int. Ed.* **2010**, *49* (46), 8612–8615.

(13) Rodriguez, A. R.; Kramer, J. R.; Deming, T. J. Enzyme-Triggered Cargo Release from Methionine Sulfoxide Containing Copolypeptide Vesicles. *Biomacromolecules* **2013**, *14* (10), 3610–3614.

(14) Harnoy, A. J.; Rosenbaum, I.; Tirosh, E.; Ebenstein, Y.; Shaharabani, R.; Beck, R.; Amir, R. J. Enzyme-Responsive Amphiphilic PEG-Dendron Hybrids and Their Assembly into Smart Micellar Nanocarriers. *J. Am. Chem. Soc.* **2014**, *136* (21), 7531–7534.

(15) Raghupathi, K. R.; Azagarsamy, M. A.; Thayumanavan, S. Guest-Release Control in Enzyme-Sensitive, Amphiphilic-Dendrimer-Based Nanoparticles through Photochemical Crosslinking. *Chem. Eur. J.* **2011**, *17* (42), 11752–11760.

(16) Phillips, D. J.; Wilde, M.; Greco, F.; Gibson, M. I. Enzymatically Triggered, Isothermally Responsive Polymers: Reprogramming Poly(Oligoethylene Glycols) to Respond to Phosphatase. *Biomacromolecules* **2015**, *16* (10), 3256–3264.

(17) Ding, Y.; Kang, Y.; Zhang, X. Enzyme-Responsive Polymer Assemblies Constructed through Covalent Synthesis and Supramolecular Strategy. *Chem. Commun.* **2015**, *51* (6), 996–1003.

(18) Blum, A. P.; Kammeyer, J. K.; Yin, J.; Crystal, D. T.; Rush, A. M.; Gilson, M. K.; Gianneschi, N. C. Peptides Displayed as High Density Brush Polymers Resist Proteolysis and Retain Bioactivity. *J. Am. Chem. Soc.* **2014**, *136* (43), 15422–15437.

(19) Samarajeewa, S.; Shrestha, R.; Li, Y.; Wooley, K. L. Degradability of Poly(Lactic Acid)-Containing Nanoparticles: Enzymatic Access through a Cross-Linked Shell Barrier. *J. Am. Chem. Soc.* **2012**, *134* (2), 1235–1242.

(20) Kumar, V.; Harris, J. T.; Ribbe, A.; Franc, M.; Bae, Y.; McNeil, A. J.; Thayumanavan, S. Construction from Destruction: Hydrogel Formation from Triggered Depolymerization-Based Release of an Enzymatic Catalyst. *ACS Macro Lett.* **2020**, 377–381.

(21) Yardley, R. E.; Kenaree, A. R.; Gillies, E. R. Triggering Depolymerization: Progress and Opportunities for Self-Immolative Polymers. *Macromolecules*. **2019**, *52* (17), 6342-6360.

(22) Peterson, G. I.; Larsen, M. B.; Boydston, A. J. Controlled Depolymerization: Stimuli-

Responsive Self-Immolative Polymers. *Macromolecules* **2012**, *45* (18), 7317–7328.

(23) DiLauro, A. M.; Lewis, G. G.; Phillips, S. T. Self-Immolative Poly(4,5-Dichlorophthalaldehyde) and Its Applications in Multi-Stimuli-Responsive Macroscopic Plastics. *Angew. Chem. Int. Ed.* **2015**, *127* (21), 6298–6303.

(24) Lewis, G. G.; Robbins, J. S.; Phillips, S. T. Phase-Switching Depolymerizable Poly(Carbamate) Oligomers for Signal Amplification in Quantitative Time-Based Assays. *Macromolecules* **2013**, *46* (13), 5177–5183.

(25) Esser-Kahn, A. P.; Sottos, N. R.; White, S. R.; Moore, J. S. Programmable Microcapsules from Self-Immolative Polymers. *J. Am. Chem. Soc.* **2010**, *132* (30), 10266–10268.

(26) Zhuang, J.; Seçinti, H.; Zhao, B.; Thayumanavan, S. Propagation of Enzyme-Induced Surface Events inside Polymer Nanoassemblies for a Fast and Tunable Response. *Angew. Chem. Int. Ed.* **2018**, *57* (24), 7111–7115.

CHAPTER 4

COOPERATIVE INTERACTION BETWEEN ENZYME RESPONSIVE POLYELECTROLYTES & SURFACTANTS: IMPLICATIONS IN HOST-GUEST AND INTERFACIAL CHEMSTRY

4.1 Introduction

Study of interaction between polyelectrolytes and surfactants of opposite charge has gained significant attention in recent years and this feature is widely used in several formulations for cosmetics, food and biomedical applications.[1–3] Mixing a polyelectrolyte with an oppositely charged surfactant can be used for significantly easier "synthesis" of a variety of self-assembled structures which are otherwise difficult to achieve using polyelectrolyte or surfactant individually.[2,4,5] The self-assembly of surfactants in presence of a polyelectrolyte is primarily driven by the increase in entropy of system due to release of counterions, as well as a decrease in the electrostatic repulsion experienced by surfactant molecules.[6,7] As a result, surfactants in the complex self-assembles at a much lower critical aggregate concentration (Figure 4.1).

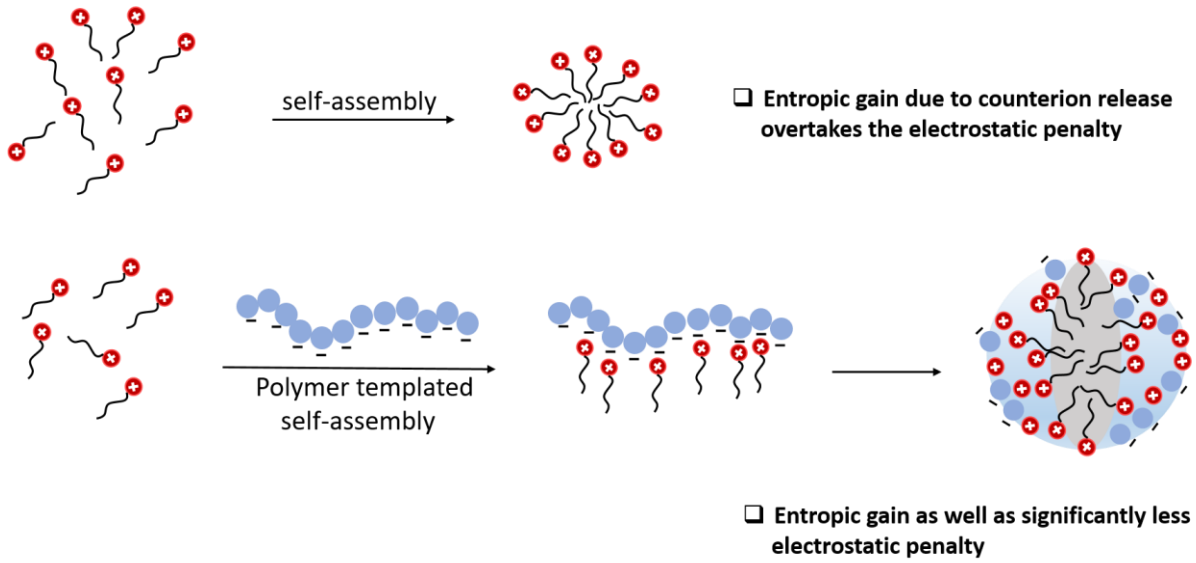

Figure 4.1: Self-assembly of surfactants in presence of polyelectrolyte.

By varying several parameters such as charge density on the polymer, salt concentration and the nature of hydrophobic tail on surfactant, several nanoscale assemblies can be achieved.[8–11] While there are many reports on understanding different architectures of polyelectrolyte-surfactant complexes and the properties they offer in solution as well as in solid phase, their stimuli responsive behavior is relatively less explored. Introduction of stimuli responsive features to polyelectrolyte-surfactant complexes offer several advantages such as in applications where molecular release in presence of a stimulus is desired. Additionally, the interfacial studies of polyelectrolyte-surfactant complexes at the liquid crystal (LC) interface is also less explored. Due to the long range orientational order in LC phase because of the alignment of constituent molecules, they possess a characteristics optical appearance.[12,13] However, introducing a polyelectrolyte-surfactant complex can change the alignment of constituent molecules in LC, resulting into a change in their optical appearance.[14] By understanding the mechanism in which complexes orient themselves at the LC interface in the absence and presence of a stimulus, their interfacial behavior could be regulated to tune the orientation of LC systems. This provides an opportunity to achieve a macroscopic response by LC based amplification of the molecular level input signal.

The depolymerizable polymer discussed in chapter 3 offers several advantages due to its charged nature. Since it is a polyelectrolyte with enzyme responsive features, it can be used to formulate enzyme responsive supramolecular host assemblies in the presence of a positively charged surfactant. This gives us an opportunity to learn the evolution in host as well as guest release features due to enzyme triggered depolymerization.

Additionally, when used at the LC interface, the alkaline phosphatase (ALP) responsive polyelectrolyte-surfactant complex can be anchored at the interface giving a characteristics optical

signal. ALP triggered depolymerization event can be used to disassemble the complex, causing a change in the orientation of LCs with an amplified optical signature that can be macroscopically visualized (Figure 4.2).

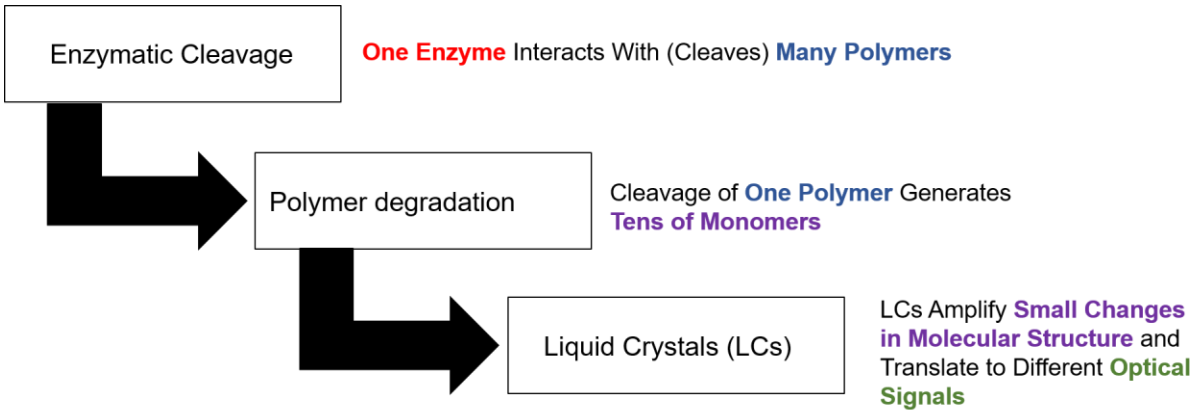

Figure 4.2: LC mediated signal amplification due to ALP triggered depolymerization.

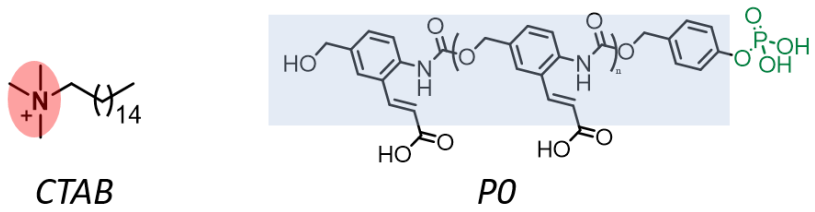

Figure 4.3: Structure of CTAB surfactant and ALP triggerable polyelectrolyte, **P0.**

Overall, the objective of this chapter is to understand the following:

1) Self-assembly of surfactants (cetyl trimethyl ammonium bromide, CTAB) in the presence of ALP triggerable polyelectrolyte, P0?
2) How do surfactants affect the degradation behavior of CTAB-P0 complex when triggered with ALP?

3) Behavior of CTAB-P0 complex at the interface of liquid crystal before and after triggering with ALP. Does the molecular event of substrate cleavage by enzyme leads to signal amplification by changing the optical signal of LCs?

4.2 Results and discussion

4.2.1 Critical aggregate concentration of CTAB in the absence and presence of P0

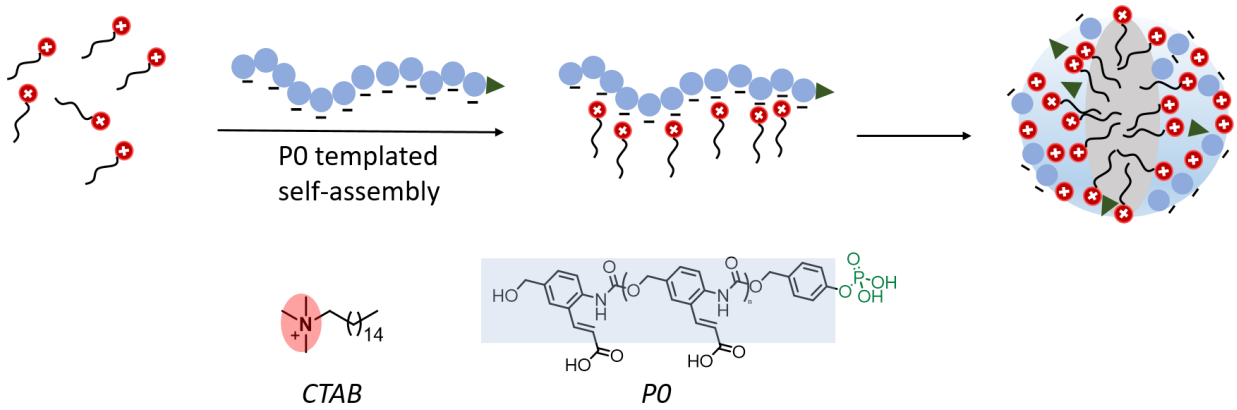

Figure 4.4: **P0** templated self-assembly of CTAB.

To understand the effect of P0 on the self-assembly behavior of CTAB (Figure 4.4), critical aggregate concentration (cac) measurements of CTAB in the absence and presence of P0 was carried out. In the absence of P0, the cac value of CTAB was 0.6 mM. However, in the presence of P0, the cac value reduced 10 times which alluded to the fact that P0 assists in the self-assembly of CTAB molecules (Figure 4.5A). It should be noted that we observed only a 10-fold decrease in the cac value while in previously published reports the decrease in cac values is significantly higher. This is attributed to low molecular weight of ~6000 for P0.

The self-assembly of CTAB-P0 complex was also studied using dynamic light scattering (DLS). At a concentration of 0.3 mM, CTAB surfactants didn't form any stable self-assembled aggregates, but in the presence of P0, stable aggregate of hydrodynamic diameter ~30 nm was observed (Figure 4.5B). CTAB-P0 complex can be used as host assemblies for hydrophobic guest molecules such

as nile red (Figure 4.5C). CTAB solution on the other hand showed significantly poor dye encapsulation behavior (Figure 4.5C). The morphology of CTAB-P0 complex was studied using transmission electron microscopy (TEM) which revealed micelle like morphology (Figure 4.5D).

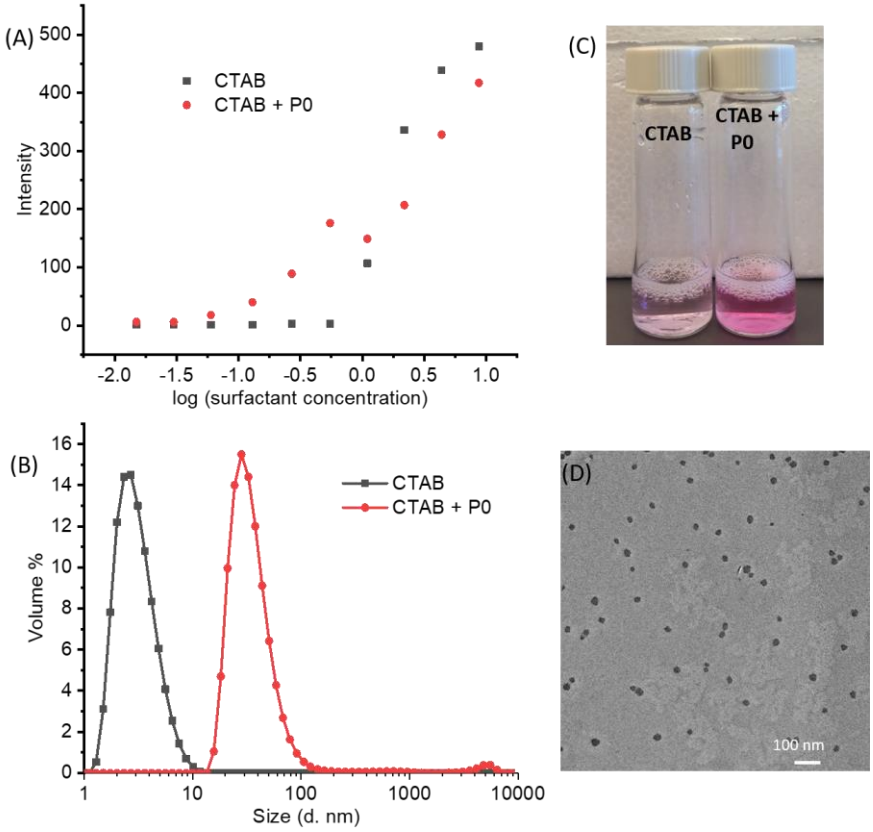

Figure 4.5: (A) Critical aggregate concentration of CTAB and CTAB + **P0** complex; (B) Dynamic light scattering profile of CTAB and CTAB + **P0** complex; (C) Nile red encapsulation behavior of CTAB and CTAB + **P0** complex; (D) TEM images of CTAB + **P0** complex.

4.2.2 Depolymerization of P0 in CTAB-P0 complex in the presence of ALP

In chapter three, we discovered that the depolymerization of P0 takes around two hours for completion (Figure 4.6A). However, when complexed with CTAB, significant reduction in depolymerization kinetics was observed and it was not complete even after 24 h. This observation was consistent with the slow depolymerization kinetics of hydrophilic polymer, P1 in the presence of PDADMAC which was discussed in chapter 3.

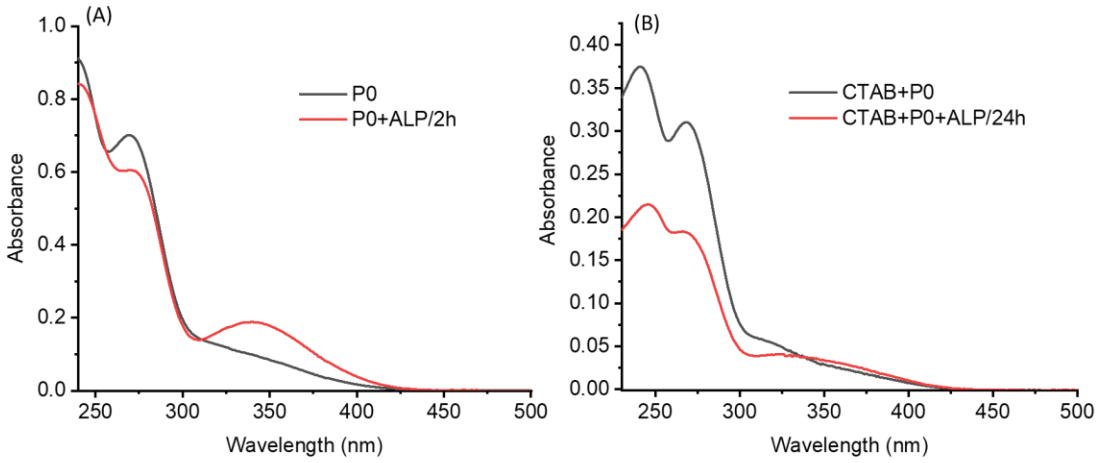

Figure 4.6: (A) Depolymerization of **P0** in presence of ALP; (B) Depolymerization of **P0** + CTAB complex in presence of ALP.

To account for this slow depolymerization, we proposed the hypothesis that when P0 is complexed with CTAB, phosphate group is buried in the hydrophobic core in a similar fashion to P1 + PDADMAC complex discussed in chapter 3. This limits the accessibility of ALP to the substrate group, thereby limiting the phosphate cleavage event and the subsequent depolymerization. To test this hypothesis, kinetics of cleavage of phosphate group from CTAB-P0 complex was monitored using ^{31}P NMR. The cleavage of phosphate group was significantly slower in the presence of CTAB which confirmed the limited accessibility of substrate by ALP (Figure 4.7).

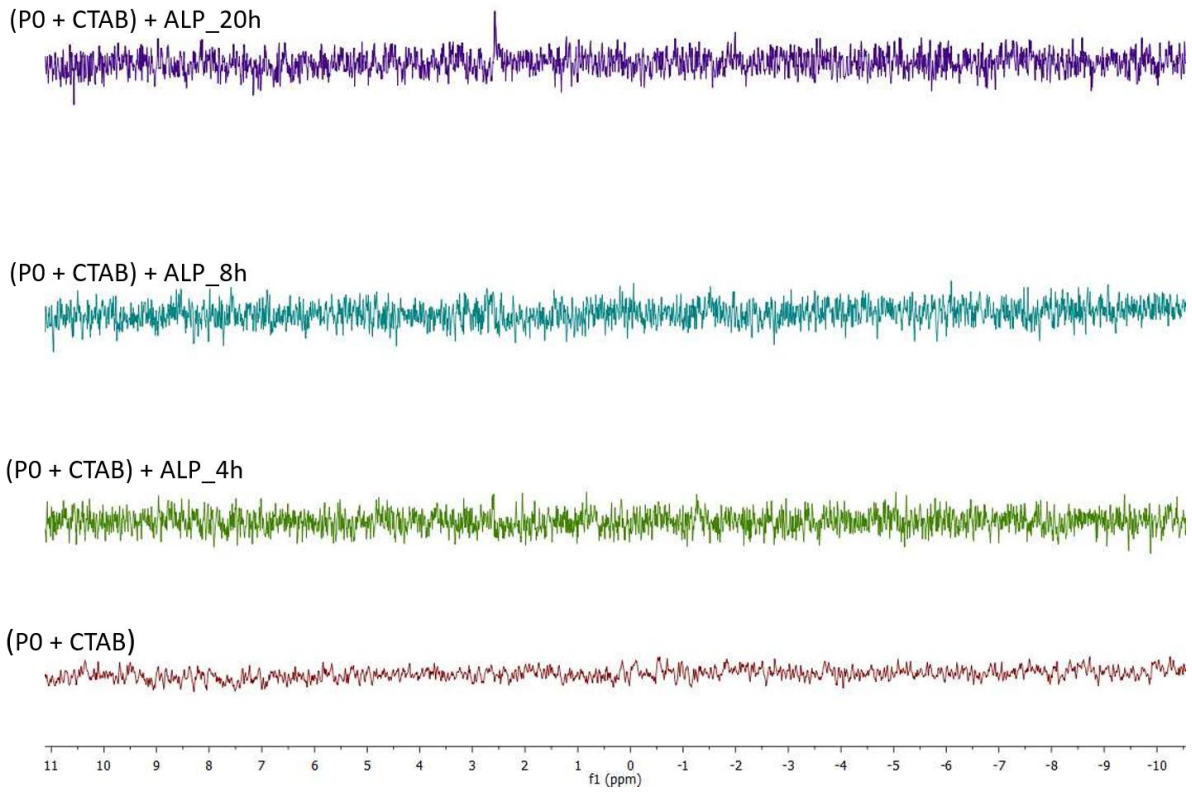

Figure 4.7: ^{31}P NMR of the kinetics of cleavage of phosphate group from CTAB-**P0** complex in presence of ALP.

To test if the rate of cleavage of phosphate group is reflected in the depolymerization kinetics, UV-Vis of the CTAB-P0 complex was measured after incubating the solution with ALP. We observed that the depolymerization kinetics was significantly slower and followed similar kinetics as the rate of cleavage of phosphate group from the complex (Figure 4.8). These results show that when P0 is complexed with CTAB, the cleavage of phosphate groups by ALP dictates the degradation of P0 in the complex. This was because upon complexation, enzyme mediated cleavage of phosphate groups which are located in the hydrophobic core of complex becomes the rate limiting step rather than the depolymerization event of P0.

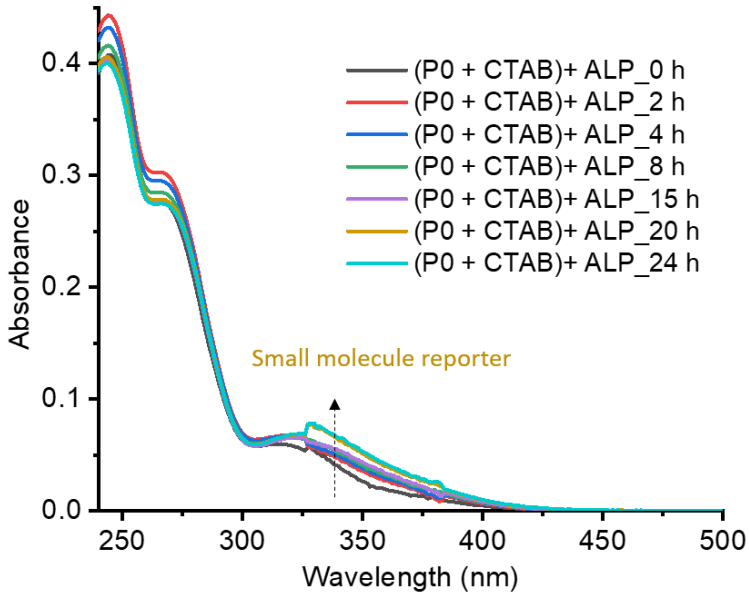

Figure 4.8: Depolymerization of **P0** in CTAB-**P0** complex in the presence of ALP.

4.2.3 Monitoring disassembly of CTAB-P0 complex

Next, we were interested in understanding the effect of degradation of CTAB-P0 complex on the guest stability. Nile red which is a hydrophobic dye, was encapsulated in the complex and its release after the disassembly of complex was monitored. Upon incubating the complex with ALP, a temporal release of nile red was observed due to its precipitation in water after complex degradation (Figure 4.9A). The kinetics of guest release was consistent with the kinetics of depolymerization of P2 in the complex implying that the host degradation feature was reflected in the guest release kinetics. The disassembly was further monitored using DLS where we observed bigger aggregates with poor correlation function after treating the complex with ALP (Figure 4.9B).

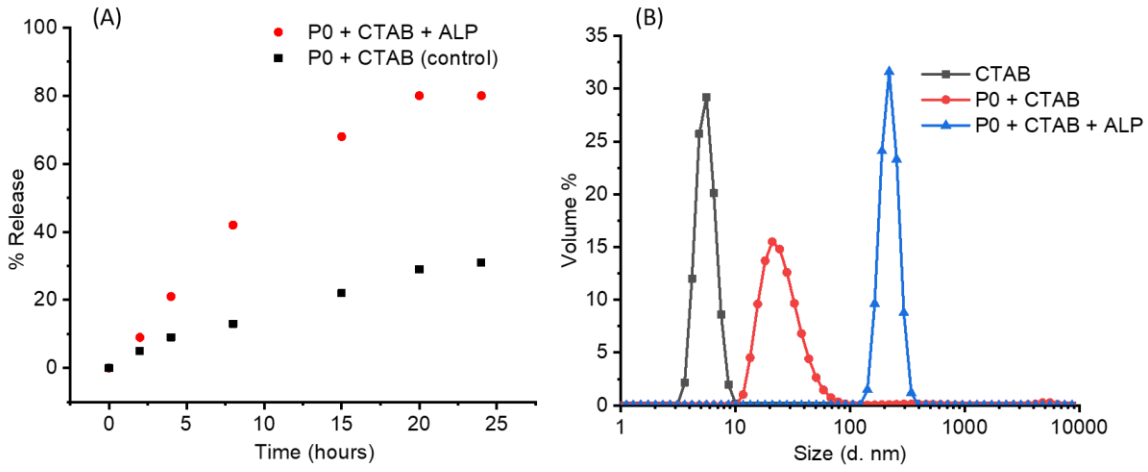

Figure 4.9: (A) Guest release profile from **P0** + CTAB host complex; (B) DLS profile of **P0** + CTAB complex when treated with ALP.

4.2.4 Liquid crystal anchoring transition of P0-CTAB complex

Earlier, in the work done by Abbott and co-workers they have found that a positively charged polyelectrolyte such as PDADMAC when complexed with sodium dodecyl sulfate (SDS) can lead to homeotropic LC anchoring transition of 5 CB liquid crystals. PDADMAC and SDS, individually leads to the planar anchoring of liquid crystals (Figure 4.10). We were interested in understanding if a similar phenomenon can be observed using CTAB-P0 complex. We hypothesized that the LC anchoring transition behavior due to CTAB-P0 complex will change if the complex is triggered with ALP, which leads to the depolymerization of P0. This would result in an amplified response to enzymatic reaction in the form of modified optical signature of the LC system.

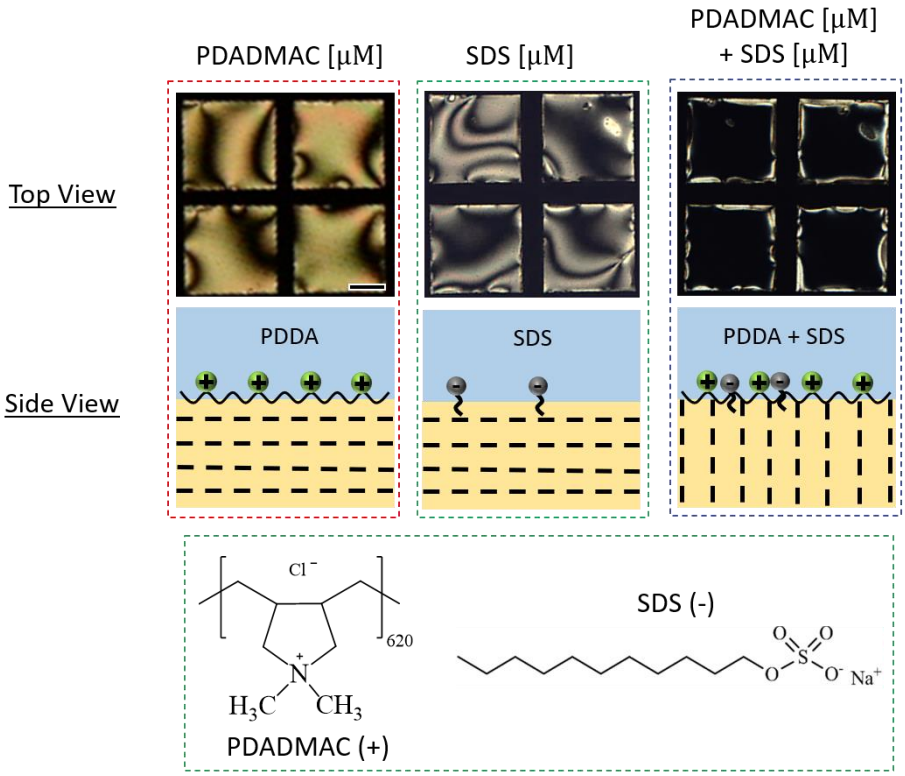

Figure 4.10: LC anchoring transition of PDADMAC + SDS complex.

To test this hypothesis, we carried out a control experiment to see the effect of surfactant on the LC anchoring transition. DTAB being a positively charged surfactant, was used for the study and we observed a homeotropic anchoring induced by DTAB. However, in the presence of P0, the anchoring transition behavior changed from homeotropic to planar. This was attributed to the π- π stacking between the aromatic groups from P0 and the aromatic groups present in 5 CB liquid crystals. To monitor the effect of ALP induced degradation of P0 from the complex on the LC anchoring transition behavior, we treated the system with ALP. 12 hours after ALP treatment, we observed the LC transition from planar to homeotropic with some planar domains (Figure 4.11).

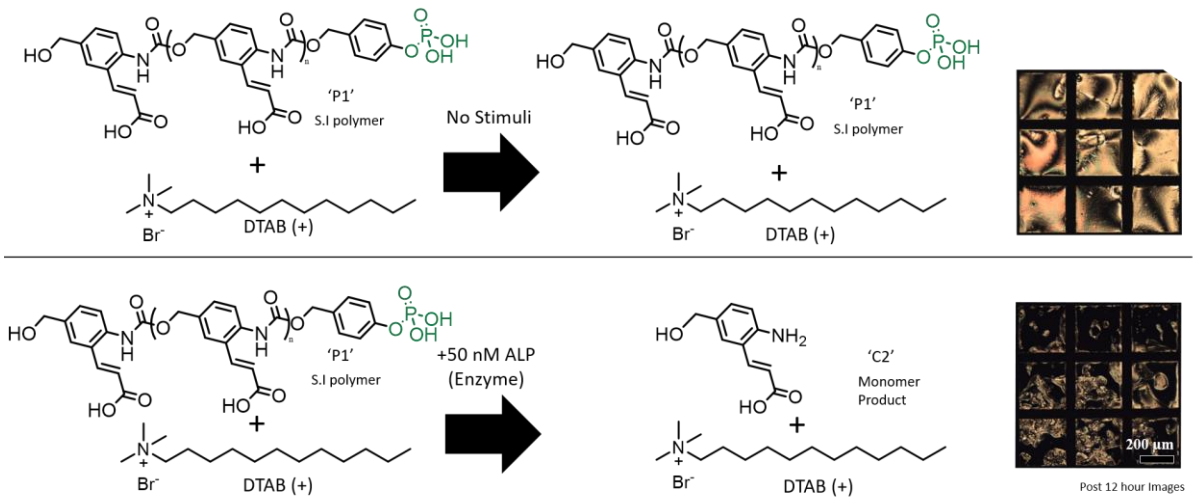

Figure 4.11: In-situ depolymerization of DTAB-**P0** complex at the LC interface.

4.3 Conclusion

In this chapter, we explored the cooperative interaction between ALP triggerable polyelectrolytes and oppositely charged surfactants. The polyelectrolyte acts as a template to assist in the self-assembly of surfactants. While the self-assembled complex could be used as a host to encapsulate hydrophobic guest molecules, the enzyme triggered degradation of polyelectrolyte in the complex was significantly slower than the depolymerization of polyelectrolyte in solution. The slow degradation was reflected in the kinetics of guest release and it was attributed to the burying of phosphate group in the complex interior which led to poor accessibility by enzyme.

These polyelectrolyte-surfactant complex undergoes planar anchoring transition at liquid crystal interface. When triggered with enzyme, the depolymerization of polyelectrolyte at the LC interface leads to a change in LC orientation which was reflected in the optical signal of the LC. Combining the depolymerization strategy with LC based signal amplification provides broad applicability of the system in sensing different analytes where a single cleavage event provides a macroscopic response in the optical response of LC.

4.4 Materials and methods

4.4.1 Instruments

- **Nuclear Magnetic Resonance (NMR)**

^{1}H NMR spectra were recorded using 400 MHz Bruker NMR spectrometer with residual proton for solvent as a standard. ^{31}P NMR spectra were recorded in 162 MHz Bruker NMR spectrometer using carbon signal of the deuterated solvent as a standard.

- **Dynamic Light Scattering (DLS)**

DLS was performed using Malvern nanozetasizer with a 637 nm laser source with noninvasive backscattering detected at 173°. Standard operating procedure was set up with the following parameters: sample equilibration for 1 min at 25 ^{o}C and then three measurements were taken while each measurement recorded 16 runs.

- **Transmission Electron Microscopy (TEM)**

The sample for DLS was drop casted on carbon coated copper grid and the sample was left for drying overnight. Subsequently, the imaging was done using JEOL-2000FX transmission electron microscope.

- **UV-Vis Spectroscopy**

UV-Vis measurement of the samples was done using PerkinElmer Lambda 35 spectrometer.

4.4.2 Preparation of LC films

LC films were prepared by depositing nematic 5CB (4’-pentyl-4-biphenylcarbonitrile) on a gold TEM grid (10 μm in thickness) placed on glass substrates. The glass substrate was coated with DMOAP which was rubbed to achieve unidirectional planar alignment. Subsequently, the LC film

was immersed in an aqueous bath containing 10 mM bicarbonate buffer and P0 + DTAB complex. To prevent evaporation of the aqueous a glass slide was used to cap off the bath. After the well is capped, the well is placed under the microscope observe the state of the LC film over time. Below is the schematic.

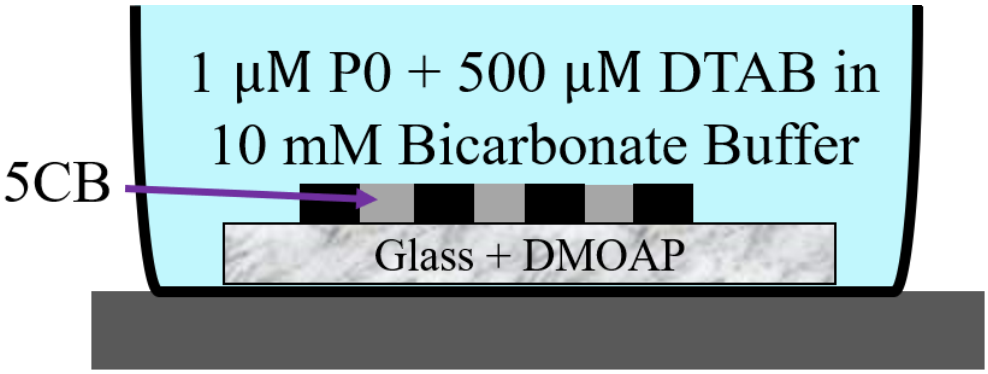

Figure 4.12: Schematic of the set up for LC film preparation.

4.5 References

(1) Macknight, W. J.; Ponomarenko, E. A.; Tirrell, D. A. Self-Assembled Polyelectrolyte - Surfactant Complexes in Nonaqueous Solvents and in the Solid State. *Acc. Chem. Res.* **1998**, *31* (12), 781–788.

(2) Ober, C. K.; Wegner, G. Polyelectrolyte-Surfactant Complexes in the Solid State: Facile Building Blocks for Self-Organizing Materials. *Adv. Mater.* **1997**, *9* (1), 17–31.

(3) Antonietti, M.; Thünemann, A. Polyelectrolyte-Lipid Complexes as Membrane Mimetic Systems. *Curr. Opin. Coll. Inter. Sci.* **1996**, *1* (5), 667–671.

(4) Antonietti, M.; Conrad, J.; Thünemann, A. Polyelectrolyte-Surfactant Complexes: A New Type of Solid, Mesomorphous Material. *Macromolecules* **1994**, *27* (21), 6007–6011.

(5) Kosmella, S.; Kötz, J.; Shirahama, K.; Liu, J. Cooperative Nature of Complex Formation in Mixed Polyelectrolyte-Surfactant Systems. *J. Phys. Chem. B* **1998**, *102* (34), 6459–6464.

(6) Tam, K. C.; Wyn-Jones, E. Insights on Polymer Surfactant Complex Structures during the Binding of Surfactants to Polymers as Measured by Equilibrium and Structural Techniques. *Chem. Soc. Rev*. **2006**, *35* (8), 693–709.

(7) Kayitmazer, A. B. Thermodynamics of Complex Coacervation. *Adv. Coll. Int. Sci*. **2017**, *239*, 169–177.

(8) Dautzenberg, H.; Jaeger, W. Effect of Charge Density on the Formation and Salt Stability of Polyelectrolyte Complexes. *Macromol. Chem. Phys.* **2002**, *203* (14), 2095–2102.

(9) Zhou, S.; Burger, C.; Yeh, F.; Chu, B. Charge Density Effect of Polyelectrolyte Chains on

the Nanostructures of Polyelectrolyte-Surfactant Complexes. *Macromolecules* **1998**, *31* (23), 8157–8163.

(10) Bai, G.; Nichifor, M.; Lopes, A.; Bastos, M. Thermodynamic Characterization of the Interaction Behavior of a Hydrophobically Modified Polyelectrolyte and Oppositely Charged Surfactants in Aqueous Solution: Effect of Surfactant Alkyl Chain Length. *J. Phys. Chem. B* **2005**, *109* (1), 518–525.

(11) Wallin, T.; Linse, P. Monte Carlo Simulations of Polyelectrolytes at Charged Micelles. 3. Effects of Surfactant Tail Length. *J. Phys. Chem. B* **1997**, *101* (28), 5506–5513.

(12) Carlton, R. J.; Hunter, J. T.; Miller, D. S.; Abbasi, R.; Mushenheim, P. C.; Tan, L. N.; Abbott, N. L. Chemical and Biological Sensing Using Liquid Crystals. *Liq. Cryst. Rev.* **2013**, *1* (1), 29–51.

(13) Miller, D. S.; Wang, X.; Abbott, N. L. Design of Functional Materials Based on Liquid Crystalline Droplets. *Chem. Mat*. **2014,** *26* (1), 496–506.

(14) Kinsinger, M. I.; Buck, M. E.; Campos, F.; Lynn, D. M.; Abbott, N. L. Dynamic Ordering Transitions of Liquid Crystals Driven by Interfacial Complexes Formed between Polyanions and Amphiphilic Polyamines. *Langmuir* **2008**, *24* (23), 13231–13236.

CHAPTER 5

ADENOSINE TRIPHOSPHATE (ATP) FUELLED DISSIPATIVE NANOSTRUCTURES

5.1 Introduction

The process of supramolecular self-assembly is ubiquitous in nature.[1] For example, the self-assembly of lipids into cell membrane, or folding of DNA into double helix are prime examples of the vitality of this process for our survival. Synthetic supramolecular structures are primarily inspired by such natural systems. It involves rational design of amphiphilic molecules, which can undergo self-assembly into different architectures depending on the non-covalent forces of interaction they experience in solution.[2–7] The self-assembly process is spontaneous in nature and as a result, the system is in a global minimum energy state which is also referred as the state of thermodynamic equilibrium where individual molecules are in equilibrium with the self-assembled structure[8] (Figure 5.1).

In natural systems however, there are several processes which are highly dynamic and cannot be achieved by the classic thermodynamically derived self-assembled structures.[9] Because these processes are energetically uphill, they require an energy input to carry out a function and are termed as dissipative or non-equilibrium supramolecular systems (Figure 5.1). For example, the growth and shrinkage of microtubules present in cytoskeleton is a highly dynamic non-equilibrium process used in several functions such as cell locomotion and division.[10–13] In this process, guanosine triphosphate (GTP) bound tubulin dimers are used as building blocks for the growth of microtubules while the hydrolysis of bound GTP leads to their shrinkage. The relative rates of addition of GTP bound building blocks (which is the input energy in this case) vs the hydrolysis of GTP to guanosine diphosphate (GDP) dictates the state of microtubules and hence, the function. In the absence of energy input, the assembly dissipates back to its equilibrium state due to the

hydrolysis of GTP. Similarly, the use of adenosine triphosphate (ATP) by enzyme kinase to carry out several enzymatic reactions for cellular metabolism is another example of natural non-equilibrium process which uses ATP as an energy input.[14–18] Synthetic supramolecular systems that mimic these dissipative natural processes can be used to tap several functions which are otherwise not possible using traditional supramolecular systems in equilibrium state.[19,20] Examples include developing autonomous material capable of adapting to the input energy to carry out a functional response. They can also be used for the fundamental understanding of the complex way in which nature has evolved to carry out non-equilibrium processes.

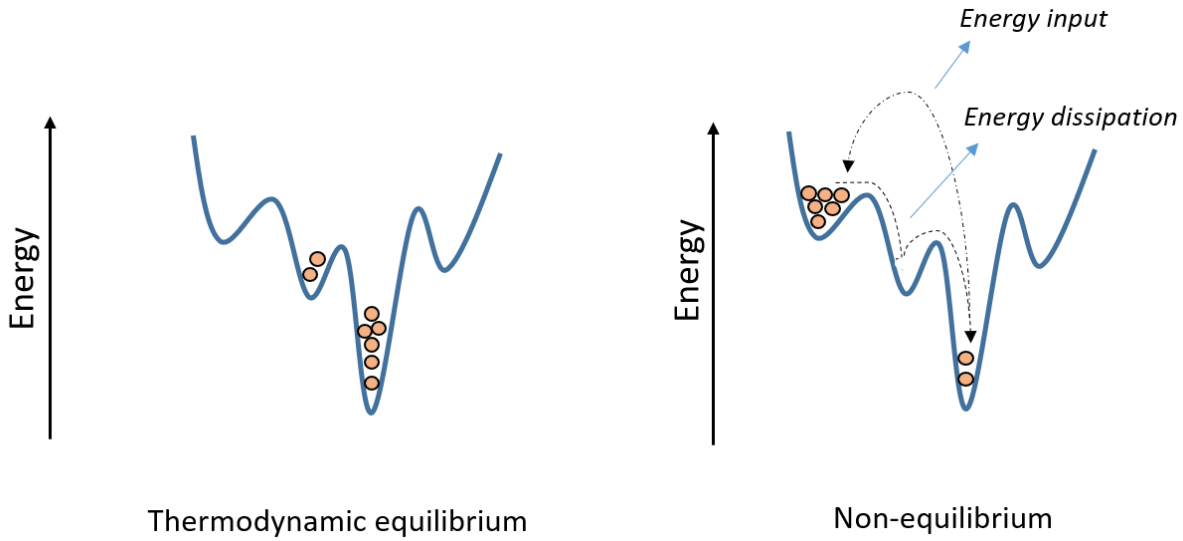

Figure 5.1: Energy profile of chemical systems under thermodynamic equilibrium and non-equilibrium states.

First step in creating dissipative synthetic systems is to design building blocks which can self-assemble into unique supramolecular nanostructures in the presence of chemical input.[21] The chemical input can modify the building blocks in a covalent or non-covalent fashion providing it

an ability to self-assemble.[22] To bring the self-assembled structure back to its building blocks, a stimulus such as pH[23,24], light[25] or enzyme[26] is used depending on the molecular design. Using this principle, the dissipative supramolecular structure can be transiently achieved as long as the chemical input is present in the system. Once the supply of chemical input ceases, transiently formed self-assembled structure can revert to its resting or thermodynamic state under the influence of stimulus. Adding different batches of chemical input provides a temporal control in the self-assembly process which can be harnessed for several functions.

There has been a surge in the development of dissipative systems in past few years. For example, ATP has been used as a chemical input for transient self-assembly of small molecule surfactants into vesicles based on charge mediated non-covalent interactions.[27] The vesicles can dissipate back to their individual building blocks upon potato apyrase mediated enzymatic hydrolysis of ATP. Similarly, dimethyl sulfate has been used as an energy input for transient formation of hydrogel by covalently modifying carboxylic acid present in the building blocks into ester groups leading to their hydrophobic association.[23] They can dissipate back into resting solution state due to pH mediated hydrolysis of ester groups. This demonstration is reminiscent of dynamic formation and shrinkage of microtubule polymers.

In this chapter, we were interested in designing synthetic dissipative system that mimics the non-equilibrium behavior of natural systems involving kinase and phosphatase enzymes using ATP as an energy input. Both enzymes work in tandem during several cellular processes such as signal transduction.[28–31] Using ATP, kinase can phosphorylate a protein substrate, which is used for downstream signaling. On the other hand, phosphatase can cleave the phosphate group from phosphorylated substrate to bring the system back to its resting state. By keeping a constant supply of ATP, natural systems maintain their non-equilibrium phosphorylated state to carry out

energetically uphill tasks. To design a synthetic mimic of this process, we utilized a supramolecular self-assembly and disassembly approach using an amphiphilic trimer molecule which contains a hydrophobic peptide sequence (KYSGYIY) as substrate for kinase (Figure 5.2A). We hypothesized that it can self-assemble into micellar nanoparticles under aqueous conditions. However, when the hydrophobic peptide sequence is phosphorylated in the presence of kinase and ATP, phosphate group is introduced at the tyrosine moieties. This changes the overall amphiphilicity of the molecule leading to a non-equilibrium self-assembled architecture. Cleavage of phosphate group by phosphatase brings the assembly back to its initial stage. We rationalized that by controlling the addition of ATP to the system, a temporal control over the non-equilibrium self-assembled state can be achieved. It can dissipate back to its resting assembled state due to dephosphorylation once the supply of ATP is ceased (Figure 5.2B)

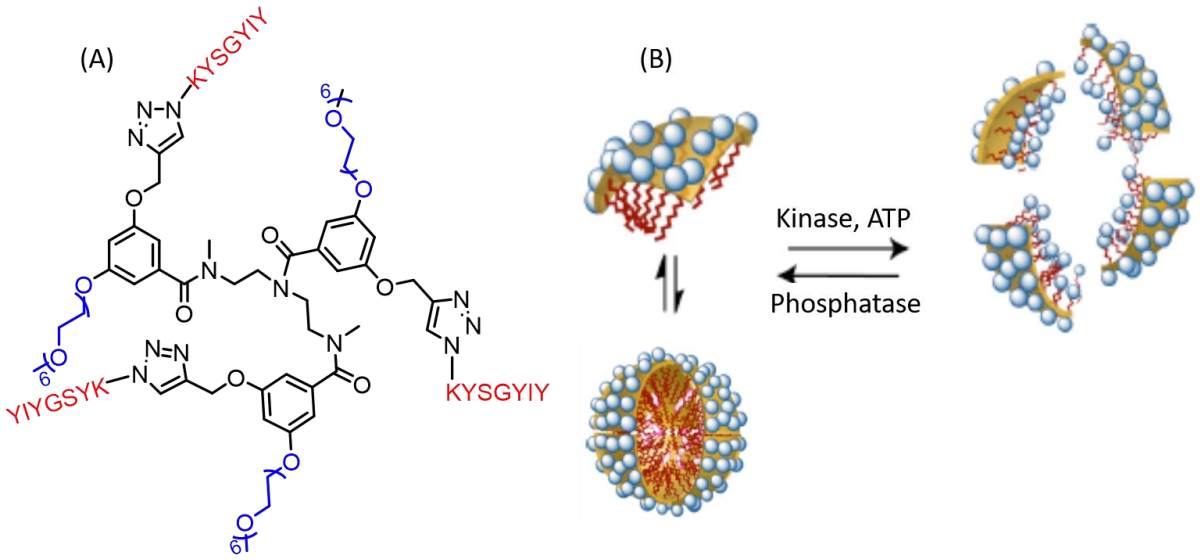

Figure 5.2: (A) Structure of amphiphilic trimer; (B) Principle of dissipative self-assembly of the trimer in the presence of ATP as an input energy.

5.2 Results and Discussion

5.2.1 Molecular design and synthetic scheme

The hydrophobic peptide sequence used in this study was commercially achieved. Amine group of the lysine at C-terminus of peptide was modified with an azide group (Figure 5.3A). This modification was further used to carry out a copper mediated click reaction with alkyne groups present in trimer to obtain the amphiphilic trimer (Figure 5.3B).

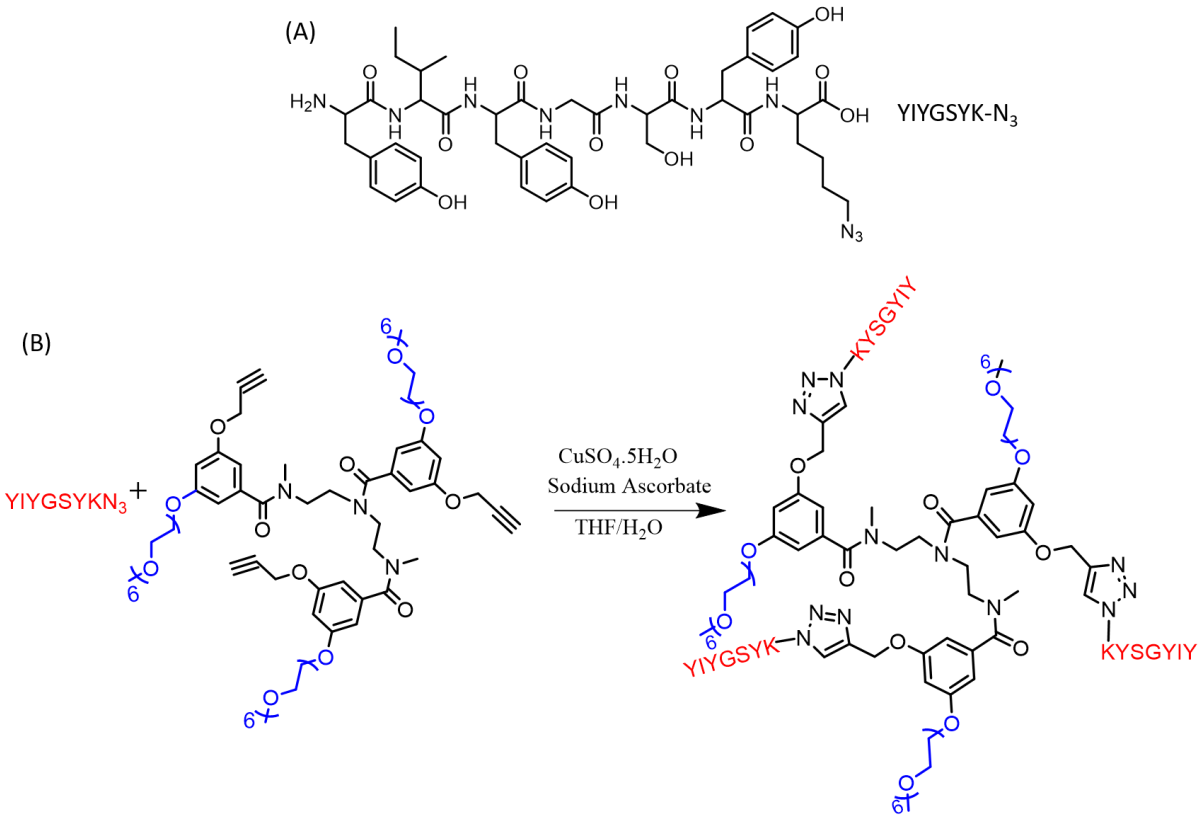

Figure 5.3: (A) Structure of the peptide sequence used as substrate for kinase; (B) Scheme of copper mediated click reaction to achieve amphiphilic trimer.

5.2.2 Phosphorylation studies of the peptide sequence YIYGSYK-N_3

Phosphorylation of peptide was done using Src kinase and ATP at 37 ^{0}C. During kinase mediated phosphorylation, one of the tyrosine residues in the peptide gets phosphorylated in the presence of ATP and ADP is produced as by-product (Figure 5.4A). In ^{31}P NMR, we observed the generation of a new peak at -0.5 ppm corresponding to the phosphate group from phosphorylated peptide in the presence of kinase and ATP (Figure 5.4B). Peaks corresponding to the phosphorous atoms from ADP were also observed.

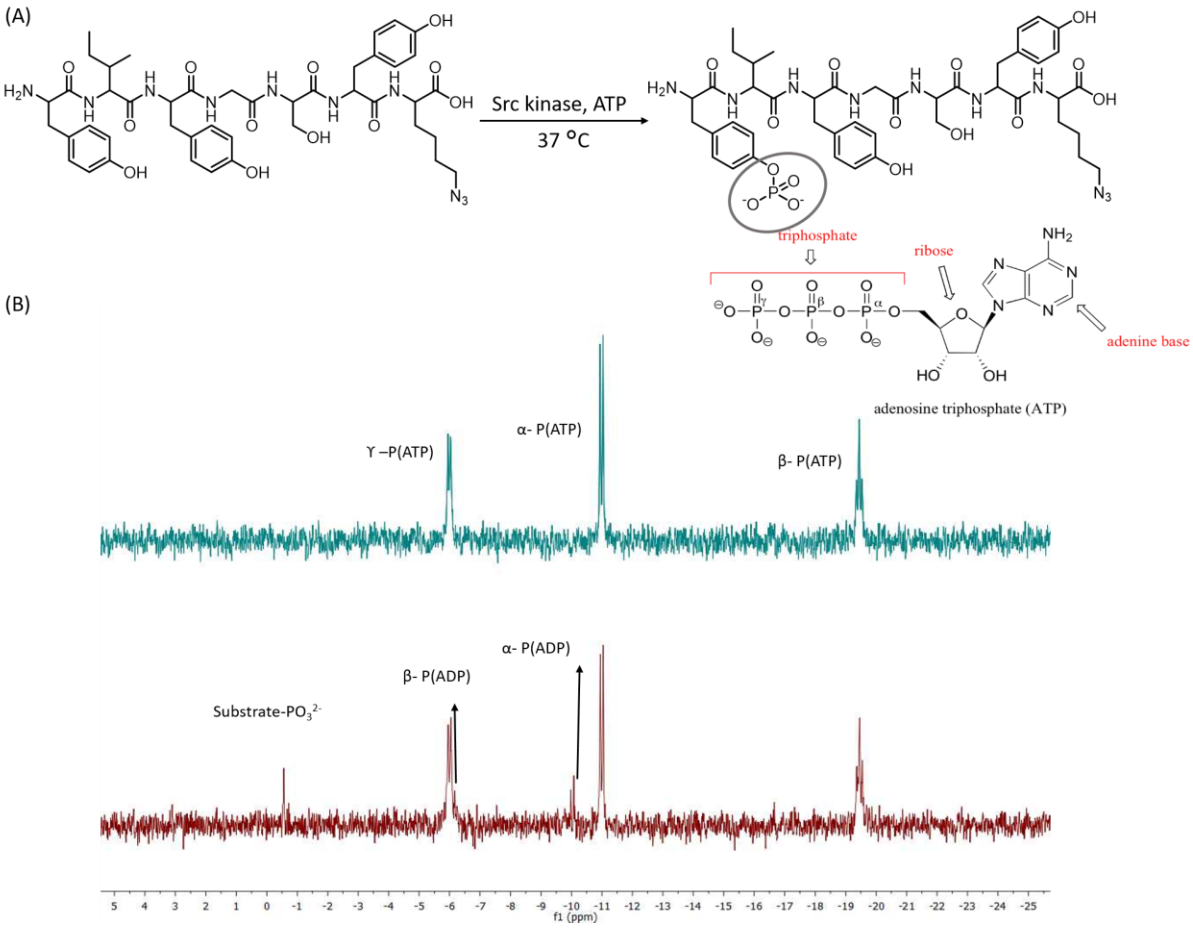

Figure 5.4: (A) Phosphorylation of peptide in the presence of Src kinase and ATP; (B) ^{31}P NMR of ATP (top spectra) and reaction mixture containing peptide, Src kinase, ATP (bottom spectra).

Peptide phosphorylation was also studied using MALDI-MS where the mass fragment corresponding to the phosphorylated peptide was observed at 1037.138.

To understand the activity of kinase, kinetics experiment of peptide phosphorylation was carried out using ^{31}P NMR. 30% peptide phosphorylation was observed in presence of kinase in 21 h (Figure 5.6). By varying various parameters such as ATP, substrate or enzyme concentration, substrate phosphorylation can be increased to 56%. It should be noted that the hydrophobic nature of peptide substrate contributed to significantly less phosphorylation because the solubility of peptide in buffer conditions was poor to start with.

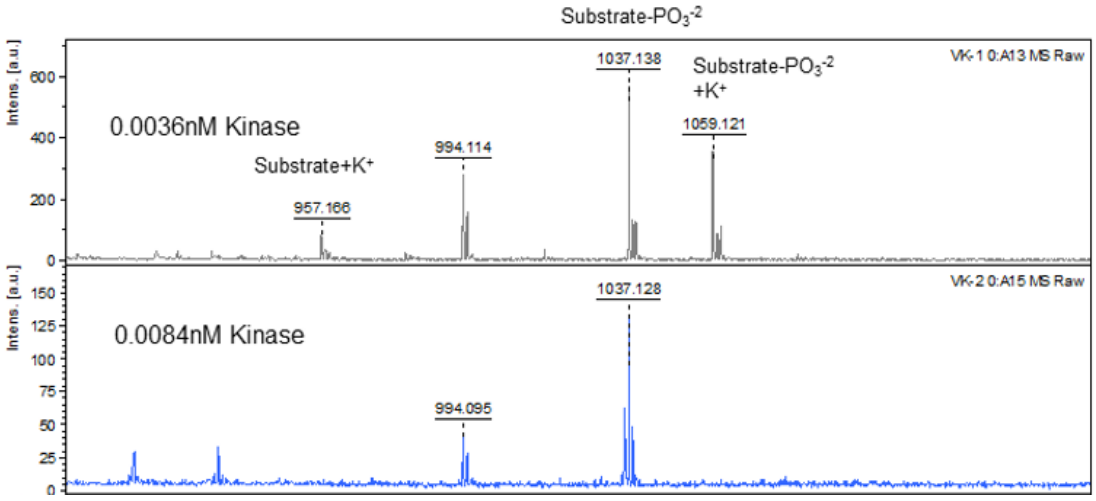

Figure 5.5: Peptide phosphorylation study using MALDI-MS at different concentration of Src kinase.

5.2.3 Dephosphorylation studies of the phosphorylated substrate

Subsequently, we studied the dephosphorylation of peptide in the presence of alkaline phosphatase (ALP). ALP cleaves phosphate group from the substrate to reform the original peptide sequence while generating phosphoric acid as a by-product. Using ^{31}P NMR spectroscopy, we observed that the kinetics of cleavage of phosphate group was significantly faster compared to phosphorylation. Within 10 min, phosphate groups from the peptide got cleaved to form phosphoric acid as a by-product (Figure 5.7).

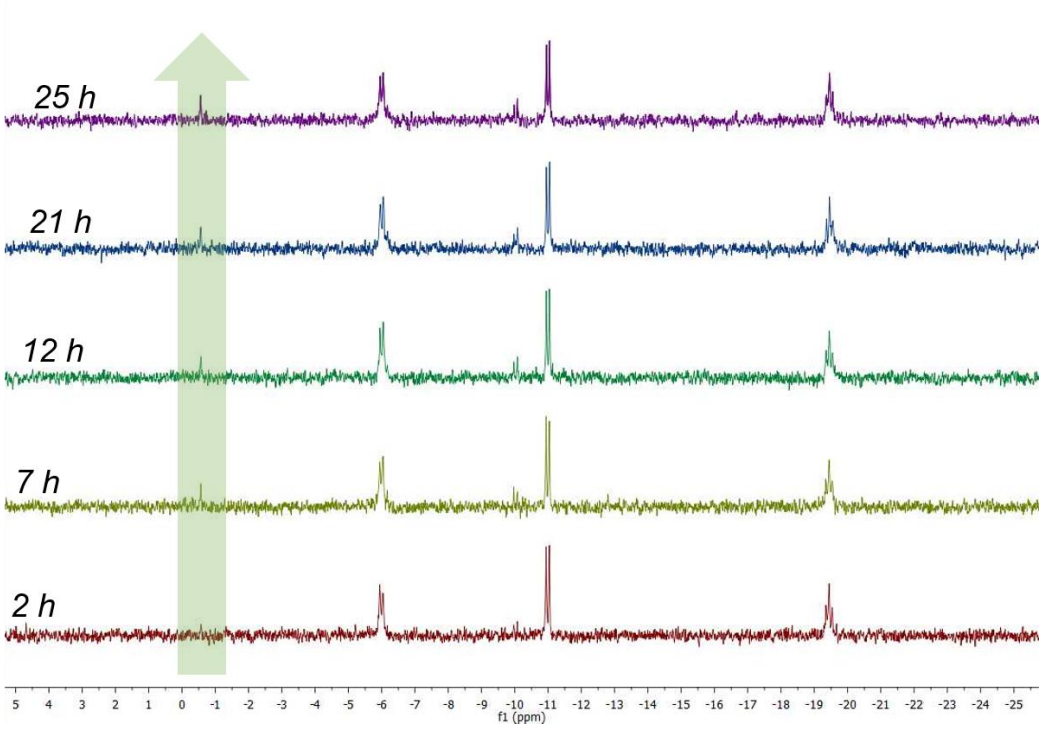

Figure 5.6: Kinetics of peptide phosphorylation in the presence of Src kinase and ATP.

While ALP cleaves the phosphate group from substrate in 10 min, it was observed that if the reaction was kept for longer duration ALP can have an enzymatic effect on ATP also. ATP can be completely hydrolyzed by ALP if incubated for a longer duration.

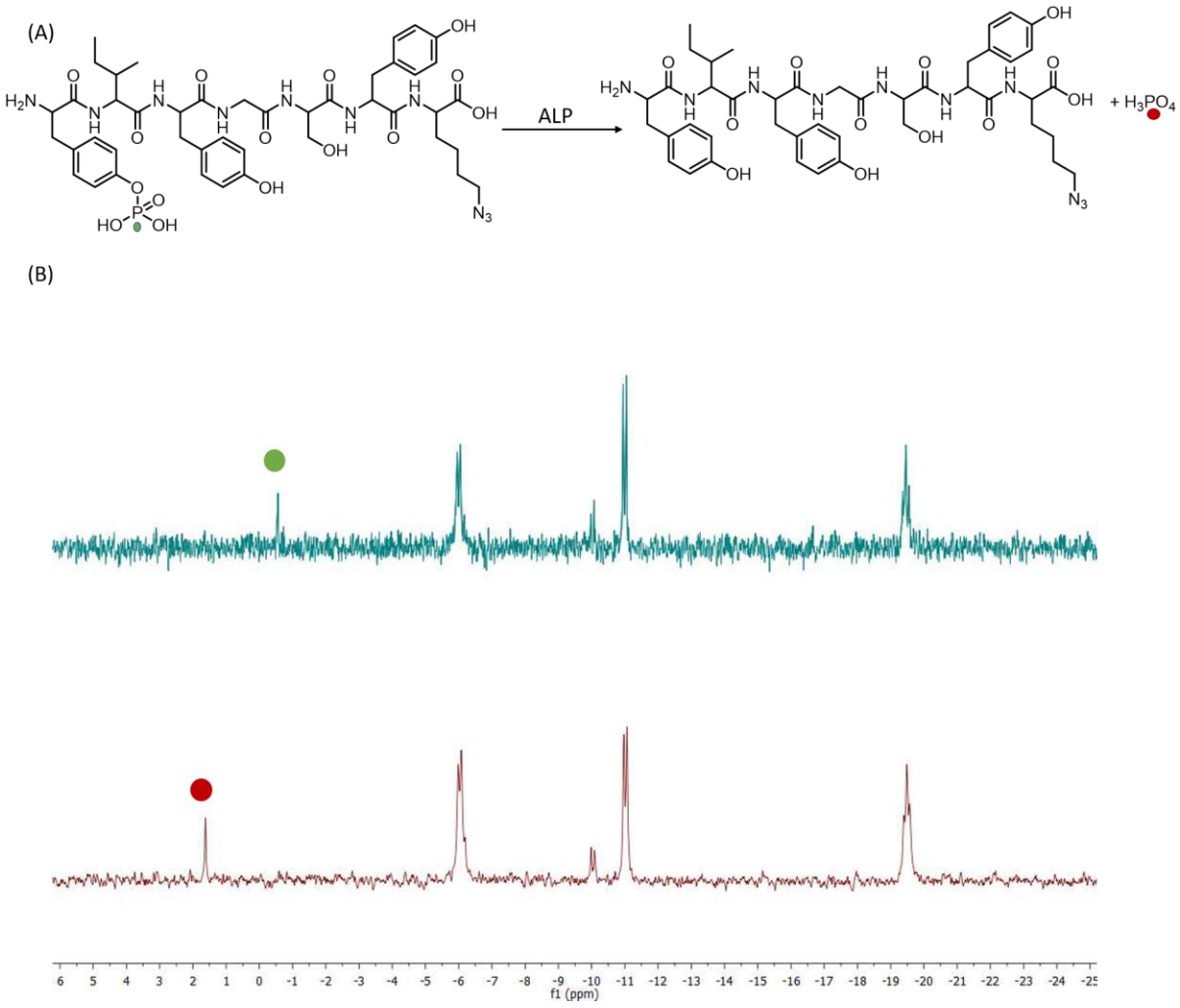

Figure 5.7: Dephosphorylation in the presence of alkaline phosphatase.

5.2.4 Trials to synthesize amphiphilic substrate for kinase

After understanding the enzymatic activity and kinetics of kinase and phosphatase, the synthesis of amphiphilic trimer was carried out. The precursor trimer for the final product was synthesized according to a previously reported procedure from our group. It contains pentaethylene glycol as hydrophilic unit while alkyne moieties were anchored on the hydrophobic unit. A copper mediated

click reaction was carried out to click the peptide substrate on the trimeric precursor to achieve the final product. Product formation was confirmed using MALDI-MS (Figure 5.8).

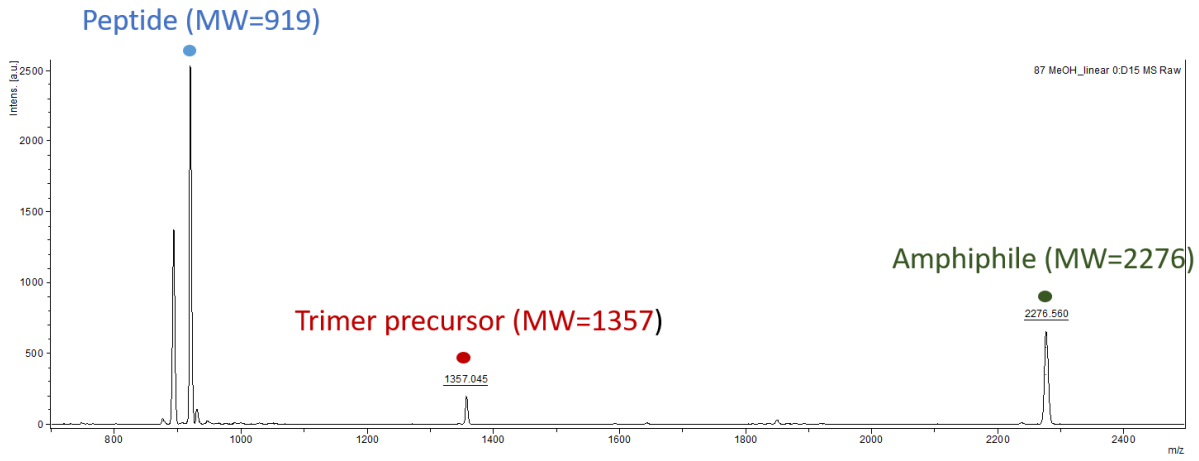

Figure 5.8: MALDI-MS spectra of reaction mixture for trimer synthesis. Note the presence of peak corresponding to the amphiphile.

Even though we observed product formation using MALDI-MS, isolating the product was a big challenge due to its high polarity. Several techniques such as normal chromatography, reverse phase chromatography and preparatory TLS were used to purify the product, but we were not successful in our attempts.

Therefore, we decided to work with a relatively simpler amphiphilic molecule (PA1) (Figure 5.9), which can be easily synthesized using solid phase peptide synthesis method.

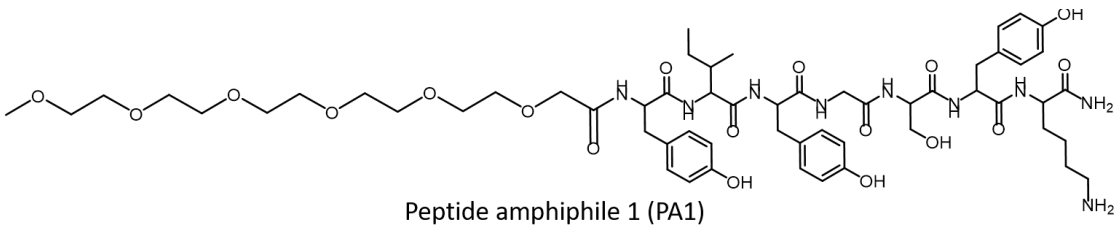

Figure 5.9: Structure of modified amphiphile for kinase.

5.2.5 Self-assembly studies of amphiphile in the absence and presence of kinase

Due to their inherent amphiphilicity, PA1 spontaneously self-assembled under aqueous conditions to form aggregates of size ~100 nm when studied using DLS (Figure 5.10A). Using TEM, micellar morphology of the aggregates was observed (Figure 5.10B).

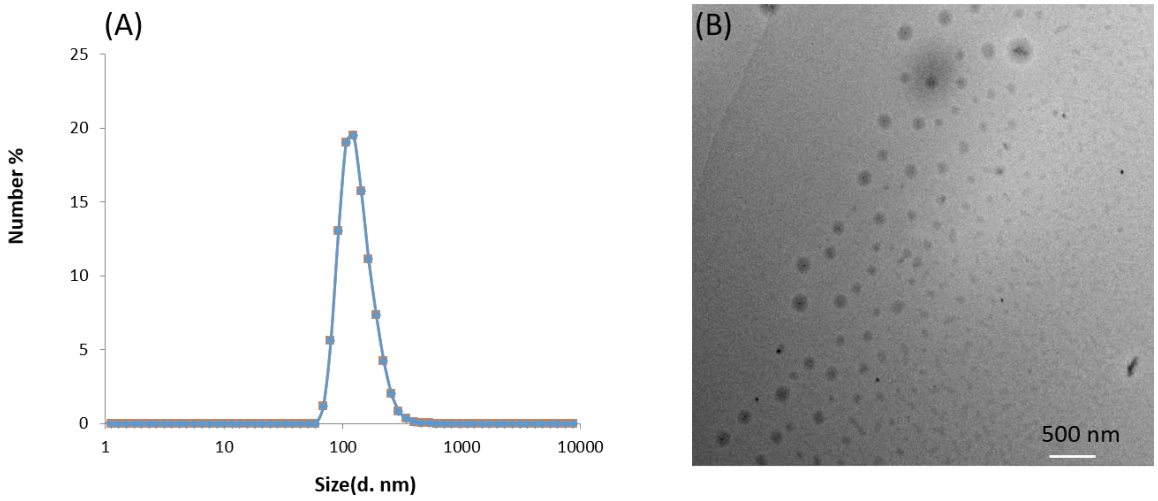

Figure 5.10: (A) DLS profile of **PA1** in water; (B) TEM image of the self-assembled **PA1.**

In the presence of kinase and ATP, peptide sequence gets phosphorylated at the tyrosine residue which changes the overall amphiphilicity of PA1. Therefore, we hypothesized that the self-assembly behavior of PA1 will change significantly after phosphorylation. To test this hypothesis, we incubated PA1 with kinase and ATP overnight, and checked the size of assemblies using dynamic light scattering. The size of aggregates reduced significantly after enzymatic treatment and we reasoned this was due to the loss in amphiphilicity of PA1 after phosphorylation which helps the molecules solubilize under aqueous conditions (Figure 5.11A).

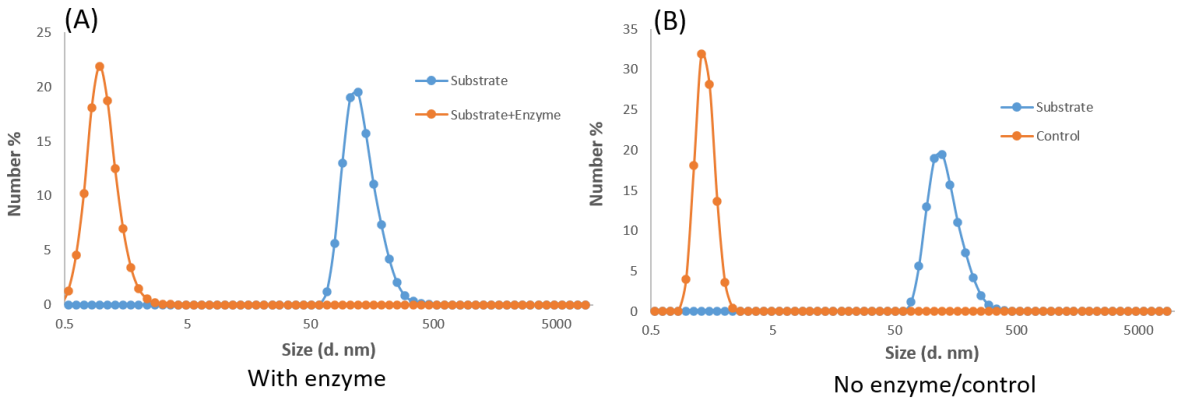

Figure 5.11: (A) DLS profile of **PA1** assemblies after incubation with kinase and ATP; (B) DLS profile of the control experiment when no enzyme and ATP were added.

As a control experiment, we tested the stability of assemblies in the absence of kinase and ATP. We observed a similar decrease in the size of aggregates which revealed that the disassembly in the presence of kinase was not due to the phosphorylation (Figure 5.11B). Rather, it was due to the unstable nature of aggregates which contributed to the disassembly observed in dynamic light scattering

5.2.6 Troubleshooting the challenges and modified approach

After encountering the challenges mentioned in previous sections, instead of designing a different amphiphile, we decided to take a step back and look at the problem more carefully.

To design dissipative systems, a forward process is required to achieve the non-equilibrium state which is sustained in the presence of energy input. The reverse process brings the system back to its resting state. To obtain the non-equilibrium state of a system at any point of time, the kinetics of forward process should be faster than the reverse process. This would allow enough population of the transformed building blocks to self-assemble under non-equilibrium conditions. When we

tried to corroborate this reasoning with the existing reports of dissipative or non-equilibrium system, they indeed had this feature. For example, in dimethyl sulfate mediated non-equilibrium formation of hydrogels, the forward process of methylation of acid groups was faster than ester hydrolysis.[23] This led to the transient formation of hydrogels. In our design hypothesis, kinase serves to bring the system in the non-equilibrium state using ATP as an energy input while phosphatase brings it back to resting state. However, if we compare the kinetics of two processes, the kinetics of phosphorylation by kinase was significantly slower compared to the kinetics of dephosphorylation. At any point of time, even if ATP is added temporally into the system, phosphatase will dominate the process to bring the system back to its resting state. Hydrolysis of ATP by phosphatase was another issue in this design hypothesis.

To navigate these issues, we decided to modify our approach by removing kinase from the system due to its poor kinetics. Instead of covalent modification of building blocks using kinase and ATP mediated phosphorylation, we decided to use non-covalent modification of building blocks to achieve the dissipative structures. Electrostatic interaction between positively charged peptide and negatively charged ATP can be used modify self-assembled peptides into a different nanostructure. Briefly, a positively charged peptide amphiphile can self-assemble into nanofibers in water but in the presence of ATP, they can interact with negative charge present in ATP to form a different self-assembled structure. Phosphatase mediated hydrolysis of ATP weakens the multivalent interactions to restore the initial peptide-based nanofibers. However, adding more ATP to the system can once again lead to self-assembly based on charge mediated interaction between peptide and ATP (Figure 5.12). This way, dissipative self-assembly of peptide can be achieved using electrostatic interaction between peptides and chemical energy input ATP.

Towards that end, we synthesized peptide sequence C17RR, with positively charged arginine groups at the C-terminus for charge mediated interactions with ATP (Figure 5.12).

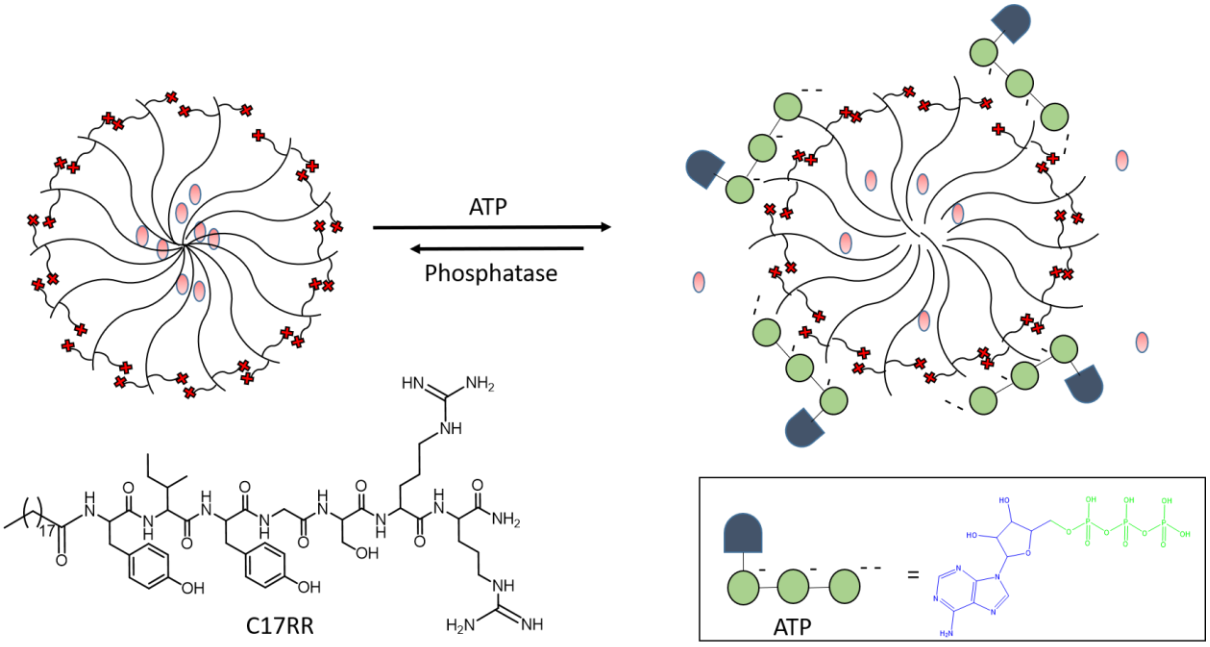

Figure 5.12: Dissipative self-assembly of **C17RR** in the presence of ATP as an energy input.

C17RR was soluble in water due to the presence of charged arginine groups. At a critical aggregate concentration of 100 µM, self-assembled aggregate of size ~50 nm was observed (Figure 5.13). To achieve ATP mediated self-assembly, an equimolar amount of ATP was added which led to the formation of precipitate. This led us to believe that ATP leads to charge mediated cross-linking of peptides, and at a sufficiently high concentration, caused inter particle cross-linking to form precipitate. Upon addition of controlled amount of ATP (20% with respect to amount of positive charge present in arginine groups), we observed stable colloidal particles with little turbidity and

the size of aggregates in the presence of ATP was ~200 nm (Figure 5.13). They were stable for weeks and no precipitation was observed.

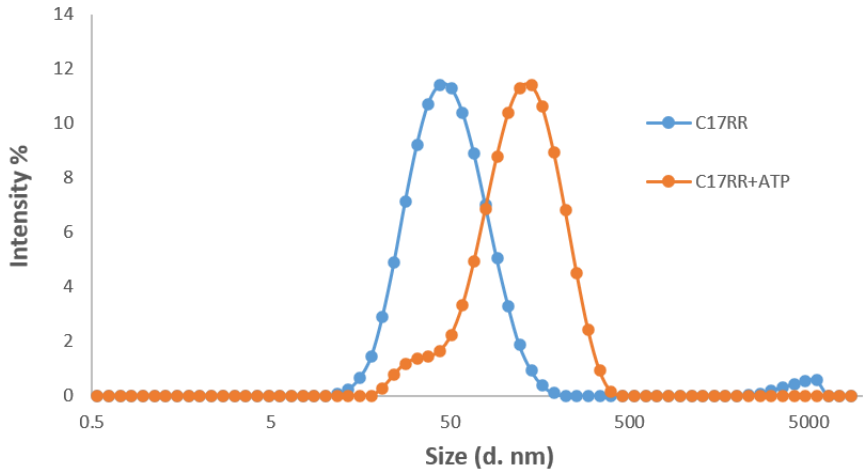

Figure 5.13: DLS profile of **C17RR** in the absence and presence of ATP.

Morphology of self-assembled C17RR was studied using TEM which revealed nanofiber like morphology of length ~50 nm (Figure 5.14A). However, in the presence of ATP, formation of significantly larger cross-linked fibers was obtained which can be attributed to ATP mediated cross-linking of the small C17RR peptide fibers (Figure 5.14B).

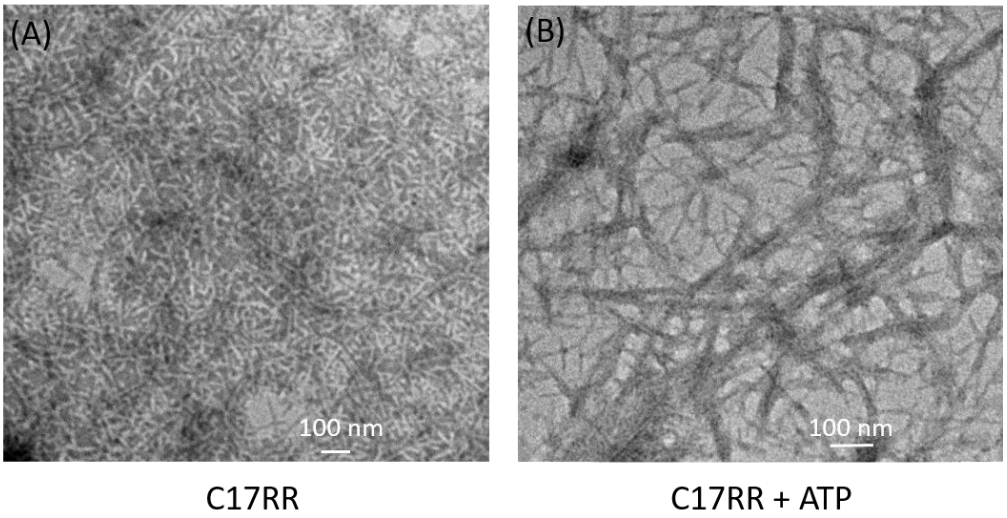

Figure 5.14: TEM images of (A) **C17RR**; (B) **C17RR** + ATP.

To test the reversibility of this process using phosphatase, C17RR+ATP solution was incubated with 3 nM alkaline phosphatase.

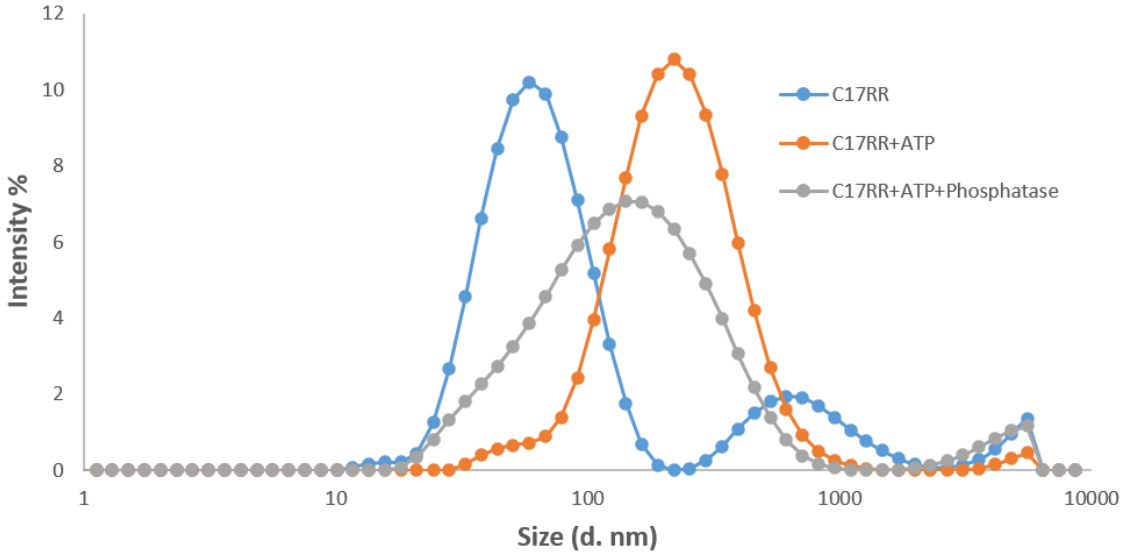

Figure 5.15: DLS profile of **C17RR**; **C17RR** + ATP and **C17RR** + ATP + Phosphatase

After treating the system with phosphatase, we didn't observe a complete reversal in the size of aggregates in DLS studies. Rather, a broad size distribution of particles was obtained which suggested the incomplete hydrolysis of ATP (Figure 5.15). In order to reinitiate the cross-linked fiber formation upon adding ATP as energy input, it was necessary that in the presence of phosphatase, the system completely reverses to its resting uncross-linked state. The presence of a mixture of uncross-linked and cross-linked assemblies made it difficult to understand the dissipative behavior of this system.

5.3 Conclusions

This chapter aimed at creating artificial systems which mimic the non-equilibrium or dissipative behavior of natural systems. Several cellular processes require kinase mediated phosphorylation in the presence of ATP as energy source and its dissipation in the presence of phosphatase for basic survival. A supramolecular self-assembly approach was used to mimic this dynamic process. Phosphorylation and dephosphorylation studies of a peptide substrate using ^{31}P NMR revealed that the kinetics of phosphorylation by kinase was significantly slower compared to phosphatase. Using this study, we learnt that to mimic the natural process, the forward process of phosphorylation in the presence of kinase needs to be faster compared to the reverse dephosphorylation process.

As an alternative, a different approach was used in which we navigated the use of kinase. Multivalent charge mediated interaction between ATP and peptide amphiphiles was used to form cross-linked nanofibers which can dissipate back to their resting state in presence of ATP. However, due to the inefficient activity of phosphatase on peptide bound ATP molecules led to a mixture of cross-linked and uncross-linked assemblies, making the system difficult to study and understand. We learnt the following key points during our attempt to design dissipative systems which should be taken care by researchers working in similar field.

1) The kinetics of forward process should be faster than the backward process to achieve dissipative systems in the presence of chemical input.
2) Ideally, one should minimize waste formation during the covalent or non-covalent modification of building blocks using chemical fuel to sustain the formation of dissipative structures over multiple cycles.
3) Use of dissipative systems to achieve functional response is less explored. It can be harnessed to achieve temporal control over material property in the presence of chemical input.

5.4 Materials and methods

5.4.1 Materials

All the peptides and rink amide resin were purchased from Novabiochem unless otherwise stated. Src, active, GST tagged human, alkaline phosphatase from calf intestine and ATP was purchased from Sigma Aldrich.

5.4.2 Instruments

- **Nuclear Magnetic Resonance (NMR)**

^{1}H NMR spectra were recorded using 400 MHz Bruker NMR spectrometer with residual proton for solvent as a standard. ^{31}P NMR spectra were recorded in 162 MHz Bruker NMR spectrometer using carbon signal of the deuterated solvent as a standard.

- **Dynamic Light Scattering (DLS)**

DLS was performed using Malvern nanozetasizer with a 637 nm laser source with noninvasive backscattering detected at 173°. Standard operating procedure was set up with the following parameters: sample equilibration for 1 min at 25 ^{o}C and then three measurements were taken while each measurement recorded 16 runs.

- **Transmission Electron Microscopy (TEM)**

The sample for DLS was drop casted on carbon coated copper grid and the sample was left for drying overnight. Subsequently, the imaging was done using JEOL-2000FX transmission electron microscope.

5.4.3 General procedure for solid phase peptide synthesis

Rink amide resin (100-200 mesh size) (200 mg, 0.072 mmol) was added in the peptide synthesizer. It was soaked by washing it with 2 mL DMF. The fmoc groups from the resin were deprotected using 2 mL of 20% piperidine solution in DMF for 10 min. Subsequently, the solution of amino acids (0.216 mmol) was prepared in 2 mL DMF, DIPEA (0.216 mmol) and HATU (0.216 mmol). It was added to the rink amide resin and the reaction was shaken multiple times over a period of 30 min. Fmoc groups were deprotected in the similar way as the rink amide deprotection. The protection deprotection cycle was continued until the final amino acid was attached to the sequence. The protection and deprotection was monitored using Kaiser test (It was prepared by mixing 5 mg ninhydrin in 100 mL ethanol, 80 g phenol in 20 mL ethanol and 2 mL of 0.001M aq. KCN in 98 mL pyridine).

5.5 References

(1) Philp, D.; Fraser Stoddart, J. Self-Assembly in Natural and Unnatural Systems. *Angew. Chem. Int. Ed.* **1996**, *35* (11), 1154–1196.

(2) Lehn, J. M. Toward Self-Organization and Complex Matter. *Science* **2002**, *295* (5564) 2400–2403.

(3) Whitesides, G. M.; Mathias, J. P.; Seto, C. T. Molecular Self-Assembly and Nanochemistry: A Chemical Strategy for the Synthesis of Nanostructures. *Science* **1991**, *254* (5036), 1312–1319.

(4) Lawrence, D. S.; Jiang, T.; Levett, M. Self-Assembling Supramolecular Complexes. *Chem. Rev.* **1995**, *95* (6), 2229–2260.

(5) Lehn, J. -M. Perspectives in Supramolecular Chemistry—From Molecular Recognition towards Molecular Information Processing and Self-Organization. *Angew. Chem. Int. Ed.* **1990**, *29* (11), 1304–1319.

(6) Whitesides, G. M.; Simanek, E. E.; Mathias, J. P.; Seto, C. T.; Chin, D. N.; Mammen, M.; Gordon, D. M. Noncovalent Synthesis: Using Physical-Organic Chemistry to Make Aggregates. *Acc. Chem. Res.* **1995**, *28* (1), 37–44.

(7) Fyfe, M. C. T.; Stoddart, J. F. Synthetic Supramolecular Chemistry. *Acc. Chem. Res.* **1997**, *30* (10), 393–401.

(8) Mattia, E.; Otto, S. Supramolecular Systems Chemistry. *Nat. Nanotechnol*. **2015**, *10* (2), 111–119.

(9) Galimov, E. M. Phenomenon of Life: Between Equilibrium and Non-Linearity. *Orig. Life*

Evol. Biosph. **2004**, *34* (6), 599–613.

(10) Heald, R.; Nogales, E. Microtubule Dynamics. *J. Cell Sci.* **2002**, *115* (1).

(11) Hess, H.; Ross, J. L. Non-Equilibrium Assembly of Microtubules: From Molecules to Autonomous Chemical Robots. *Chem. Soc. Rev.* **2017**, *46* (18), 5570–5587.

(12) Cassimeris, L.; Pryer, N. K.; Salmon, E. D. Real-Time Observations of Microtubule Dynamic Instability in Living Cells. *J. Cell Biol.* **1988**, *107* (6 I), 2223–2231.

(13) Honore, S.; Pasquier, E.; Braguer, D. Understanding Microtubule Dynamics for Improved Cancer Therapy. *Cellular and Molecular Life Sciences* **2005**, *62* (24), 3039–3056.

(14) Berenbaum, F.; Humbert, L.; Bereziat, G.; Thirion, S. Concomitant Recruitment of ERK1/2 and P38 MAPK Signalling Pathway Is Required for Activation of Cytoplasmic Phospholipase A2 via ATP in Articular Chondrocytes. *J. Biol. Chem.* **2003**, *278* (16), 13680–13687.

(15) De Keyzer, J.; Van Der Does, C.; Driessen, A. J. M. The Bacterial Translocase: A Dynamic Protein Channel Complex. *Cellular and Molecular Life Sciences* **2003**, *60* (10), 2034–2052.

(16) Riccio, A. Dynamic Epigenetic Regulation in Neurons: Enzymes, Stimuli and Signaling Pathways. *Nat. Neurosc.* **2010**, *13* (11), 1330–1337.

(17) Tatsumi, T.; Shiraishi, J.; Keira, N.; Akashi, K.; Mano, A.; Yamanaka, S.; Matoba, S.; Fushiki, S.; Fliss, H.; Nakagawa, M. Intracellular ATP Is Required for Mitochondrial Apoptotic Pathways in Isolated Hypoxic Rat Cardiac Myocytes. *Cardiovasc. Res.* **2003**, *59* (2), 428–440.

(18) Hilgemann, D. W. Cytoplasmic ATP-dependent Regulation of Ion Transporters and Channels: Mechanisms and Messengers. *Annu. Rev. Physiol.* **1997**, *59* (1), 193–220.

(19) Van Esch, J. H.; Klajn, R.; Otto, S. Chemical Systems out of Equilibrium. *Chem. Soc. Rev*. **2017**, *46* (18), 5474–5475.

(20) Van Rossum, S. A. P.; Tena-Solsona, M.; Van Esch, J. H.; Eelkema, R.; Boekhoven, J. Dissipative Out-of-Equilibrium Assembly of Man-Made Supramolecular Materials. *Chem. Soc. Rev*. **2017**, *46* (18), 5519–5535.

(21) De, S.; Klajn, R. Dissipative Self-Assembly Driven by the Consumption of Chemical Fuels. *Adv. Mater.* **2018**, *30* (41), 1706750.

(22) Rieß, B.; Grötsch, R. K.; Boekhoven, J. The Design of Dissipative Molecular Assemblies Driven by Chemical Reaction Cycles. *Chem* **2019**, *6* (3), 552–578.

(23) Boekhoven, J.; Hendriksen, W. E.; Koper, G. J. M.; Eelkema, R.; Van Esch, J. H. Transient Assembly of Active Materials Fueled by a Chemical Reaction. *Science* **2015**, *349* (6252), 1075–1079.

(24) Boekhoven, J.; Brizard, A. M.; Kowlgi, K. N. K.; Koper, G. J. M.; Eelkema, R.; Van Esch, J. H. Dissipative Self-Assembly of a Molecular Gelator by Using a Chemical Fuel. *Angew. Chem. Int. Ed.* **2010**, *49* (28), 4825–4828.

(25) Klajn, R.; Bishop, K. J. M.; Grzybowski, B. A. Light-Controlled Self-Assembly of Reversible and Irreversible Nanoparticle Suprastructures. *Proc. Natl. Acad. Sci. U. S. A.* **2007**, *104* (25), 10305–10309.

(26) Dhiman, S.; Jain, A.; Kumar, M.; George, S. J. Adenosine-Phosphate-Fueled, Temporally

Programmed Supramolecular Polymers with Multiple Transient States. *J. Am. Chem. Soc.* **2017**, *139* (46), 16568–16575.

(27) Maiti, S.; Fortunati, I.; Ferrante, C.; Scrimin, P.; Prins, L. J. Dissipative Self-Assembly of Vesicular Nanoreactors. *Nat. Chem.* **2016**, *8* (7), 725–731.

(28) Wirth, A.; Benyó, Z.; Lukasova, M.; Leutgeb, B.; Wettschureck, N.; Gorbey, S.; Orsy, P.; Horváth, B.; Maser-Gluth, C.; Greiner, E.; et al. G12-G13-LARG-Mediated Signaling in Vascular Smooth Muscle Is Required for Salt-Induced Hypertension. *Nat. Med.* **2008**, *14* (1), 64–68.

(29) Geiger, D.; Scherzer, S.; Mumm, P.; Stange, A.; Marten, I.; Bauer, H.; Ache, P.; Matschi, S.; Liese, A.; Al-Rasheid, K. A. S.; et al. Activity of Guard Cell Anion Channel SLAC1 Is Controlled by Drought-Stress Signaling Kinase-Phosphatase Pair. *Proc. Natl. Acad. Sci. U. S. A.* **2009**, *106* (50), 21425–21430.

(30) Wettschureck, N.; Offermanns, S. Rho/Rho-Kinase Mediated Signaling in Physiology and Pathophysiology. *J. Mol. Med.* **2002**, *80* (10), 629–638.

(31) Lee, S. C.; Lan, W.; Buchanan, B. B.; Luan, S. A Protein Kinase-Phosphatase Pair Interacts with an Ion Channel to Regulate ABA Signaling in Plant Guard Cells. *Proc. Natl. Acad. Sci. U. S. A.* **2009**, *106* (50), 21419–21424.

CHAPTER 6

SUMMARY AND FUTURE DIRECTIONS

6.1 Summary

Depolymerizable and dissipative chemical systems have great potential to be used as a tool in the development of smart materials. The sensitivity of depolymerizable systems to a stimulus giving an amplified response is desirable in applications where a trace amount of input signal leads to a macroscopic change in the property of material. For example, by coating surfaces with materials synthesized using depolymerizable systems and healing agents encapsulated within, we can potentially protect the coated surfaces. By triggering the materials with external stimuli such as UV light, triggered release of healing agents from the material can be used to treat the damaged surface. A proof of concept of such demonstration was shown in chapter 1. Upon UV illumination, enzyme containing vesicles were degraded leading to enzyme release and formation of cross-linked network hydrogel. The strength of hydrogel can be controlled by tuning the duration of UV illumination which dictated the amount of enzyme getting released and hence the cross-linking.

In biological systems, enzymes are expressed in a very complex way. This requires synthesis of enzyme responsive materials which can show a rapid as well as sustained response when treated with enzyme. Because of the sensitivity of depolymerizable systems to enzymes as stimuli, they are excellent candidate for biological applications. However, in the existing literature, there are limited reports to achieve a rapid functional response due to poor accessibility of substrate by enzyme. Chapter 3 was aimed at overcoming this shortcoming. By modifying ALP triggerable polymer in a hydrophobic, materials which show rapid degradation in response to ALP was

formulated using emulsion techniques. The location of phosphate group in the formulated material, was crucial for rapid enzymatic response.

Most of the studies related to depolymerizable systems have been carried out in bulk solution or in solid state. However, triggered depolymerization at the interface of two phases is equally interesting because molecular change in one phase can affect the property of the other. If the depolymerization event in one phase leads to a macroscopic and observable change in the property of other, the system could serve as a sensing tool to detect trace amount of stimulus. To address this gap in knowledge, a depolymerizable polyelectrolyte-surfactant complex was studied at the interface of liquid crystals in chapter 4. Before triggering with ALP, the complex showed planar anchoring transitions at the interface. However, after ALP triggered depolymerization, the small molecule byproducts and surfactant showed homeotropic with some planar anchoring domains, which was reflected in the optical signature of liquid crystals. This is a demonstration of utilizing a trace enzymatic stimulus to bring a macroscopic change in the property of material through depolymerization.

Chapter 5 was different from the preceding chapters in terms of concept. Dissipative systems are ubiquitous in natural system where they show functional response in presence of energy input such as ATP or GTP. However, there are only few reported synthetic dissipative systems which show functional response in presence of a chemical input. In this chapter, with an aim to develop synthetic dissipative systems, an amphiphilic system which can show dynamic self-assembly in presence of kinase & phosphatase and ATP as energy input was studied. However, due to significantly different kinetics of kinase and phosphatase, the desired self-assembly features in the system was not observed. Potential solution to the problems encountered in this chapter are discussed in the future directions section.

6.2 Future directions

6.2.1 Future directions for chapter 2

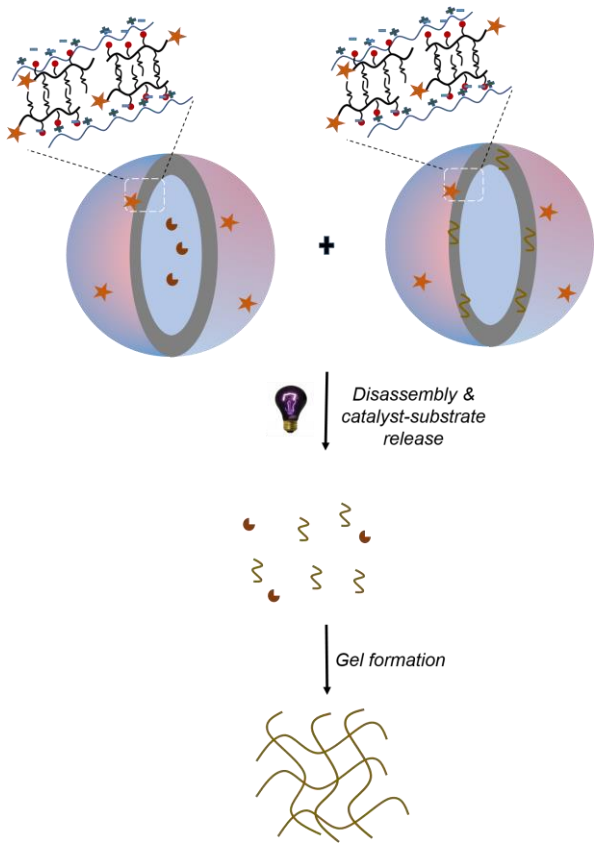

Figure 6.1: Compartmentalization of enzyme as well as substrate in a nanocontainer and its triggered release to form hydrogel.

As an extension of the methodology developed for on demand cross-linking of materials, it would be advantageous to compartmentalize the catalyst as well as substrate inside nanoparticles. In the current study, enzymatic substrate was dispersed in the aqueous bulk which limits its use in coating applications. Compartmentalization of catalyst and substrate into capsule like structures, could be advantageous in coating surfaces because the capsules can be easily dispersed in a medium for coating a substrate. Triggering the capsules containing catalyst and substrate using stimuli can lead to surface curing. Another advantage of this strategy is that it provides an opportunity to cure

surfaces using an external stimulus at room temperature. While existing techniques require high temperature to cure a surface, it significantly increases the energy cost. Triggered release of catalyst and substrate from capsules to cure surfaces provides an ideal methodology to significantly reduce the energy cost in coating applications.

6.2.2 Future directions for chapter 3

In this chapter, we outlined the conditions for a rapid degradation of materials synthesized using depolymerizable polymers. To achieve an even broader range of response, strategies need to be developed for achieving controlled and sustained degradation. This could be accomplished by varying enzyme concentration in the case of polyelectrolyte complexes. Since the poor accessibility of substrate by enzyme was leading to a slower degradation response, increasing enzyme concentration can help to improve the degradation kinetics and achieve intermediate depolymerization kinetics of the poly-ion complex.

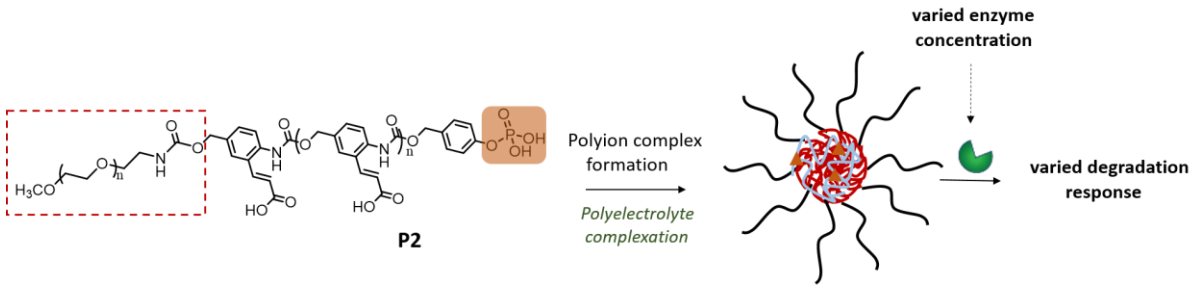

Figure 6.2: Varied degradation response of poly-ion complex in response to enzyme concentration.

6.2.3 Future directions for chapter 4

This chapter involved polyelectrolyte-surfactant complex formation using depolymerizable polyelectrolyte and CTAB surfactant. The key thing we learnt in this study was the interfacial behavior of complex and its varied response in presence of ALP. There is plenty of opportunities

in terms of the use of surfactants and lipids with varying tail length to achieve a variety of nanoarchitectures. By taking advantage of the depolymerization feature, in situ transformation of the morphology of materials can be accomplished.

6.2.4 Future directions for chapter 5

Most research focused on this topic deals with the use of fuel to achieve the dissipative self-assembled structure which can revert to its thermodynamic state when the energy input is ceased. Although our approach in this chapter seemed reasonable on paper, its execution was challenging due to significantly slow phosphorylation kinetics by enzyme kinase. However, during the process, we learnt that to design dissipative systems, the forward kinetics leading to the dissipative self-assembly needs to be faster than the backward kinetics. In the past few years, significant attention has been given to the use of a variety of chemistry that can lead to self-assembly under dissipative conditions or upon fuel consumption. It is one of the directions in which constant effort is being made. However, in order to achieve a dynamic functional response, it is required that we take advantage of the dissipative self-assembled structure.

For example, in the work done by Maiti et al, they took advantage of the dissipative vesicular structures to carry out a transient chemical reaction between two non-polar substrates. By using the dissipative self-assembly as a tool to achieve a dynamic functional response, one can think of designing autonomous materials which does a function only in the presence of energy input. Once the input energy is consumed, it shuts itself off. To restart the process, the system needs to be supplied more chemical input. This opens up a significantly exciting area of materials with adaptive and dynamic functions.

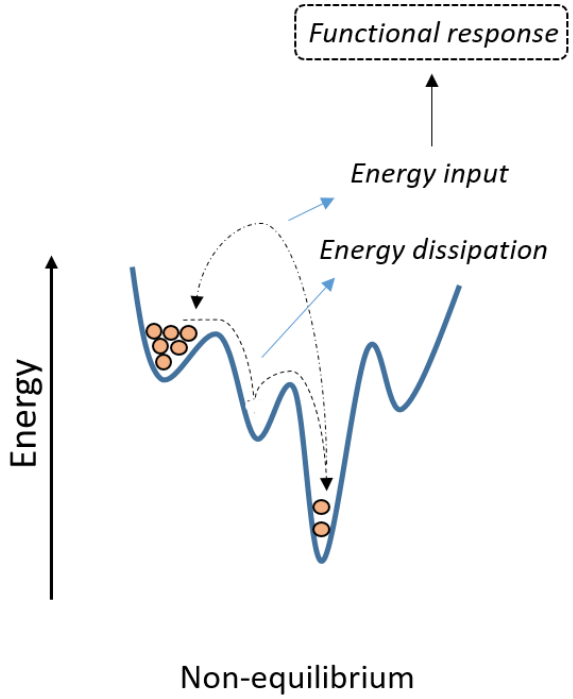

Figure 6.3: Energy profile of dissipative systems showing functional response when supplied with an energy input.

BIBLIOGRAPHY

Amir, R. J.; Pessah, N.; Shamis, M.; Shabat, D. Self-Immolative Dendrimers. *Angew. Chem. Int. Ed.* **2003**, *42* (37), 4494–4499.

Alouane, A.; Labruère, R.; Le Saux, T.; Schmidt, F.; Jullien, L. Self-Immolative Spacers: Kinetic Aspects, Structure-Property Relationships, and Applications. *Angew. Chem. Int. Ed*. **2015**, *54* (26), 7492–7509.

Aso, C.; Tagami, S.; Kunitake, T. Polymerization of Aromatic Aldehydes. II. Cationic Cyclopolymerization of Phthalaldehyde. *J. Polym. Sci. Part A-1 Polym. Chem.* **1969**, *7* (2), 497–511.

Ahmad, H.; Sehgal, S.; Mishra, A.; Gupta, R. Mimosa Pudica L. (Laajvanti): An Overview. *Pharm. Rev.* 2012, 6 (12), 115–124.

Alouane, A.; Labruère, R.; Le Saux, T.; Schmidt, F.; Jullien, L. Self-Immolative Spacers: Kinetic Aspects, Structure-Property Relationships, and Applications. *Angew. Chem. Int. Ed.* **2015**, *54* (26), 7492–7509.

Antonietti, M.; Thünemann, A. Polyelectrolyte-Lipid Complexes as Membrane Mimetic Systems. *Curr. Opin. Colloid Interface Sci.* **1996**, *1* (5), 667–671.

Antonietti, M.; Conrad, J.; Thünemann, A. Polyelectrolyte-Surfactant Complexes: A New Type of Solid, Mesomorphous Material. *Macromolecules* **1994**, *27* (21), 6007–6011.

Azagarsamy, M. A.; Sokkalingam, P.; Thayumanavan, S. Enzyme-Triggered Disassembly of Dendrimer-Based Amphiphilic Nanocontainers. *J. Am. Chem. Soc.* **2009**, *131* (40), 14184–14185.

Borrelle, S. B.; Rochman, C. M.; Liboiron, M.; Bond, A. L.; Lusher, A.; Bradshaw, H.; Provencher, J. F. Why We Need an International Agreement on Marine Plastic Pollution. *Proc. Nat. Acad. Sci. U. S. A.* **2017,** *114* (38), 9994–9997.

Boekhoven, J.; Hendriksen, W. E.; Koper, G. J. M.; Eelkema, R.; Van Esch, J. H. Transient Assembly of Active Materials Fueled by a Chemical Reaction. *Science* **2015**, *349* (6252), 1075–1079.

Baker, M. S.; Kim, H.; Olah, M. G.; Lewis, G. G.; Phillips, S. T. Depolymerizable Poly(Benzyl Ether)-Based Materials for Selective Room Temperature Recycling. *Green Chem.* **2015**, *17* (9), 4541–4545.

Bai, G.; Nichifor, M.; Lopes, A.; Bastos, M. Thermodynamic Characterization of the Interaction Behavior of a Hydrophobically Modified Polyelectrolyte and Oppositely Charged Surfactants in Aqueous Solution: Effect of Surfactant Alkyl Chain Length. *J. Phys. Chem. B* **2005**, *109* (1), 518–525.

Berenbaum, F.; Humbert, L.; Bereziat, G.; Thirion, S. Concomitant Recruitment of ERK1/2 and P38 MAPK Signalling Pathway Is Required for Activation of Cytoplasmic Phospholipase A2 via ATP in Articular Chondrocytes. *J. Biol. Chem.* **2003**, *278* (16), 13680–13687.

Boekhoven, J.; Hendriksen, W. E.; Koper, G. J. M.; Eelkema, R.; Van Esch, J. H. Transient Assembly of Active Materials Fueled by a Chemical Reaction. *Science* **2015**, *349* (6252), 1075–1079.

Boekhoven, J.; Brizard, A. M.; Kowlgi, K. N. K.; Koper, G. J. M.; Eelkema, R.; Van Esch, J. H. Dissipative Self-Assembly of a Molecular Gelator by Using a Chemical Fuel. *Angew. Chem. Int. Ed.* **2010**, *49* (28), 4825–4828.

Blum, A. P.; Kammeyer, J. K.; Yin, J.; Crystal, D. T.; Rush, A. M.; Gilson, M. K.; Gianneschi, N. C. Peptides Displayed as High Density Brush Polymers Resist Proteolysis and Retain Bioactivity. *J. Am. Chem. Soc.* **2014**, *136* (43), 15422–15437.

Carl, P. L.; Chakravarty, P. K.; Katzenellenbogen, J. A. A Novel Connector Linkage Applicable in Prodrug Design. *J. Med. Chem.* **1981**, *24* (5), 479–480.

Chen, E. K. Y.; McBride, R. A.; Gillies, E. R. Self-Immolative Polymers Containing Rapidly Cyclizing Spacers: Toward Rapid Depolymerization Rates. *Macromolecules* **2012**, *45* (18), 7364–7374.

Carlton, R. J.; Hunter, J. T.; Miller, D. S.; Abbasi, R.; Mushenheim, P. C.; Tan, L. N.; Abbott, N. L. Chemical and Biological Sensing Using Liquid Crystals. *Liq. Cryst. Rev.* **2013**, *1* (1), 29–51.

Cassimeris, L.; Pryer, N. K.; Salmon, E. D. Real-Time Observations of Microtubule Dynamic Instability in Living Cells. *J. Cell Biol.* **1988**, *107* (6 I), 2223–2231.

Cassimeris, L.; Pryer, N. K.; Salmon, E. D. Real-Time Observations of Microtubule Dynamic Instability in Living Cells. *J. Cell Biol.* **1988**, *107* (6 I), 2223–2231.

De Gracia Lux, C.; Joshi-Barr, S.; Nguyen, T.; Mahmoud, E.; Schopf, E.; Fomina, N.; Almutairi, A. Biocompatible Polymeric Nanoparticles Degrade and Release Cargo in Response to Biologically Relevant Levels of Hydrogen Peroxide. *J. Am. Chem. Soc.* **2012**, *134* (38), 15758–15764.

DiLauro, A. M.; Lewis, G. G.; Phillips, S. T. Self-Immolative Poly(4,5-Dichlorophthalaldehyde) and Its Applications in Multi-Stimuli-Responsive Macroscopic Plastics. *Angew. Chem. Int. Ed.* **2015**, *127* (21), 6298–6303.

DeWit, M. A.; Gillies, E. R. A Cascade Biodegradable Polymer Based on Alternating Cyclization and Elimination Reactions. *J. Am. Chem. Soc.* **2009**, *131* (51), 18327–18334.

Dhanasekaran, S. M.; Barrette, T. R.; Ghosh, D.; Shah, R.; Varambally, S.; Kurachi, K.; Pienta, K. J.; Rubin, M. A.; Chinnaiyan, A. M. Delineation of Prognostic Biomarkers in Prostate Cancer. *Nature* **2001**, *412* (6849), 822–826.

De Gracia Lux, C.; McFearin, C. L.; Joshi-Barr, S.; Sankaranarayanan, J.; Fomina, N.; Almutairi, A. Single UV or near IR Triggering Event Leads to Polymer Degradation into Small Molecules. *ACS Macro Lett.* **2012**, *1* (7), 922–926.

Dhiman, S.; Jain, A.; Kumar, M.; George, S. J. Adenosine-Phosphate-Fueled, Temporally Programmed Supramolecular Polymers with Multiple Transient States. *J. Am. Chem. Soc.* **2017**, *139* (46), 16568–16575.

Dhiman, S.; Jain, A.; George, S. J. Transient Helicity: Fuel-Driven Temporal Control over Conformational Switching in a Supramolecular Polymer. *Angew. Chem. Int. Ed.* **2017**, *56* (5), 1329–1333.

Downing, S. W.; Spitzer, R. H.; Koch, E. A.; Salo, W. L. The Hagfish Slime Gland Thread Cell. I. A Unique Cellular System for the Study of Intermediate Filaments and Intermediate Filament-Microtubule Interactions. *J. Cell Biol.* **1984**, *98* (2), 653–669.

Dhanasekaran, S. M.; Barrette, T. R.; Ghosh, D.; Shah, R.; Varambally, S.; Kurachi, K.; Pienta, K. J.; Rubin, M. A.; Chinnaiyan, A. M. Delineation of Prognostic Biomarkers in Prostate Cancer. *Nature* **2001**, *412* (6849), 822–826.

Ding, Y.; Kang, Y.; Zhang, X. Enzyme-Responsive Polymer Assemblies Constructed through Covalent Synthesis and Supramolecular Strategy. *Chem. Commun.* **2015**, *51* (6), 996–1003.

Dautzenberg, H.; Jaeger, W. Effect of Charge Density on the Formation and Salt Stability of Polyelectrolyte Complexes. *Macromol. Chem. Phys.* **2002**, *203* (14), 2095–2102.

De Keyzer, J.; Van Der Does, C.; Driessen, A. J. M. The Bacterial Translocase: A Dynamic Protein Channel Complex. *Cellular and Molecular Life Sciences* **2003**, *60* (10), 2034–2052.

De, S.; Klajn, R. Dissipative Self-Assembly Driven by the Consumption of Chemical Fuels. *Adv. Mater.* **2018**, *30* (41), 1706750.

Esser-Kahn, A. P.; Sottos, N. R.; White, S. R.; Moore, J. S. Programmable Microcapsules from Self-Immolative Polymers. *J. Am. Chem. Soc.* **2010**, *132* (30), 10266–10268.

Ergene, C.; Palermo, E. F. Cationic Poly(Benzyl Ether)s as Self-Immolative Antimicrobial Polymers. *Biomacromolecules* **2017**, *18* (10), 3400–3409.

Fomina, N.; McFearin, C.; Sermsakdi, M.; Edigin, O.; Almutairi, A. UV and Near-IR Triggered Release from Polymeric Nanoparticles. *J. Am. Chem. Soc.* **2010**, *132* (28),

9540–9542.

Fudge, D. S.; Levy, N.; Chiu, S.; Gosline, J. M. Composition, Morphology and Mechanics of Hagfish Slime. *J. Exp. Biol.* **2005**, *208* (24), 4613–4625.

Fyfe, M. C. T.; Stoddart, J. F. Synthetic Supramolecular Chemistry. *Acc. Chem. Res.* **1997**, *30* (10), 393–401.

Gnaim, S.; Shabat, D. Self-Immolative Chemiluminescence Polymers: Innate Assimilation of Chemiexcitation in a Domino-like Depolymerization. *J. Am. Chem. Soc.* **2017**, *139* (29), 10002–10008.

Galimov, E. M. Phenomenon of Life: Between Equilibrium and Non-Linearity. *Orig. Life Evol. Biosph.* **2004**, *34* (6), 599–613.

Geiger, D.; Scherzer, S.; Mumm, P.; Stange, A.; Marten, I.; Bauer, H.; Ache, P.; Matschi, S.; Liese, A.; Al-Rasheid, K. A. S.; et al. Activity of Guard Cell Anion Channel SLAC1 Is Controlled by Drought-Stress Signaling Kinase-Phosphatase Pair. *Proc. Natl. Acad. Sci. U. S. A.* **2009**, *106* (50), 21425–21430.

Haward, M. Plastic Pollution of the World's Seas and Oceans as a Contemporary Challenge in Ocean Governance. *Nat. Commun.* **2018**, 9 (1), 1-3.

Haba, K.; Popkov, M.; Shamis, M.; Lerner, R. A.; Barbas, C. F.; Shabat, D. Single-Triggered Trimeric Prodrugs. *Angew. Chem. Int. Ed.* **2005**, *44* (5), 716–720.

Heald, R.; Nogales, E. Microtubule Dynamics. *J. Cell Sci.* **2002**, *115* (1).

Hu, J.; Zhang, G.; Liu, S. Enzyme-Responsive Polymeric Assemblies, Nanoparticles and Hydrogels. *Chem. Soc. Rev.* **2012**, *41* (18), 5933–5949.

Harnoy, A. J.; Rosenbaum, I.; Tirosh, E.; Ebenstein, Y.; Shaharabani, R.; Beck, R.; Amir, R. J. Enzyme-Responsive Amphiphilic PEG-Dendron Hybrids and Their Assembly into Smart Micellar Nanocarriers. *J. Am. Chem. Soc.* **2014**, *136* (21), 7531–7534.

Heald, R.; Nogales, E. Microtubule Dynamics. *J. Cell Sci.* **2002**, *115* (1).

Hess, H.; Ross, J. L. Non-Equilibrium Assembly of Microtubules: From Molecules to Autonomous Chemical Robots. *Chem. Soc. Rev.* **2017**, *46* (18), 5570–5587.

Honore, S.; Pasquier, E.; Braguer, D. Understanding Microtubule Dynamics for Improved Cancer Therapy. *Cellular and Molecular Life Sciences* **2005**, *62* (24), 3039–3056.

Hilgemann, D. W. Cytoplasmic ATP-dependent Regulation of Ion Transporters and Channels: Mechanisms and Messengers. *Annu. Rev. Physiol.* **1997**, *59* (1), 193–220.

Klajn, R.; Bishop, K. J. M.; Grzybowski, B. A. Light-Controlled Self-Assembly of Reversible and Irreversible Nanoparticle Suprastructures. *Proc. Natl. Acad. Sci. U. S. A.*

2007, *104* (25), 10305–10309.

Koch, E. A.; Spitzer, R. H.; Pithawalla, R. B.; Parry, D. A. An Unusual Intermediate Filament Subunit from the Cytoskeletal Biopolymer Released Extracellularly into Seawater by the Primitive Hagfish (Eptatretus Stouti). *J. Cell Sci.* **1994**, *107* (11), 3133-3144.

Kim, H.; Mohapatra, H.; Phillips, S. T. Rapid, On-Command Debonding of Stimuli-Responsive Cross-Linked Adhesives by Continuous, Sequential Quinone Methide Elimination Reactions. *Angew. Chemi. Int. Ed.* **2015**, *127* (44), 13255–13259.

Kogej, K.; Theunissen, E.; Reynaers, H. Effect of Polyion Charge Density on the Morphology of Nanostructures in Polyelectrolyte−Surfactant Complexes. *Langmuir* **2002**, *18* (23), 8799–8805.

Kishimura, A. Development of Polyion Complex Vesicles (PICsomes) from Block Copolymers for Biomedical Applications. *Polymer Journal* **2013**, *45* (9), 892–897.

Kang, J. H.; Asai, D.; Kim, J. H.; Mori, T.; Toita, R.; Tomiyama, T.; Asami, Y.; Oishi, J.; Sato, Y. T.; Niidome, T.; et al. Design of Polymeric Carriers for Cancer-Specific Gene Targeting: Utilization of Abnormal Protein Kinase Cα Activation in Cancer Cells. *J. Am. Chem. Soc.* **2008**, *130* (45), 14906–14907.

Kim, K.; Bae, B.; Kang, Y. J.; Nam, J. M.; Kang, S.; Ryu, J. H. Natural Polypeptide-Based Supramolecular Nanogels for Stable Noncovalent Encapsulation. *Biomacromolecules* **2013**, *14* (10), 3515–3522.

Kayitmazer, A. B. Thermodynamics of Complex Coacervation. *Adv. Coll. Int. Sci*. **2017**, *239*, 169–177.

Kosmella, S.; Kötz, J.; Shirahama, K.; Liu, J. Cooperative Nature of Complex Formation in Mixed Polyelectrolyte-Surfactant Systems. *J. Phys. Chem. B* **1998**, *102* (34), 6459–6464.

Kinsinger, M. I.; Buck, M. E.; Campos, F.; Lynn, D. M.; Abbott, N. L. Dynamic Ordering Transitions of Liquid Crystals Driven by Interfacial Complexes Formed between Polyanions and Amphiphilic Polyamines. *Langmuir* **2008**, *24* (23), 13231–13236.

Kumar, V.; Harris, J. T.; Ribbe, A.; Franc, M.; Bae, Y.; McNeil, A. J.; Thayumanavan, S. Construction from Destruction: Hydrogel Formation from Triggered Depolymerization-Based Release of an Enzymatic Catalyst. *ACS Macro Lett.* **2020**, 377–381.

Li, S.; Szalai, M. L.; Kevwitch, R. M.; McGrath, D. V. Dendrimer Disassembly by Benzyl Ether Depolymerization. *J. Am. Chem. Soc.* **2003**, *125* (35), 10516–10517.

Liu, G.; Wang, X.; Hu, J.; Zhang, G.; Liu, S. Self-Immolative Polymersomes for High-

Efficiency Triggered Release and Programmed Enzymatic Reactions. *J. Am. Chem. Soc.* **2014**, *136* (20), 7492–7497.

Liu, G.; Zhang, G.; Hu, J.; Wang, X.; Zhu, M.; Liu, S. Hyperbranched Self-Immolative Polymers (HSIPs) for Programmed Payload Delivery and Ultrasensitive Detection. *J. Am. Chem. Soc.* **2015**, *137* (36), 11645–11655.

Lewis, G. G.; Robbins, J. S.; Phillips, S. T. Phase-Switching Depolymerizable Poly(Carbamate) Oligomers for Signal Amplification in Quantitative Time-Based Assays. *Macromolecules* **2013**, *46* (13), 5177–5183.

Lewis, G. G.; Robbins, J. S.; Phillips, S. T. Point-of-Care Assay Platform for Quantifying Active Enzymes to Femtomolar Levels Using Measurements of Time as the Readout. *Anal. Chem.* **2013**, *85* (21), 10432–10439.

Lopes, G. R.; Pinto, D. C. G. A.; Silva, A. M. S. Horseradish Peroxidase (HRP) as a Tool in Green Chemistry. *RSC Adv.* **2014**, *4* (70), 37244–37265.

Li, Y.; Liu, G.; Wang, X.; Hu, J.; Liu, S. Enzyme-Responsive Polymeric Vesicles for Bacterial-Strain-Selective Delivery of Antimicrobial Agents. *Angew. Chem. Int. Ed.* **2016**, *128* (5), 1792–1796.

Li, N.; Cai, H.; Jiang, L.; Hu, J.; Bains, A.; Hu, J.; Gong, Q.; Luo, K.; Gu, Z. Enzyme-Sensitive and Amphiphilic PEGylated Dendrimer-Paclitaxel Prodrug-Based Nanoparticles for Enhanced Stability and Anticancer Efficacy. *ACS Appl. Mater. Interfaces* **2017**, *9* (8), 6865–6877.

Lawrence, D. S.; Jiang, T.; Levett, M. Self-Assembling Supramolecular Complexes. *Chem. Rev.* **1995**, *95* (6), 2229–2260.

Lehn, J. -M. Perspectives in Supramolecular Chemistry—From Molecular Recognition towards Molecular Information Processing and Self-Organization. *Angew. Chem. Int. Ed.* **1990**, *29* (11), 1304–1319.

Lehn, J. M. Toward Self-Organization and Complex Matter. *Science* **2002**, *295* (5564) 2400–2403.

Lee, S. C.; Lan, W.; Buchanan, B. B.; Luan, S. A Protein Kinase-Phosphatase Pair Interacts with an Ion Channel to Regulate ABA Signaling in Plant Guard Cells. *Proc. Natl. Acad. Sci. U. S. A.* **2009**, *106* (50), 21419–21424.

Mattia, E.; Otto, S. Supramolecular Systems Chemistry. *Nat. Nanotechnol.* **2015**, *10* (2), 111-119.

Maiti, S.; Fortunati, I.; Ferrante, C.; Scrimin, P.; Prins, L. J. Dissipative Self-Assembly of Vesicular Nanoreactors. *Nat. Chem.* **2016**, *8* (7), 725–731.

Michon, T.; Chenu, M.; Kellershon, N.; Desmadril, M.; Guéguen, J. Horseradish Peroxidase Oxidation of Tyrosine-Containing Peptides and Their Subsequent Polymerization: A Kinetic Study. *Biochemistry* **1997**, *36* (28), 8504–8513.

Macknight, W. J.; Ponomarenko, E. A.; Tirrell, D. A. Self-Assembled Polyelectrolyte - Surfactant Complexes in Nonaqueous Solvents and in the Solid State. *Acc. Chem. Res.* **1998**, *31* (12), 781–788.

Miller, D. S.; Wang, X.; Abbott, N. L. Design of Functional Materials Based on Liquid Crystalline Droplets. *Chem. Mat*. **2014,** *26* (1), 496–506.

Olah, M. G.; Robbins, J. S.; Baker, M. S.; Phillips, S. T. End-Capped Poly(Benzyl Ethers): Acid and Base Stable Polymers That Depolymerize Rapidly from Head-to-Tail in Response to Specific Applied Signals. *Macromolecules* **2013**, *46* (15), 5924–5928.

Ober, C. K.; Wegner, G. Polyelectrolyte-Surfactant Complexes in the Solid State: Facile Building Blocks for Self-Organizing Materials. *Adv. Mater.* **1997**, *9* (1), 17–31.

Patchornik, A.; Amit, B.; Woodward, R. B. Photosensitive Protecting Groups. *J. Am. Chem. Soc*. **1970**, *92* (21), 6333–6335.

Peterson, G. I.; Larsen, M. B.; Boydston, A. J. Controlled Depolymerization: Stimuli-Responsive Self-Immolative Polymers. *Macromolecules* **2012**, *45* (18), 7317–7328.

Phillips, D. J.; Wilde, M.; Greco, F.; Gibson, M. I. Enzymatically Triggered, Isothermally Responsive Polymers: Reprogramming Poly(Oligoethylene Glycols) to Respond to Phosphatase. *Biomacromolecules* **2015**, *16* (10), 3256–3264.

Philp, D.; Fraser Stoddart, J. Self-Assembly in Natural and Unnatural Systems. *Angew. Chem. Int. Ed.* **1996**, *35* (11), 1154–1196.

Roth, M. E.; Green, O.; Gnaim, S.; Shabat, D. Dendritic, Oligomeric, and Polymeric Self-Immolative Molecular Amplification. *Chem. Rev*. **2016**, *116* (3), 1309–1352.

Robinson, P. K. Enzymes: Principles and Biotechnological Applications. *Essays Biochem.* **2015**, *59*, 1–41.

Rieß, B.; Grötsch, R. K.; Boekhoven, J. The Design of Dissipative Molecular Assemblies Driven by Chemical Reaction Cycles. *Chem* **2019**, *6* (3), 552–578.

Robinson, P. K. Enzymes: Principles and Biotechnological Applications. *Essays Biochem.* **2015**, *59*, 1–41.

Rodriguez, A. R.; Kramer, J. R.; Deming, T. J. Enzyme-Triggered Cargo Release from Methionine Sulfoxide Containing Copolypeptide Vesicles. *Biomacromolecules* **2013**, *14* (10), 3610–3614.

Raghupathi, K. R.; Azagarsamy, M. A.; Thayumanavan, S. Guest-Release Control in Enzyme-Sensitive, Amphiphilic-Dendrimer-Based Nanoparticles through Photochemical Crosslinking. *Chem. Eur. J.* **2011**, *17* (42), 11752–11760.

Riccio, A. Dynamic Epigenetic Regulation in Neurons: Enzymes, Stimuli and Signaling Pathways. *Nat. Neurosc*. **2010**, *13* (11), 1330–1337.

Shabat, D. Self-Immolative Dendrimers as Novel Drug Delivery Platforms. *J. Polym. Sci. Part A Polym. Chem.* **2006**, *44* (5), 1569–1578.

Seo, W.; Phillips, S. T. Patterned Plastics That Change Physical Structure in Response to Applied Chemical Signals. *J. Am. Chem. Soc.* **2010**, *132* (27), 9234–9235.

Sagi, A.; Weinstain, R.; Karton, N.; Shabat, D. Self-Immolative Polymers. *J. Am. Chem. Soc.* **2008**, *130* (16), 5434–5435.

Sui, Z.; Jaber, J. A.; Schlenoff, J. B. Polyelectrolyte Complexes with PH-Tunable Solubility. *Macromolecules* **2006**, *39* (23), 8145–8152.

Spulber, M.; Najer, A.; Winkelbach, K.; Glaied, O.; Waser, M.; Pieles, U.; Meier, W.; Bruns, N. Photoreaction of a Hydroxyalkyphenone with the Membrane of Polymersomes: A Versatile Method to Generate Semipermeable Nanoreactors. *J. Am. Chem. Soc.* **2013**, *135* (24), 9204–9212.

Sato, H.; Takino, T.; Okada, Y.; Cao, J.; Shinagawa, A.; Yamamoto, E.; Seiki, M. A Matrix Metalloproteinase Expressed on the Surface of Invasive Tumour Cells. *Nature* **1994**, *370* (6484), 61–65.

Seo, W.; Phillips, S. T. Patterned Plastics That Change Physical Structure in Response to Applied Chemical Signals. *J. Am. Chem. Soc.* **2010**, *132* (27), 9234–9235.

Sisco Bayse, G.; Michaels, A. W.; Morrison, M. The Peroxidase-Catalyzed Oxidation of Tyrosine. *BBA - Enzymol.* **1972**, *284* (1), 34–42.

Samarajeewa, S.; Shrestha, R.; Li, Y.; Wooley, K. L. Degradability of Poly(Lactic Acid)-Containing Nanoparticles: Enzymatic Access through a Cross-Linked Shell Barrier. *J. Am. Chem. Soc.* **2012**, *134* (2), 1235–1242.

Tam, K. C.; Wyn-Jones, E. Insights on Polymer Surfactant Complex Structures during the Binding of Surfactants to Polymers as Measured by Equilibrium and Structural Techniques. *Chem. Soc. Rev*. **2006**, *35* (8), 693–709.

Tatsumi, T.; Shiraishi, J.; Keira, N.; Akashi, K.; Mano, A.; Yamanaka, S.; Matoba, S.; Fushiki, S.; Fliss, H.; Nakagawa, M. Intracellular ATP Is Required for Mitochondrial Apoptotic Pathways in Isolated Hypoxic Rat Cardiac Myocytes. *Cardiovasc. Res.* **2003**, *59* (2), 428–440.

Van Esch, J. H.; Klajn, R.; Otto, S. Chemical Systems out of Equilibrium. *Chem. Soc. Rev.* **2017**, *46* (18), 5474–5475.

Van Rossum, S. A. P.; Tena-Solsona, M.; Van Esch, J. H.; Eelkema, R.; Boekhoven, J. Dissipative Out-of-Equilibrium Assembly of Man-Made Supramolecular Materials. *Chem. Soc. Rev.* **2017**, *46* (18), 5519–5535.

Volkov, A. G.; Adesina, T.; Markin, V. S.; Jovanov, E. Kinetics and Mechanism of Dionaea Muscipula Trap Closing. *Plant Physiol.* **2008**, *146* (2), 694–702.

Vince, J.; Hardesty, B. D. Plastic Pollution Challenges in Marine and Coastal Environments: From Local to Global Governance. *Restor. Ecol.* **2017**, *25* (1), 123–128.

Wong, C.; Stylianopoulos, T.; Cui, J.; Martin, J.; Chauhan, V. P.; Jiang, W.; Popovíc, Z.; Jain, R. K.; Bawendi, M. G.; Fukumura, D. Multistage Nanoparticle Delivery System for Deep Penetration into Tumor Tissue. *Proc. Natl. Acad. Sci. U. S. A.* **2011**, *108* (6), 2426–2431.

Wen, J.; Anderson, S. M.; Du, J.; Yan, M.; Wang, J.; Shen, M.; Lu, Y.; Segura, T. Controlled Protein Delivery Based on Enzyme-Responsive Nanocapsules. *Adv. Mater.* **2011**, *23* (39), 4549–4553.

Wang, C.; Chen, Q.; Wang, Z.; Zhang, X. An Enzyme-Responsive Polymeric Superamphiphile. *Angew. Chem. Int. Ed.* **2010**, *49* (46), 8612–8615.

Whitesides, G. M.; Simanek, E. E.; Mathias, J. P.; Seto, C. T.; Chin, D. N.; Mammen, M.; Gordon, D. M. Noncovalent Synthesis: Using Physical-Organic Chemistry to Make Aggregates. *Acc. Chem. Res.* **1995**, *28* (1), 37–44.

Whitesides, G. M.; Mathias, J. P.; Seto, C. T. Molecular Self-Assembly and Nanochemistry: A Chemical Strategy for the Synthesis of Nanostructures. *Science* **1991**, *254* (5036), 1312–1319.

Wirth, A.; Benyó, Z.; Lukasova, M.; Leutgeb, B.; Wettschureck, N.; Gorbey, S.; Orsy, P.; Horváth, B.; Maser-Gluth, C.; Greiner, E.; et al. G12-G13-LARG-Mediated Signaling in Vascular Smooth Muscle Is Required for Salt-Induced Hypertension. *Nat. Med.* **2008**, *14* (1), 64–68.

Wettschureck, N.; Offermanns, S. Rho/Rho-Kinase Mediated Signaling in Physiology and Pathophysiology. *J. Mol. Med.* **2002**, *80* (10), 629–638.

Wang, W.; Alexander, C. Self-Immolative Polymers. *Angew. Chem. Int. Ed.* **2008**, *47* (41) 7804–7806.

Weinstain, R.; Sagi, A.; Karton, N.; Shabat, D. Self-Immolative Comb-Polymers: Multiple-Release of Side-Reporters by a Single Stimulus Event. *Chem. - A Eur. J.* **2008**,

14 (23), 6857–6861.

Wallin, T.; Linse, P. Monte Carlo Simulations of Polyelectrolytes at Charged Micelles. 3. Effects of Surfactant Tail Length. *J. Phys. Chem. B* **1997**, *101* (28), 5506–5513.

Weinstain, R.; Baran, P. S.; Shabat, D. Activity-Linked Labeling of Enzymes by Self-Immolative Polymers. *Bioconjug. Chem.* **2009**, *20* (9), 1783–1791.

Wang, Q.; Schlenoff, J. B. The Polyelectrolyte Complex/Coacervate Continuum. *Macromolecules* **2014**, *47* (9), 3108–3116.

Xiao, Y.; Li, H.; Zhang, B.; Cheng, Z.; Li, Y.; Tan, X.; Zhang, K. Modulating the Depolymerization of Self-Immolative Brush Polymers with Poly(Benzyl Ether) Backbones. *Macromolecules* **2018**, *51* (8), 2899–2905.

Yardley, R. E.; Kenaree, A. R.; Gillies, E. R. Triggering Depolymerization: Progress and Opportunities for Self-Immolative Polymers. *Macromolecules*. **2019**, *52* (17), 6342-6360.

Yang, Z.; Gu, H.; Fu, D.; Gao, P.; Lam, J. K.; Xu, B. Enzymatic Formation of Supramolecular Hydrogels. *Adv. Mater.* **2004**, *16* (16), 1440–1444.

Zhuang, J.; Seçinti, H.; Zhao, B.; Thayumanavan, S. Propagation of Enzyme-Induced Surface Events inside Polymer Nanoassemblies for a Fast and Tunable Response. *Angew. Chem. Int. Ed.* **2018**, *57* (24), 7111–7115.

Zhou, S.; Burger, C.; Yeh, F.; Chu, B. Charge Density Effect of Polyelectrolyte Chains on the Nanostructures of Polyelectrolyte-Surfactant Complexes. *Macromolecules* **1998**, *31* (23), 8157–8163.

Zhao, H.; Sterner, E. S.; Coughlin, E. B.; Theato, P. O-Nitrobenzyl Alcohol Derivatives: Opportunities in Polymer and Materials Science. *Macromolecules* **2012**, *45* (4), 1723–1736.

Zustiak, S. P.; Leach, J. B. Characterization of Protein Release from Hydrolytically Degradable Poly(Ethylene Glycol) Hydrogels. *Biotechnol. Bioeng.* **2011**, *108* (1), 197–206.